


Fall 2012

# The contribution of oxidative stress in the protein damage and DNA lesion in Alzheimer's disease neuropathology

Cheng Zhang

Follow this and additional works at: <https://digitalcommons.latech.edu/dissertations>

 Part of the [Biochemistry Commons](#), [Biomedical Engineering and Bioengineering Commons](#), and the [Neuroscience and Neurobiology Commons](#)

---

**THE CONTRIBUTION OF OXIDATIVE STRESS IN  
THE PROTEIN DAMAGE AND DNA LESION  
IN ALZHEIMER'S DISEASE  
NEUROPATHOLOGY**

by

Cheng Zhang, B.Eng., M.S.

A Dissertation Presented in Partial Fulfillment  
of the Requirements of the Degree  
Doctor of Philosophy

COLLEGE OF ENGINEERING AND SCIENCE  
LOUISIANA TECH UNIVERSITY

November 2012

UMI Number: 3534296

All rights reserved

INFORMATION TO ALL USERS

The quality of this reproduction is dependent upon the quality of the copy submitted.

In the unlikely event that the author did not send a complete manuscript and there are missing pages, these will be noted. Also, if material had to be removed, a note will indicate the deletion.



UMI 3534296

Published by ProQuest LLC 2012. Copyright in the Dissertation held by the Author.

Microform Edition © ProQuest LLC.

All rights reserved. This work is protected against unauthorized copying under Title 17, United States Code.



ProQuest LLC  
789 East Eisenhower Parkway  
P.O. Box 1346  
Ann Arbor, MI 48106-1346

LOUISIANA TECH UNIVERSITY

THE GRADUATE SCHOOL

JULY 17, 2012

Date

We hereby recommend that the dissertation prepared under our supervision by

Cheng Zhang, B.Eng., M.S.

Entitled The Contribution of Oxidative Stress in the Protein Damage and  
DNA Lesion in Alzheimer's Disease Neuropathology

be accepted in partial fulfillment of the requirements for the Degree of  
Doctor of Philosophy in Biomedical Engineering

Junefeng

Supervisor of Dissertation Research

Stan Jones

Head of Department

Department

Recommendation concurred in:

Alvin

[Signature]  
[Signature]

Advisory Committee

Approved:

M. K. Kawachandran

Director of Graduate Studies

Stan Napp

Dean of the College

Approved:

Terrence M. Conathy

Dean of the Graduate School

## ABSTRACT

Glutathione (GSH) plays an essential role in the intracellular antioxidant defense against the oxidant radicals, especially the  $\cdot\text{OH}$  radical. To understand the early and progressive cellular changes in Alzheimer's disease (AD) development, we investigated reduced glutathione/oxidized glutathione (GSH/GSSG) status in a double mutated AD transgenic mouse model (B6.Cg-Tg), which carries Swedish amyloid precursor protein mutation ( $\text{APP}_{\text{swe}}$ ) and exon 9 deletion of the PSEN1 gene. Likewise, *S*-glutathionylation (Pr-SSG) is a specific post-translational modification (PTM) of cysteine residues by the addition of glutathione. *S*-glutathionylated proteins induced by oxidative stress play an essential role in understanding the pathogenesis of the aging and age related disorder. In addition, 8-Hydroxy-2'-deoxyguanosine (8-OHdG) is one of the major forms of DNA oxidative damage, and is commonly analyzed as an excellent marker of DNA lesions. The purpose of this research was to develop a sensitive method to accurately and rapidly quantify the 8-OHdG by using capillary electrophoresis with laser-induced fluorescence detection (CE-LIF). The method involved the use of specific antibody to detect DNA lesions (8-OHdG) and consecutive fluorescence labeling.

Here, we quantified and compared both GSH/GSSG and mixed-disulfide (Pr-SSG) levels in blood samples and three anatomic positions in the brain (cerebrum, cerebellum, and hippocampus) at 3 age stages (1-, 5-, and 11-month-old) of AD transgenic (Tg)/wild type (WT) mice. The study was designed to characterize and

provide insight into the glutathione redox state of both brain tissues and blood samples at different disease stages of this Tg model. The GSH/GSSG ratio in AD-Tg brain tissue started at a higher value at 1-month, fell at the transitional period at 5-month, right before the onset of amyloid plaque, followed by an increase in GSSG and an associated decrease of GSH/GSSG at 11-month. Besides, the high basal levels of Pr-SSG in hippocampus suggest a potential for increased oxidative damage under oxidized conditions and increased GSSG in this vulnerable region.

Moreover, we developed an approach to aid in the early diagnosis of AD by using principal component analysis (PCA) based spectral analysis of oxidized protein electrophoretic profiling. We found that the combination of capillary electrophoresis and PCA analysis of *S*-glutathionylation distribution characterization can be used in the sample classification and molecular weight (Mw) prediction. PCA can project the *S*-glutathionyl electrophoretic data into one of six different groups of mice brain and blood samples based on disease progressions and genotype differences. The prediction of the main protein Mw regions that are most susceptible to *S*-glutathionylation damages in mice brains and blood samples are located at 8.4~20.3 kDa and 13.2~37.2 kDa.

Furthermore, the urine sample with 8-OHdG fluorescently labeled along with other constituents was resolved by the capillary electrophoretic system and the lesion of interest was detected using a fluorescence detector. The low detection limit of 9.0 amol proves the method sensitive enough for the detection and quantification of 8-OHdG in untreated urine samples. The relative standard deviation (RSD) was found to be 11.32% for migration time, and 5.52% for the peak area.

## APPROVAL FOR SCHOLARLY DISSEMINATION

The author grants to the Prescott Memorial Library of Louisiana Tech University the right to reproduce, by appropriate methods, upon request, any or all portions of this Dissertation. It is understood that "proper request" consists of the agreement, on the part of the requesting party, that said reproduction is for his personal use and that subsequent reproduction will not occur without written approval of the author of this Dissertation. Further, any portions of the Dissertation used in books, papers, and other works must be appropriately referenced to this Dissertation.

Finally, the author of this Dissertation reserves the right to publish freely, in the literature, at any time, any or all portions of this Dissertation.

Author Chy Zhou

Date 09-21-12

## TABLE OF CONTENTS

ABSTRACT .....	iii
LIST OF FIGURES .....	x
LIST OF TABLES .....	xiv
ACKNOWLEDGMENTS .....	xv
CHAPTER 1 INTRODUCTION .....	1
1.1    Alzheimer's Disease .....	1
1.2    Glutathione Redox Cycle.....	2
1.3    Oxidized Protein .....	3
1.4    DNA Lesion.....	4
CHAPTER 2 METHODS.....	8
2.1    General Methods.....	8
2.1.1  Transgenic Mice and Genotyping.....	8
2.1.2  Cell Culture.....	9
2.1.3  Sample Preparation .....	9
2.1.4  Protein Concentration Measurement.....	10
2.1.5  Data Analysis.....	10
2.2    High Performance Liquid Chromatography .....	10
2.2.1  Measurement of GSH and GSSG .....	10
2.2.2  Pr-SSG Determination .....	11
2.2.3  Determination of Enzymatic Activity .....	12
2.3    Capillary Electrophoresis.....	12



2.3.1	<i>In Vitro</i> S-glutathionylation of BSA .....	12
2.3.2	S-glutathionyl Level Determination.....	12
2.3.3	Pr-SSG Derivatization and Detection .....	13
2.3.4	Validation of the Developed Method.....	15
2.3.5	CE Instrument .....	15
2.3.6	Mw Determination .....	16
2.3.7	Urine Collection and Labeling.....	17
2.3.8	Labeling of Test Model.....	17
2.3.9	Separation Condition .....	18
2.4	Principle Component Analysis .....	18
2.4.1	Principle Component Analysis .....	18
2.4.2	K-means Clustering Algorithm.....	20
2.4.3	Probability of Gaussian Distribution .....	21
CHAPTER 3 RESULTS .....		22
3.1	Glutathione Redox Status .....	22
3.1.1	Genotyping.....	22
3.1.2	Brain Weight.....	22
3.1.3	Tissue Glutathione Status .....	24
3.1.4	Blood Glutathione Status .....	27
3.1.5	Mixed-disulfide Status.....	28
3.1.6	Enzymatic Activity .....	30
3.2	Oxidized Protein .....	32
3.2.1	Grx-catalyzed Deglutathionylation.....	32
3.2.2	Detection and Validation .....	32
3.2.3	Evaluation of NEM Removal.....	35

3.2.4	Assessment of Blocking Efficiency .....	37
3.2.5	Assay Reproducibility and Accuracy .....	38
3.2.6	<i>S</i> -glutathionylation Determination.....	41
3.2.7	Monitoring Pr-SSG in Mice Brain.....	43
3.2.8	Pr-SSG in Protein Profiles .....	47
3.2.9	Principal Component Analysis .....	50
3.2.10	Prediction of Molecular Weight .....	53
3.2.11	Sample Categorization.....	55
3.3	Damaged DNA .....	62
3.3.1	Calibration Curve .....	62
3.3.2	Analysis of 8-OHdG in Mice Urine .....	64
3.3.3	Assay Repeatability and Accuracy.....	67
CHAPTER 4 DISCUSSION.....		69
4.1	Glutathione Homeostasis .....	69
4.1.1	Age Effect .....	70
4.1.2	Genotype Effect .....	72
4.1.3	Specific Brain Region Effect .....	73
4.2	Pr-SSG Profiles.....	75
4.2.1	Pr-SSG Electrophoretic Profiles .....	76
4.2.2	Diagnostic Use.....	78
4.2.3	Protein Biomarkers .....	79
4.2.4	Spectral Separation .....	80
4.2.5	Transgenic Mouse Model .....	81
4.3	8-OHdG Detection.....	82
APPENDIX A CHEMICALS AND REAGENTS.....		84

A.1	GSH and GSSG Determination .....	85
A.2	Pr-SSG Detection.....	85
A.3	8-OHdG Detection.....	86
APPENDIX B	ANIMAL USE APPROVAL.....	87
REFERENCES	.....	89

## LIST OF FIGURES

Figure 1:	Glutathione Redox Cycle. Oxidative stress, which is a disturbance of glutathione homeostasis, induced by Reactive Oxygen Species (ROS). Superoxide dismutase and Glutathione (GSH) are considered as the first line of defense against superoxide anions and $\cdot\text{OH}$ radicals produced in mammalian cells. Glutathione presents primarily in its reduced form (GSH), which can be converted to the oxidized form (GSSG) under glutathione peroxidase (GPx). GSSG is then recycled to GSH by glutathione reductase (GR) in the presence of reduced nicotinamide adenine dinucleotide phosphate (NADPH) .....	3
Figure 2:	Formation of 8-hydroxy-2'-deoxyguanosine (8-OHdG) by oxidative stress .....	5
Figure 3:	Mechanism of deglutathionylation and detection of <i>S</i> -glutathionylated proteins (Pr-SSG). (a) Schematic representation of the method to detect Pr-SSG by labeling with Dylight 488 maleimide. (b) Deglutathionylation assay is divided by 3 steps. (1) The Pr-SSG is reduced by glutaredoxin (Grx). (2) The oxidized Grx (Grx-SSG) intermediate is transferred to glutathione (GSH). (3) Glutathione reductase (GR) reduces oxidized glutathione (GSSG) with presence of nicotinamide adenine dinucleotide phosphate (NADPH).....	14
Figure 4:	Transformation of migration time (a) to molecular weight (Mw) value. (b) Log of molecular mass of standard proteins as a function of their electrophoretic mobility.....	17
Figure 5:	A schematic block diagram describing overall experimental procedure .....	19
Figure 6:	Comparison of wet brain weight in cerebrum, cerebellum, hippocampus, and total weight of AD-Tg/WT mice at 3 age stages. Data are presented as means $\pm$ SEM for 30 animals. Age effect: 1-month vs. 5-month vs. 11-month. +++ $P < 0.001$ . Genotype effect: Tg vs. WT. * $P < 0.05$ . Tissue effect: hippocampus vs. cerebrum vs. cerebellum. †† $P < 0.01$ , ††† $P < 0.001$ .....	23

- Figure 7: Glutathione (GSH) and oxidized glutathione (GSSG) levels and GSH/GSSG ratio in 1-, 5- and 11-month-old Tg and WT specific brain regions. Both (A) GSH and (B) GSSG levels were determined by reverse-phase high performance liquid chromatography (HPLC) following derivatization of samples with 1-fluoro-2, 4-dinitrobenzene (FDNB) as described in Methods; and (C) calculated GSH/GSSG ratio. GSH and GSSG are expressed as nmol/mg proteins and presented as means  $\pm$  SEM (n=5/group). Age effect: 1-month vs. 5-month vs. 11-month. + P < 0.05, ++ P < 0.01. Genotype effect: Tg vs. WT. \* P < 0.05. Tissue effect: hippocampus vs. cerebrum vs. cerebellum. † P < 0.05, †† P < 0.01, ††† P < 0.001 ..... 25
- Figure 8: Levels of S-glutathionylated proteins (Pr-SSG) in specific brain regions in 1-, 5- and 11-month-old Tg and WT mice. Data are expressed as nmol/mg proteins and presented as means  $\pm$  SEM. Error bars do not appear in panel A, because samples cannot be detectable in cerebrum, cerebellum and blood of WT mice. Age effect: 1-month vs. 5-month vs. 11-month. + P < 0.05. Genotype effect: Tg vs. WT. \* P < 0.05, \*\* P < 0.01 ..... 29
- Figure 9: Activities of glutathione reductase (GR) and glutathione peroxidase (GPx) in AD-Tg/WT mouse brain at 1-, 5- and 24-month. Data are expressed as nmol/min/ml and presented as means  $\pm$  SEM. Age effect: 1-month vs. 5-month vs. 11-month. +P<0.05, ++ P < 0.01 ..... 31
- Figure 10: *In vitro* S-glutathionylated bovine serum albumin (BSA-SSG) and validation of the method using controls. (1) Electropherograms of Dylight 488 maleimide; (2) BSA-SSG; (3) BSA-SSG without glutaredoxin (Grx) reduction; (4) BSA-SSG pretreated with dithiothreitol (DTT); (5) native BSA. Hydrodynamic injection at pH 8 and 11 kpa for 4 s; separation in gel containing 15% dextran (64-76 kDa), 0.5% SDS, 20 mM Tris and 20 mM Tricine at -570 V/cm. 1 & 2 indicate Dylight 488 maleimide. Top trace is offset in the y-axis for the clarity ..... 34
- Figure 11: Comparison of desalting efficiency using spin columns at different times. Completely removing blocking reagents is crucial in this experiment. Remaining N-ethylmaleimide (NEM) can cause unnecessary blocking to freshly formed thiol groups. Double the desalting times will solve this problem. Top trace shows clear peaks for maleimide and S-glutathionylated bovine serum albumin (BSA-SSG) (1 and 2 indicate Dylight 488 maleimide using spin columns for 6 times). Bottom trace shows no peak for BSA-SSG (1' and 2' indicate Dylight 488 maleimide using spin columns for 3 times). All the experimental conditions are the same as in Figure 10. Top trace is offset in the y-axis for the clarity ..... 36

- Figure 12: Comparison of blocking efficiency between Iodoacetic acid (IAA) and N-ethylmaleimide (NEM) at three concentration conditions. S-glutathionylated bovine serum albumin (BSA-SSG) samples were reacted with IAA and NEM, respectively. Top 3 traces indicate 10, 30 and 40 mM IAA with solid lines. Bottom 3 traces indicate 10, 30 and 40 mM NEM. 1 & 2 indicate Dylight 488 maleimide. All the experimental conditions are the same as in Figure 10. Top trace is offset in the y-axis for the clarity..... 38
- Figure 13: Electropherograms of a series of dilution (1-, 1.3-, 2-, 4-fold) of S-glutathionylated bovine serum albumin (BSA-SSG) labeled with Dylight 488 maleimide. 1 & 2: Dylight 488 maleimide. All the experimental conditions are the same as in Figure 10. Top trace is offset in the y-axis for the clarity..... 40
- Figure 14: Quantitative electrophoretic profiling of menadione (MQ) mediated S-glutathionylation (Pr-SSG) in human colon adenocarcinoma (HT-29) cells and Pr-SSG of brain tissues and blood in AD-Tg/WT mice. (a) Electropherograms of Pr-SSG from HT-29 cells labeled with Dylight 488 maleimide. Trace 1 demonstrates Pr-SSG from MQ treated HT-29 cells. Traces 2 and 3 indicate MQ untreated HT-29 cells and MQ treated HT-29 cells without deglutathionylation, respectively. (b) Electropherograms of Pr-SSG in cerebrum of AD-Tg/WT mice at 5-month. (c) Electropherograms of Pr-SSG from 3 anatomical positions (cerebrum, cerebellum and hippocampus) in brain tissue and blood sample of AD-Tg mouse. (d) Electropherograms of Pr-SSG from 3 anatomic brain regions and blood of AD-WT mouse. 1 & 2: Dylight 488 maleimide. All the experimental conditions are the same as in Figure 10. Top trace is offset in the y-axis for the clarity..... 42
- Figure 15: Gel condition test for S-glutathionylated protein (Pr-SSG) in cerebrum of AD-Tg/WT mice at 5-month old using gel matrix containing 10% dextran (Mw: 64-76KDa), 0.5% SDS, 20 mM Tris and 20 mM Tricine. 1: Dylight 488 maleimide. All the experimental conditions are the same as in Figure 10. Top trace is offset in the y-axis for the clarity..... 45
- Figure 16: Melting curves (A) and melting peaks (B) of App gene. Melting temperature ( $T_m$ ) of App gene is  $86.0 \pm 0.6$  °C (peak area=18) ..... 46
- Figure 17: Electropherograms of S-glutathionylated protein (Pr-SSG) of Tg (a)/WT (b) mouse brain and Tg (c)/WT (d) blood at 1-, 5- and 11-month-old. Yellow arrows point out Pr-SSG peaks at the 3 age stages. The unlabeled peaks belong to Dylight 488 maleimide. Pr-SSG levels in AD-Tg/WT brain (e) and blood (f) samples at the 3 age groups. Age effect: 1-month vs. 5-month vs. 11-month. +++P < 0.001. Genotype effect: Tg vs. WT. \* P < 0.05, \*\* P < 0.01, \*\*\*P < 0.001 ..... 49

- Figure 18: The score plots of PCA analysis for the brain (a) and blood (b) *S*-glutathionylated protein electropherograms ..... 51
- Figure 19: Principle component analysis (PCA) of brain Pr-SSG electropherograms. Score plot of PCA-analyzed samples using the first three PCs for the three Tg (a) and WT (b) groups ..... 52
- Figure 20: Loading vector of the first principle component (PC) of mice PCA in brain (a) and blood (b). The loading vector represents how variables contribute to the variance explained by the first PC. The variables with the most contribution found above the threshold (dashed line)..... 54
- Figure 21: Boxplots for 5-fold cross-validation classification accuracy data for age/genotype groups of brain and blood *S*-glutathionylated protein. (a) and (b) show the binary classification accuracies for the discrimination of genotype in the three age groups. (c) shows the three-class age discrimination in Tg and WT mice using blood and brain samples. (d) shows the overall six-group classification of both age & genotype. In each of these subplots, the horizontal dotted line represents the accuracy of a chance (random) classifier. The mean classification accuracy for each group is also shown on the top of the each bar chart ..... 56
- Figure 22: Results of the receiver operating characteristic (ROC) analyses generated by the threshold percentage votes needed to classify a *S*-glutathionylation electropherogram. The area under the curve was calculated as 1 and 0.9867 for brain (a) and blood (b), respectively ..... 61
- Figure 23: Electropherograms of validation tests in positive and negative controls. (1) a complex with  $1000 \text{ ng}\cdot\mu\text{L}^{-1}$  8-hydroxy-2'-deoxyguanosine (8-OHdG) standard; (2) a complex with  $10 \text{ ng}\cdot\mu\text{L}^{-1}$  8-OHdG standard; (3) a complex with primary and secondary antibody; (4) secondary antibody alone; (5) primary antibody alone. Hydrodynamic injection at pH 9.5 and 0.5 psi for 5 s; separation in 20mM sodium tetraborate buffer at 400 V/cm. Arrowhead: secondary antibody; Arrow: 8-OHdG complex. Top trace is offset in the y-axis for the clarity ..... 63
- Figure 24: Electropherograms of calibration curve of 8-hydroxy-2'-deoxyguanosine (8-OHdG) standard with different concentrations. Arrowhead: secondary antibody; Arrow: 8-OHdG complex. All the experimental conditions are the same as in Figure 23. Top trace is offset in the y-axis for the clarity ..... 64
- Figure 25: Electropherograms of urine sample and 8-hydroxy-2'-deoxyguanosine (8-OHdG) standard. Arrowhead: secondary antibody; Arrow: 8-OHdG complex. All the experimental conditions are the same as in Figure 23 ..... 65

## LIST OF TABLES

Table 1: The sequence of oligomers .....	9
Table 2: Blood glutathione status .....	28
Table 3: S-glutathionyl contents .....	44
Table 4: PCA variance in brain tissues and blood samples .....	53
Table 5: Probability of membership in the six age/genotype group—brain.....	58
Table 6: Probability of membership in the six age/genotype group—blood.....	59



## ACKNOWLEDGMENTS

This dissertation could not have been written without my advisor Dr. June Feng, who inspired and challenged me throughout my academic career. She never accepted less than my best efforts.

Special thanks to Dr. Tak Yee Aw's research team for experimental training and technical support.

I also want to thank my committee members in the Department of Biomedical Engineering at Louisiana Tech University for their constructive advices and stimulating suggestions.

Most especially, I would like to express my gratitude to my family and friends whose love and patience enabled me to complete this work.

Lastly, I thank the Louisiana Biomedical Research Network (LBRN) for funding and supporting our research.

# CHAPTER 1

## INTRODUCTION

### 1.1 Alzheimer's Disease

In 2011, there were 5.1 million cases of Alzheimer's disease (AD) in the U.S., while the number of individuals affected by AD is expected to increase over double with the expanded aging population by 2050 [1]. The prevalence of AD patients will reach up to 106.8 million people worldwide by 2050. In other words, 1 in 85 persons has the risk of getting AD in 38 years [2]. It was also estimated that the primary family members and other relatives had put in 17 billion hours of unpaid care that was commensurate with more than \$202 billion in 2010 [1]. Many studies suggest that unpaid caregivers often suffer from depression and stress that can directly result in low life qualities and high financial challenges. According to the report from the Center of Disease Control (CDC), the medical and nursing care bills might cost \$1 trillion annually by 2050 [3]. Moreover, the National Institutes of Health (NIH) will soon add an additional \$50 million along with the \$450 million/year funding in dementia or AD research this year. "The science of Alzheimer's disease has reached a very interesting juncture. We would love to be able to come up with a way of bringing forward an even larger amount of support," NIH director Dr. Francis Collins said in Feb. 8th, 2012.

AD often has a long stage of neuropathological changes and cognitive decline starting at a molecular level, possibly decades earlier than when the decline is detected by neuropsychological testing [4, 5]. Oxidative stress induced by reactive oxygen species (ROS) and a disturbance of glutathione homeostasis in the brain has been implicated as a contributing factor to Alzheimer's disease [6].

## 1.2 Glutathione Redox Cycle

The homeostasis of the brain redox status is mainly controlled by glutathione (GSH) that functions in radical scavenging and protecting cells from oxidative stress [7, 8]. GSH is the most abundant non-protein thiol [9] and is the first line of defense against superoxide anions and  $\cdot\text{OH}$  radicals produced in mammalian cells [10, 11]. Free (non-protein bound) glutathione exists primarily in its reduced form (GSH), which can be oxidized to glutathione disulfide (GSSG) during oxidative stress [12]. GSH is regenerated from GSSG in the glutathione redox cycle catalyzed by GSSG reductase (GR) at the expense of reduced nicotinamide adenine dinucleotide phosphate (NADPH). GSSG, when elevated, can promote protein-protein or protein-lipid cross-linkage [13]; the generation of protein mixed-disulfides (Pr-SSG) involves thiol/disulfide exchange between GSSG and Cys residues on proteins [14]. Thus, enhanced levels of GSSG may increase formation of Pr-SSG [15] shown in Figure 1.

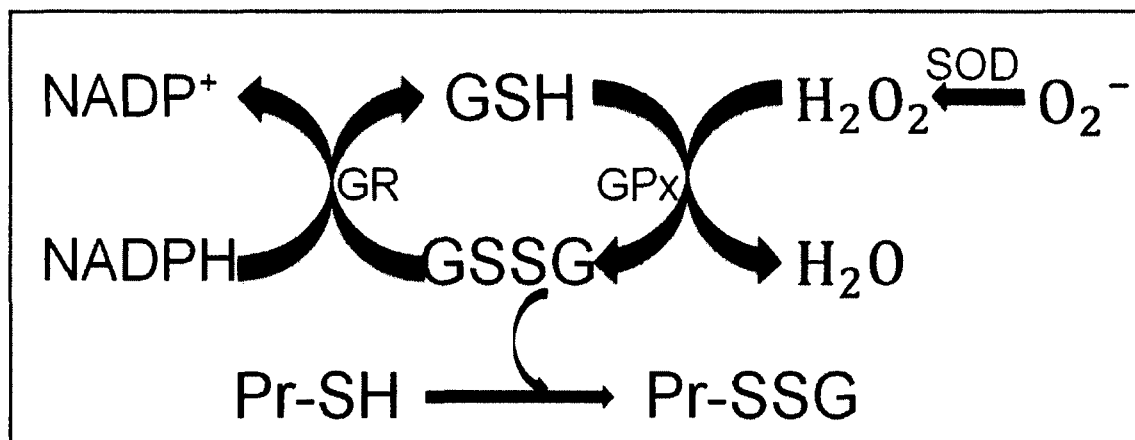


Figure 1: Glutathione Redox Cycle. Oxidative stress, which is a disturbance of glutathione homeostasis, induced by Reactive Oxygen Species (ROS). Superoxide dismutase and Glutathione (GSH) are considered as the first line of defense against superoxide anions and  $\cdot OH$  radicals produced in mammalian cells. Glutathione presents primarily in its reduced form (GSH), which can be converted to the oxidized form (GSSG) under glutathione peroxidase (GPx). GSSG is then recycled to GSH by glutathione reductase (GR) in the presence of reduced nicotinamide adenine dinucleotide phosphate (NADPH).

### 1.3 Oxidized Protein

GSH exists in both free and protein-bound (*S*-glutathionylated) forms. The free form of glutathione exists primarily in its reduced form (GSH), which can be converted to the oxidized glutathione disulfide (GSSG) during oxidative stress. The *S*-glutathionylation of protein (Pr-SSG), representing an important post-translational modification (PTM), plays an essential role in studying the etiology of the aging disorder, such as Alzheimer's disease (AD). The pathway to generate Pr-SSG involves thiol/disulfide exchange between GSSG and thiol residues at Cys residues on proteins [14]. GSSG, when elevated, can promote this thiol/disulfide exchange and cause a greater expression of Pr-SSG [15]. Currently, the *S*-glutathionylation is investigated to elucidate pathological changes in AD, because some proteins are sensitive to cysteine oxidation initiated by increased oxidative stress in an AD brain [16, 17]. Using a redox proteomic

approach, several proteins have been identified as specific targets of *S*-glutathionylation in AD [16, 17]. For instance, Glyceraldehyde 3 phosphate dehydrogenase (GAPDH), a well-known enzyme in intermediary metabolism, plays a crucial role in AD [17]. These oxidatively modified proteins in the AD brain demonstrate impaired protein function, which result in altered cell function, apoptosis and the development of amyloid plaques [16, 17]. Also, studies show that *S*-glutathionylation has potential to serve for redox regulation mechanism [18]. Several methods have been developed so far to quantify the free (non-protein bound) glutathione. To study GSH, proteins existing as the most abundant component in biological samples are removed by either acidification or ultrafiltration to eliminate interference [19, 20]. Additionally, prior to the chromatographic or electrophoretic analysis of GSH, determination of total GSH requires the reduction of all disulfide, which can be achieved enzymatically by glutathione reductase (GR) [21] or chemically with various reducing compounds such as Dithiothreitol (DTT) [22, 23].

#### 1.4 DNA Lesion

Both nuclear and mitochondrial DNA from various tissues and white blood cells are subjected to oxidative damage [24]. They interact with reactive oxygen species (ROS) including superoxide anion radical ( $O_2^-$ ), hydrogen peroxide ( $H_2O_2$ ), hydroxyl radicals ( $\bullet OH$ ), and further produce more than 20 oxidized DNA adducts. Among them, one of the major types of DNA damage is 8-hydroxy-2'-deoxyguanosine (8-OHdG) shown in Figure 2 and is considered as the most commonly used biomarker for evaluation of cellular oxidative stress. The role of 8-OHdG is implicated in aging and the development of neurodegenerative disease such as Alzheimer's disease (AD). It has been a well-

studied biomarker of oxidative stress, since it can cause mutations through CG to AT trans versions [25]. Because guanine has the lowest oxidation potential when compared with the other DNA bases, it is easy to oxidize and further forms the most abundant and important marker of oxidative damage stress. The mechanism of formation involves attack on the C8 of guanine by the hydroxyl radical followed by the formation of guanine C8-OH adduct radical that may undergo two separate pathways: (1) FapyGua formation or (2) subsequent oxidation and formation of 8-oxoguanine [26].

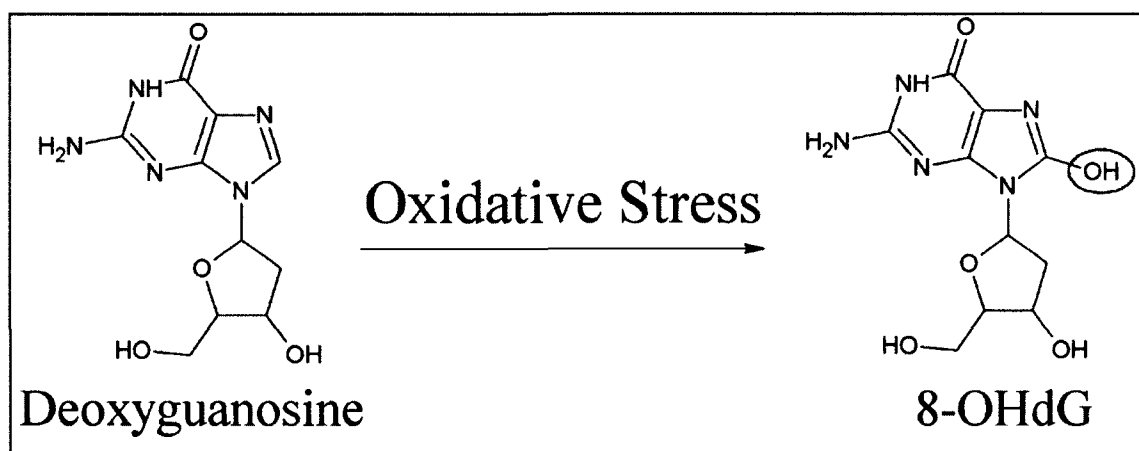


Figure 2: Formation of 8-hydroxy-2'-deoxyguanosine (8-OHdG) by oxidative stress.

Oxidative DNA damage accumulates in the brain. Oxidative damage is a contributing factor for development of Alzheimer's disease and is a major component of aging. Age-dependent increases of 8-OHdG were found in various tissues, such as the human pituitary gland [27], the liver and kidney of rats [28, 29], the human cerebral cortex and the cerebellum brain [30]. Because high oxygen is consumed by the brain, AD brains are most likely susceptible to oxidative damage. The evidence indicates that oxidative DNA damage is the feature of AD in the brain and ventricular CSF [31, 32]. The gas chromatography/mass spectrometry (GC/MS) study of temporal and parietal

lobes of the brains of AD patients revealed statistically significant increases of 8-OHdG in the AD patients when compared to the control subjects [32]. Studies have reported that the levels of 8-OHdG were increased in the mitochondrial DNA of patients with late AD when compared to nuclear DNA [32-34]. 8-OHdG levels were characterized as elevated in mitochondrial DNA in the cerebral cortex of AD patients compared with controls [35]. Another study detected higher levels of 8-OHdG in the nuclear DNA of lymphocytes in patient that have AD disease [36]. A recent study by Lovell's group found the significant increase in 8-OHdG in multiple brain regions, including frontal, temporal and parietal lobes in mild cognitive impairment (MCI) subjects [32]. These findings suggest oxidative DNA damage occurs at the earliest detectable phase of AD, and it may serve as a prescreening tool for AD and play a critical role in AD pathogenesis.

Oxidative DNA damage is also found in the urine. After 8-OH-dGTP is formed in the nucleotide pool, the pyrophosphate can be removed by the enzyme MTH1 to yield 8OH-dGMP. Afterwards, it is digested by 5'(3')-nucleotidase to produce 8-OHdG. Without further metabolism, 8-OHdG is excreted in urine [37, 38]. Because the amount of 8-OHdG excreted in the urine corresponds to the average rate of oxidative damage in the whole body, it can be potentially used as a medical test of early screening for different diseases. Measurement of excreted repair products in urine indicates the average rate of the damage in the total body, while the abundance of oxidized bases in nuclear or mitochondrial DNA represents the concentration in the specific local tissues/cells. Compared to DNA samples, urine is a better matrix for analyzing 8-OHdG, since DNA isolation and digestion techniques usually are the source of artificial formation of 8-OHdG [39]. Also, because 8-OHdG is excreted in the urine, it can be used as a non-

invasive assay for determining the levels of in vivo oxidative lesions in the early development various diseases, such as cancer, diabetes, atherosclerosis and neurological disorders [40]. Here, we focus on the development of a sensitive assay to monitor 8-OHdG in AD urine sample. This method has a great potential to serve as a platform to evaluate the effect of AD therapy. Overall, my research has been focused on three projects, which are (1) the study of glutathione redox status, (2) the prediction of S-glutahtionylated protein profile, and (3) the detection of damaged DNA.



## CHAPTER 2

### METHODS

#### 2.1 General Methods

##### 2.1.1 Transgenic Mice and Genotyping

AD-Tg mice [B6.Cg-Tg (APP<sup>swe</sup>, PSEN1<sup>dE9</sup>) 85Dbo/J, stock no. 005864, Bar Harbor, ME] were purchased from Jackson Laboratory. Real time polymerase chain reaction (qPCR) and melting curve analysis (HRM) were used for genotyping of the AD-Tg mice. The primer sets for the *APP* transgenic gene are (forward 5'-GAC TGA CCA CTC GAC CAG GTT CTG-3', reverse 5'-CTT GTA AGT TGG ATT CTC ATA TCC G-3') [41]. Primer sets for the *PSI* mutant gene are (forward 5'-AAT AGA GAA CGG CAG GAG CA-3', reverse 5'-GCC ATG AGG GCA CTA ATC AT-3') as shown in Table 1. DNA was extracted by immersing a mouse tail snip in 25 mM NaOH/0.2 mM EDTA at 98° C for 1 hour. The extracted DNA samples were mixed with 40 mM Tris-HCl (pH 5.5) and centrifuged at 4,000 rpm for 3 min. The sequence of APP gene was amplified by quantitative PCR and then analyzed by melting curve analysis using a LC 32 Scanner (Idaho Technology, Utah). The melting temperature of the App gene is 86.0 ± 0.6° C.

Table 1: The sequence of oligomers.

Oligos	Sequence	Use
APP forward	5'-GAC TGA CCA CTC GAC CAG GTT CTG-3'	PCR
APP reverse	5'-CTT GTA AGT TGG ATT CTC ATA TCC G-3'	PCR

### 2.1.2 Cell Culture

The human colon epithelial cell line HT-29 was used as a proof of principle in this method and was grown in McCoy's medium supplemented with 10% fetal bovine serum, penicillin (100 units/ml), streptomycin (100 units/ml), and incubated in 5% CO<sub>2</sub> at 37° C [42]. For the menadione (MQ)-mediated oxidative stress treatment, cells were treated with 200 μM MQ for 30 min in serum-free DMEM (Dulbecco's Modified Eagle's medium) [43]. After gentle rinsing, scraping cells into cold phosphate-buffered saline (PBS) with a scraper and then centrifugation (radius of rotor = 10 cm) at 112×g, cell pellets were harvested and immediately frozen in liquid nitrogen. For cell lysis, cells were sonicated in 250 μL 1X PBS with 2% SDS for 20 min at 4° C [44]. The same procedures were applied to untreated HT-29 cells.

### 2.1.3 Sample Preparation

In this initial study, whole blood samples and brain tissue were isolated from one pair of 5-month AD-Tg/wild type (WT) mice. The mice were anesthetized using sodium pentobarbital (60 mg/kg) through an *intraperitoneal* injection and perfused transcardially with ice-cold saline. The brains were rapidly removed and dissected on ice to harvest three brain regions including the cerebrum, the cerebellum and the hippocampus. The sample was rinsed with ice cold PBS and stored in -80° C for further study. After homogenization of the brain tissues, proteins from each preparation was precipitated in

5% trichloroacetic acid (TCA) at 4° C for 15 min, and centrifuged at 10,000×g for 5 min. The protein pellets were kept and then dissolved in PBS solution with 5% SDS at pH 8 [45, 46]. All procedures for the handling of mice were approved by the Institutional Animal Care and Use Committee at Louisiana Tech University.

#### 2.1.4 Protein Concentration Measurement

The BCA assay kit was used to measure the protein concentration according to the manufacturer's protocol. The absorbance of the protein samples at 562 nm was determined by a NanoDrop 2000/2000c Spectrophotometer.

#### 2.1.5 Data Analysis

Igor Pro software (Wavemetrics, Lake Oswego, OR) was utilized to analyze data and electrophorograms, including migration time and peak area for each individual sample. To generate a calibration curve of *S*-glutathionyls, *in vitro* *S*-glutathionylated bovine serum albumin (BSA-SSG) was used for plotting *S*-glutathionyls amounts with respect to fluorescence peak area. Therefore, amounts of Pr-SSG from HT-29 cells and brain tissue and whole blood of AD-Tg/W mice were calculated based on this curve. Statistical analysis between groups was done by one-way ANOVA. A value of  $P < 0.05$  was accepted as significant. All values are expressed as mean  $\pm$  SEM;  $n=5$  for each group.

## 2.2 High Performance Liquid Chromatography

### 2.2.1 Measurement of GSH and GSSG

The levels of GSH and GSSG in brain homogenates and blood samples of AD-Tg/WT mice at 3 stages were measured using HPLC [43] after TCA precipitation. Acid-soluble GSH and GSSG were derivatized as follows. GSH was first reacted with 80 mM

iodoacetic acid (IAA), a thiol alkylating agent to form the S-carboxymethyl derivatives of free thiols [47]. Then 6% 1-fluoro-2, 4-dinitrobenzene (FDNB) was added to react with free amine groups to form 2, 4-dinitrophenyl derivatives [48]. The chromatograph of GSH and GSSG derivatives was performed on a 250 mm × 4.6 mm Alltech Lichrosorb NH<sub>2</sub> 10- $\mu$ m column using a Shimadzu HPLC system. GSH and GSSG contents were expressed as nanomole per milligram protein, which allowed the calculation of the glutathione redox ratio (GSH/GSSG).

### 2.2.2 Pr-SSG Determination

Pr-SSG was determined using a modified Ellman's assay. After TCA precipitation and centrifugation at 10,000×g for 5 min, the protein pellets were obtained and then dissolved in 1X PBS solution with 5% SDS at pH 8 [45]. After the protein pellets completely dissolved, the samples were split into two sets. Set I was pretreated with 40  $\mu$ l immobilized TCEP gel to reduce all disulfides in Pr-SSG to protein thiols (Pr-SH) at 37° C for 30 min with occasional shaking. Set I (containing reduced Pr-SH and native Pr-SH) and Set II (containing only native Pr-SH) were incubated at room temperature for 15 min with 70  $\mu$ l phosphate buffer (1.5 mM KH<sub>2</sub>PO<sub>4</sub>, 6.36 mM K<sub>2</sub>HPO<sub>4</sub>, 1.57 mM EDTA) containing 3.95 mM DTNB. Total Pr-SH (Set I) and native Pr-SH (Set II) were determined spectro-photometrically at 412 nm [49]. The concentration of disulfides in Pr-SSG (nmol disulfides/mg of protein) was expressed as half of the thiols determined from the difference between Set II and Set I [50]. The quantity of mixed-disulfide is overestimated because other cysteine modifications such as S-nitrosylation and S-sulfenation also occur and are reduced by TCEP in sample preparation from Set I group. However, this overestimation is minimal and negligible

since mixed-disulfide (Pr-SSG) is much more predominant with nearly 1000 fold higher expression than endogenously low abundant nitrosylated proteins (1-200 picomole/mg protein) [51-53].

### 2.2.3 Determination of Enzymatic Activity

Glutathione reductase (GR) and glutathione peroxidase (GPx) activities (nmol/min/ml) were determined using commercial GR and GPx assay kits from Cayman Chemical Company. In total, the brain tissues from three pairs of mice at each three stages (1-, 5- and 24-month old) were analyzed and the sample preparations were followed according to the manufacture protocol.

## 2.3 Capillary Electrophoresis

### 2.3.1 *In Vitro S*-glutathionylation of BSA

Five mg/ml BSA solution was obtained by dissolving BSA in 50 mM Tris/1 mM EDTA with 0.1% SDS at pH 7.5, and mixed with 5 mM DTT at 37° C for 1 hour [54]. Because native BSA has few free thiol groups, DTT was used to reduce exposed disulfides from denatured BSA after treating with 0.1% SDS [55]. DTT was then removed by using spin columns before subjecting BSA to 2.5 mM diamide at 37° C for 30 min to generate *S*-glutathionylation *in vitro* [54, 55]. After desalting using spin columns to remove diamide, final concentration of *in vitro S*-glutathionylated BSA was 5 mg/ml.

### 2.3.2 *S*-glutathionyl Level Determination

The *S*-glutathionyl level in BSA-SSG was determined using modified Ellman's assay [46, 56]. After neutralizing the BSA-SSG to pH 8, the samples were split into two sets (40 µl of 5 mg/ml *S*-glutathionylated BSA each). Set I was pretreated with 40 µl

immobilized TCEP gel to reduce all disulfides into thiols at 37° C for 30 min with occasional shaking. Hence, Set I contains total thiols of Pr-SH (reduced Pr-SH and native Pr-SH), whereas Set II contains only native Pr-SH. Both sets were incubated with 70  $\mu$ l phosphate buffer (1.5 mM KH<sub>2</sub>PO<sub>4</sub>, 6.36 mM K<sub>2</sub>HPO<sub>4</sub>, 1.57 mM EDTA) that contains 3.95 mM DTNB at room temperature for 15 min. Total Pr-SH and native Pr-SH were subsequently determined spectrometrically at 412 nm from Sets I and II, respectively [49]. Hence, the concentration of *S*-glutathionyls in BSA-SSG (nmol glutathionyls/mg of BSA) was quantified and determined as half of the thiols difference between Set II and Set I.

### 2.3.3 Pr-SSG Derivatization and Detection

This procedure comprises of blocking the native thiols using N-ethylmaleimide (NEM), the deglutathionylation of SSG into free sulfhydryl (-SH) group followed with fluorescence labeling of the newly formed SH group by Dylight 488 maleimide (as shown in Figure 3a). The derivatized samples were then separated using size-based capillary gel electrophoresis with laser induced fluorescence (CE-LIF) detector. The deglutathionylation assay (depicted in Figure 3b) is based on the precise enzymatic recycling reaction using Grx-3, and includes the following three steps [57, 58]: (1) Specific reduction of Pr-SSG by Grx-3 to generate newly formed Pr-SH, (2) The tripeptide, GSH from Grx-SSG intermediate is transferred to GSH to generate GSSG, and (3) Glutathione reductase (GR) reduces GSSG with the presence of NADPH.

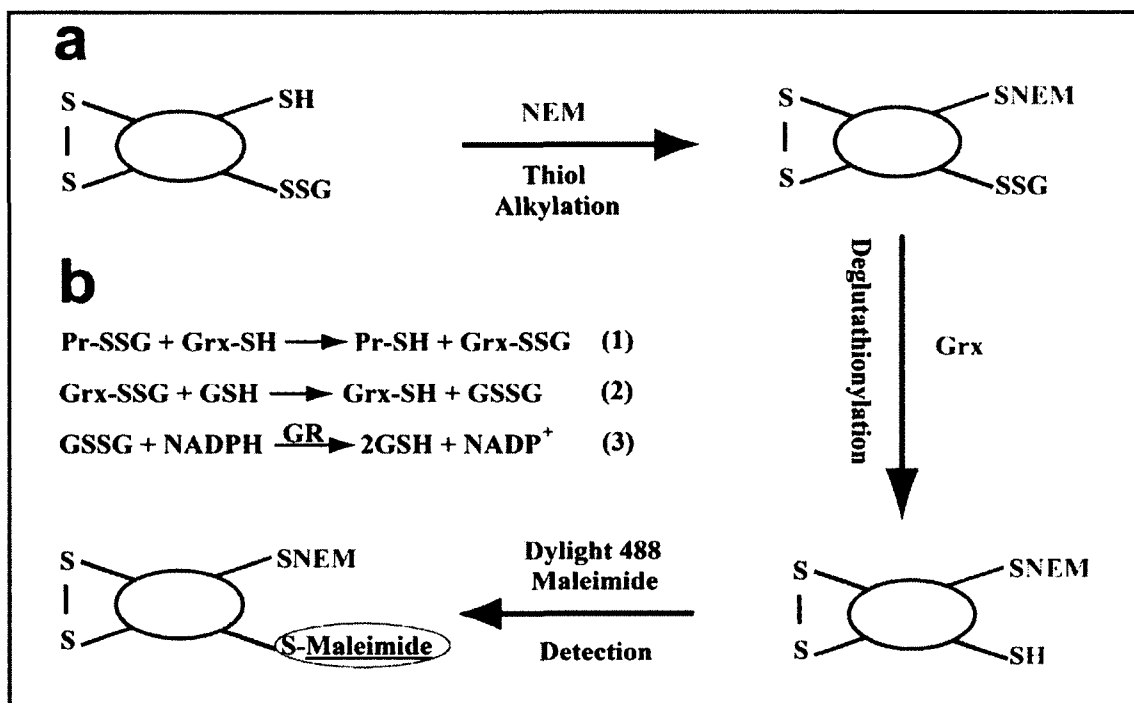


Figure 3: Mechanism of deglutathionylation and detection of *S*-glutathionylated proteins (Pr-SSG). (a) Schematic representation of the method to detect Pr-SSG by labeling with Dylight 488 maleimide. (b) Deglutathionylation assay is divided by 3 steps. (1) The Pr-SSG is reduced by glutaredoxin (Grx). (2) The oxidized Grx (Grx-SSG) intermediate is transferred to glutathione (GSH). (3) Glutathione reductase (GR) reduces oxidized glutathione (GSSG) with presence of nicotinamide adenine dinucleotide phosphate (NADPH).

Briefly, for alkylation of free thiol groups, a 20  $\mu\text{l}$  protein sample of each preparation (*in vitro* BSA-SSG, MQ induced HT-29 cells, brain tissues and whole blood from AD mouse model) was incubated in 40 mM NEM and 25 mM HEPES, 0.2 mM EDTA, 0.01 mM neocuproine and 2.5% SDS at pH 7.7 for 30 min at 4° C [44, 54]. The excess NEM was removed by extensive wash (6 washes) with spin columns (molecular weight cut-off 3 kDa). The washing solvent was PBS at pH 7.4 and each wash involved centrifugation at 4000 $\times$ g for 20 min. For deglutathionylation, the blocked Pr-SSG sample was subsequently incubated with 2.5  $\mu\text{g/ml}$  Grx-3, 4 U/ml GSSG reductase, 1 mM GSH, 1 mM NADPH for 50 min at 37° C [58]. The excess GSH and NADPH were removed by

using spin columns again. Last, for the labeling of newly generated free thiols, 2  $\mu$ l of 12.5 mM Dylight 488 maleimide was used and vortex mixed overnight. The excess dye was later removed by spin columns with obtaining a final volume of the protein sample of 100  $\mu$ l.

#### 2.3.4 Validation of the Developed Method

Various controls were performed to validate the selectivity of *S*-glutathionyl labeling of the method. These controls included: (a) 1.25  $\mu$ M Dylight 488 maleimide dye alone; (b) BSA-SSG without Grx-3 catalyzed deglutathionylation step; (c) BSA-SSG pretreated with 5 mM DTT to reduce the protein bound disulfides; (d) native BSA without *S*-glutathionylation; and (e) MQ treated HT-29 cells without Grx-3 reduction.

Additionally, we investigated (i) desalting efficiency of NEM and (ii) NEM alkylating efficiency. Excess blocking reagent needs to be removed before deglutathionylation to avoid alkylation of freshly reduced disulfides, which could cause underestimation of Pr-SSG. On the other hand, incomplete NEM blocking of free thiols will result in false artifacts of Pr-SSG signals.

#### 2.3.5 CE Instrument

CE with LIF has been considered as a highly efficient, sensitive and fast analytical separation technique for the analysis of low abundance of proteins. A commercial capillary electrophoresis instrument, Beckman Coulter P/ACE MDQ system (Fullerton, CA) was used for the analysis of modified protein or damaged DNA. For excitation, the LIF detector used an argon-ion laser (488 nm line, 3 MW) that was directed to a detector window in the capillary using a fiber optic [59]. A 520DF20 bandpass filter (~510-530 nm) was used to select the Dylight 488 fluorescence emission



before the photo-multiplier tube (PMT). The PMT output signals were sampled at 4 Hz. Separation was carried out using a 30.8-cm-long, 50- $\mu\text{m}$ -i.d., 361- $\mu\text{m}$ -o.d. fused-silica capillary. UltraTrol LN, a class of linear polyacrylamide made of *N*-substituted acrylamide copolymers, was used for pre-coating the capillary walls to decrease the electroosmotic flow (EOF) and inhibit protein binding to the capillary wall [60]. The sample was injected hydrodynamically at 11 kPa for 4 seconds into the capillary containing the sieving matrix buffer, which consisted of 15% dextran (64-76 kDa), 0.5% SDS, 20 mM Tris and 20 mM Tricine. Separation was performed at -570 V/cm. The capillary was reconditioned between consecutive runs with sequential pressure-driven flushes (20 psi) of 0.5 M sodium hydroxide for 5 min, H<sub>2</sub>O for 3 min, the dynamic coating reagent UltraTrol LN for 2 min, the separation buffer for 2 min, and the sieving matrix buffer for 4 min. The separation buffer consisted of 20 mM Tris, 20 mM Tricine and 0.5% SDS at pH 8.

#### 2.3.6 Mw Determination

Five protein standards, including trypsin inhibitor, GAPDH, albumin from chicken egg white, BSA, BGG with different molecular mass ranging from 20 to 140 kDa, were measured using CGE-LIF. To transform the migration time into protein molecular weight (*M<sub>w</sub>*), the standard curve between the logarithm of the protein's size and electrophoretic mobility was calculated. The relationship is shown in Figure 4.

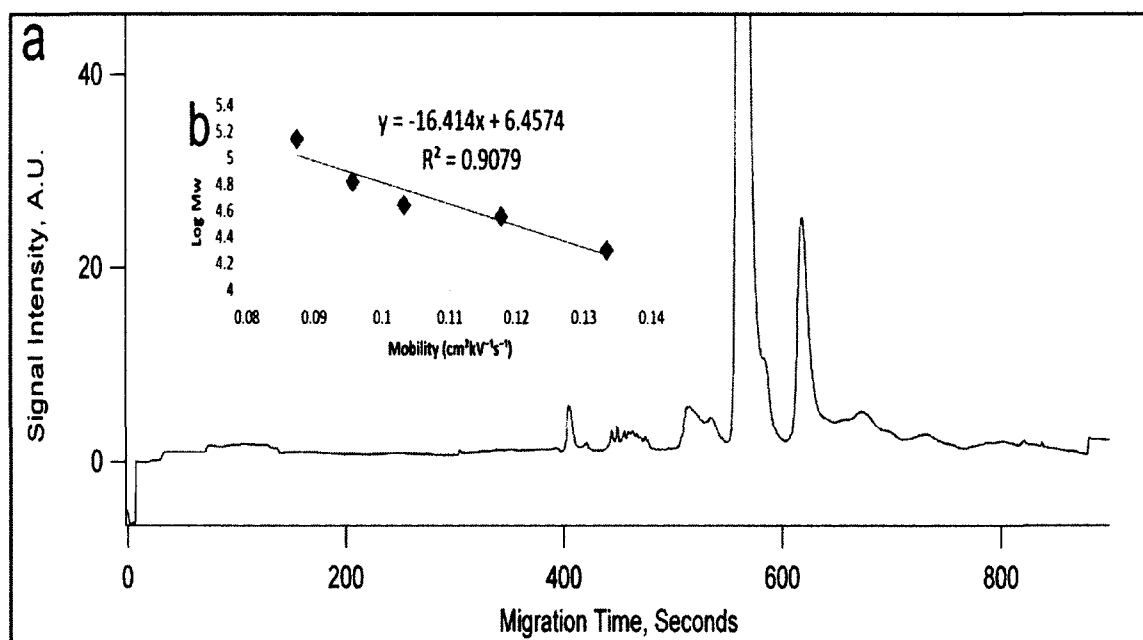


Figure 4: Transformation of migration time (a) to molecular weight (Mw) value. (b) Log of molecular mass of standard proteins as a function of their electrophoretic mobility.

### 2.3.7 Urine Collection and Labeling

Urine samples were collected from male, 11-month-old, AD transgenic mice. After collection, the samples were centrifuged for 10 min at 4000 rpm and the supernatants were collected and stored at  $-20^{\circ}\text{C}$  for further analysis. In order to detect 8-OHdG in the AD mice urine samples, a 20  $\mu\text{L}$  urine sample was incubated with 20  $\mu\text{L}$  mix of the primary (40  $\text{ng}\cdot\mu\text{L}^{-1}$ ) and 10  $\mu\text{L}$  secondary antibody (40  $\text{ng}\cdot\mu\text{L}^{-1}$ ) for 1h on orbital shaker, 500 rpm, at room temperature.

### 2.3.8 Labeling of Test Model

A DNA oxidative stress model, 8-OHdG was used to test the labeling scheme and validate the LIF detector response. 8-OHdG (1 mg) was suspended in 50  $\mu\text{L}$  DMSO and 9950  $\mu\text{L}$  of water to reach a final concentration of 100  $\text{ng}\cdot\mu\text{L}^{-1}$  (or 353  $\mu\text{M}$ ). Anti-8-OHdG and the secondary Alexa 488 antibody were diluted in water. To generate the calibration curve, five 8-OHdG standards with final concentrations of 10, 8, 6, 4, and 2

$\text{ng}\cdot\mu\text{L}^{-1}$  were prepared. Twenty  $\mu\text{L}$  of 8-OHdG standard, 20  $\mu\text{L}$  of primary antibody (40  $\text{ng}\cdot\mu\text{L}^{-1}$ ), and 10  $\mu\text{L}$  of secondary antibody (40  $\text{ng}\cdot\mu\text{L}^{-1}$ ) complex were mixed. 8-OHdG was incubated on the orbital shaker with anti-8-OHdG antibody at room temperature at 500 rpm for 1h. The secondary antibody was added to the mix and the sample was incubated for another hour on an orbital shaker at 500 rpm. Five 8-OHdG standard complexes were injected in the CE-LIF instrument to generate the standard curve and further estimate the limit of detection.

### 2.3.9 Separation Condition

Sodium Tetraborate buffer (pH 9.5) was used as the carrier electrolyte for all determinations. Samples were injected into the capillary containing the separation buffer using hydrodynamic injection mode at a pressure of 0.5 psi with 5 sec injection time. The separations were performed at 400 V/cm. Measurements were carried out at constant temperature, 25° C. The capillaries were preconditioned using methanol for 5 min, followed by 1M NaOH for 10 min, 1M HCl for 10 min, water for 10 min, and sodium tetraborate buffer for 10 min. After each run the capillaries were washed with 1M NaOH for 5 min, followed by water for 2 min and sodium tetraborate buffer for 3 min.

## 2.4 Principle Component Analysis

### 2.4.1 Principle Component Analysis

PCA was then applied to the Pr-SSG profiling spectrum data to extract the reduced feature set. The molecular weights of the Pr-SSG were predicted after PCA. Based on the distribution of the electropherographical data projected onto the PCs, K-means clustering technique [61] and probability for Gaussian distribution [62, 63] were

applied to classify the age and genotype of the samples from the complex *S*-glutathionyl profiles. A block diagram summary of the overall procedure is illustrated in Figure 5.

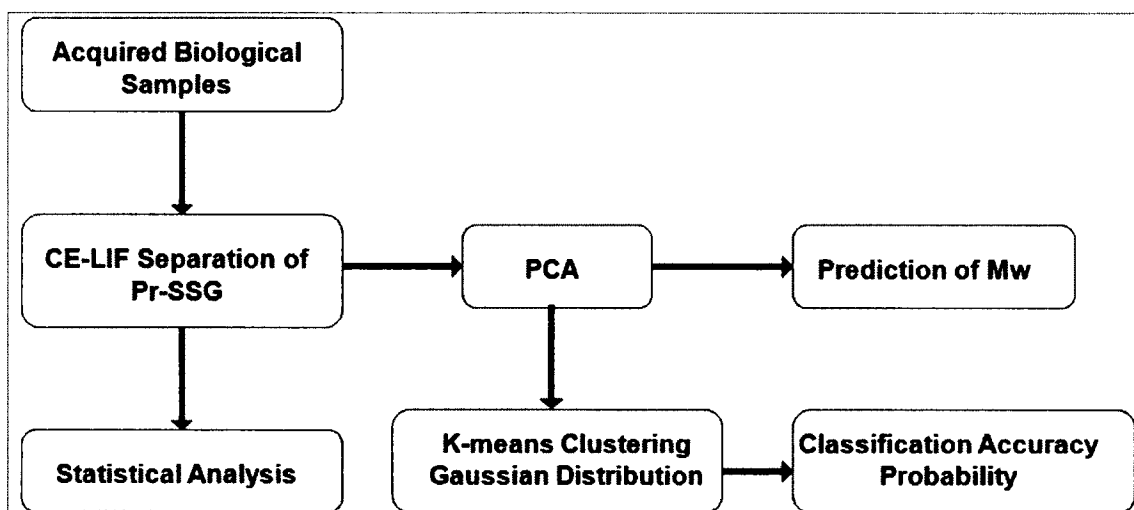


Figure 5: A schematic block diagram describing overall experimental procedure.

The Statistical Pattern Recognition Toolbox (STPRtool) in Matlab was used in this study [62]. The electrophoretic data was transformed into a set of uncorrelated PCs. These PCs were ranked according to each of their contributions based on the data variance; data complexity was then reduced by eliminating redundant, orthogonal, and independent PCs. The electrophoretic data from six groups (consisting of different genotype and age) contain many features that are difficult to directly visualize and capture. So, to classify the data samples into one of the six groups based on their electrophoretic profiles, PCA was used to project the data onto PCs with large data variances. The variance in each component is easily calculated by corresponded eigenvalues divided by total eigenvalues. PCA score was used to inform us of the cumulative variance of the data. Up to 80.10% of the total variance within the data can be accounted for using three PCs. Every electropherogram has 3600 data points which are

migration time points with their corresponding fluorescence intensity values and each data point was treated as an independent variable. A PC was considered significant when the contribution to total variances was greater than 1%. Each sample was analyzed in triplicate and averaged to have the result in a single average electropherogram for the individual sample. If the Mahalanobis distance of samples from the center of the score plot was greater than the threshold, it was tagged as an outlier and eliminated from the data set.

#### 2.4.2 K-means Clustering Algorithm

K-means clustering algorithm [61, 62] was used to partition the data set in clusters based on the genotype and age. A 5-fold cross-validation procedure [64] was used to evaluate different classification tasks. Eighty percent (80%) of the data for each study was randomly chosen to be the training set. The mean value of the training data set belonging to the same group was computed in the three dimensional PC feature space. The remaining 20% of the data was assigned to be the testing set. Each data point in the testing set was assigned to the nearest known cluster. The classification accuracy was defined to be the percentage of correctly identified testing data point. The data randomization, clustering, and testing procedure were repeated five times. Overall, twelve classifiers were created (six using blood, and six using brain Pr-SSG data) as outlined: (a) 3 – Genotype classifiers, one at the each age (1-month WT vs. Tg; 5-month WT vs. Tg; 11-month WT vs. Tg). (b) 2 – Age classifiers, one for each genotype (WT: 1-month vs. 5-month vs. 11-month; Tg: 1-month vs. 5-month vs. 11-month). (c) 1 – Combination genotype and age classifier (1-month WT vs. 1-month Tg vs. 5-month WT vs. 5-month TG vs. 11-month WT vs. 11-month Tg).

### 2.4.3 Probability of Gaussian Distribution

A Leave-One-Out cross-validation method [65] was used to test the probability of membership of each data point to each genotype and age. A multivariate Gaussian probability density function was used,

$$N(x|\mu, \Sigma) = \frac{1}{(2\pi)^{D/2}} \frac{1}{|\Sigma|^{1/2}} \exp\left\{-\frac{1}{2}(x - \mu)^T \Sigma^{-1}(x - \mu)\right\} \quad \text{Eq. 1}$$

where  $x$  indicates each data point vector,  $\mu$  represents the mean vector, and  $\Sigma$  is the covariance matrix (a positive-definite and symmetric matrix). The output vector is the probability density function between Gaussians. The probability of membership for the each point  $x$  was obtained by adding the six probabilities (from the six groups) and normalizing it to give a sum of 1. The probability of membership represents the probability that the data point belongs to one of the Gaussians [62, 63]. The whole procedure was repeated for brain tissues and blood samples.

## CHAPTER 3

### RESULTS

#### 3.1 Glutathione Redox Status

##### 3.1.1 Genotyping

Melting analysis of the PCR products generated with DNA from Tg showed a decrease in the fluorescence of the double stranded DNA LCGreen dye (Data not shown). When the melting curves were converted to melting peaks by plotting (-dF/dT vs. T), a melting peak was observed with apparent  $T_m$  of  $86.26 \pm 0.6^\circ \text{C}$ , which is the  $T_m$  specific for *APP* gene. Since no *APP* transgenic genes existed in WT individuals, no *APP* gene was amplified and gave rise to a flat melting curve with no fluorescence intensity. Moreover, no single melting peak was observed in the converted -dF/dT vs. T plot. Hence, this assay could easily distinguish AD transgenic mice from WT individuals.

##### 3.1.2 Brain Weight

The wet weight of all mouse brain samples of each anatomic position (cerebrum, cerebellum and hippocampus) in AD-Tg/WT mice at 3 age stages were measured before tissue homogenization. The overall mean brain weights were  $0.52 \pm 0.02$  and  $0.51 \pm 0.02$  g,  $0.50 \pm 0.01$  and  $0.56 \pm 0.01$  g,  $0.49 \pm 0.03$  and  $0.41 \pm 0.01$  g for Tg and WT mice at 1-, 3-, and 11-month-old, respectively. One-way ANOVA for total brain weights of wild type mice showed a significant age effect ( $P < 0.005$ ). Compared to the 5-month-old,

total brain weight of WT mice lost 7.64% at 11-month as indicated in Figure 6. Moreover, the total mouse brain weight exhibited genotype difference between Tg and WT for 5- and 11-month-old ( $P < 0.001$ ); higher brain weight was observed in WT at 5-month-old, whereas increased brain weight was shown in Tg at 11-month-old. Also, at 5-month-old, WT has significantly lower cerebrum weight than its Tg counterpart ( $P = 0.03$ ).

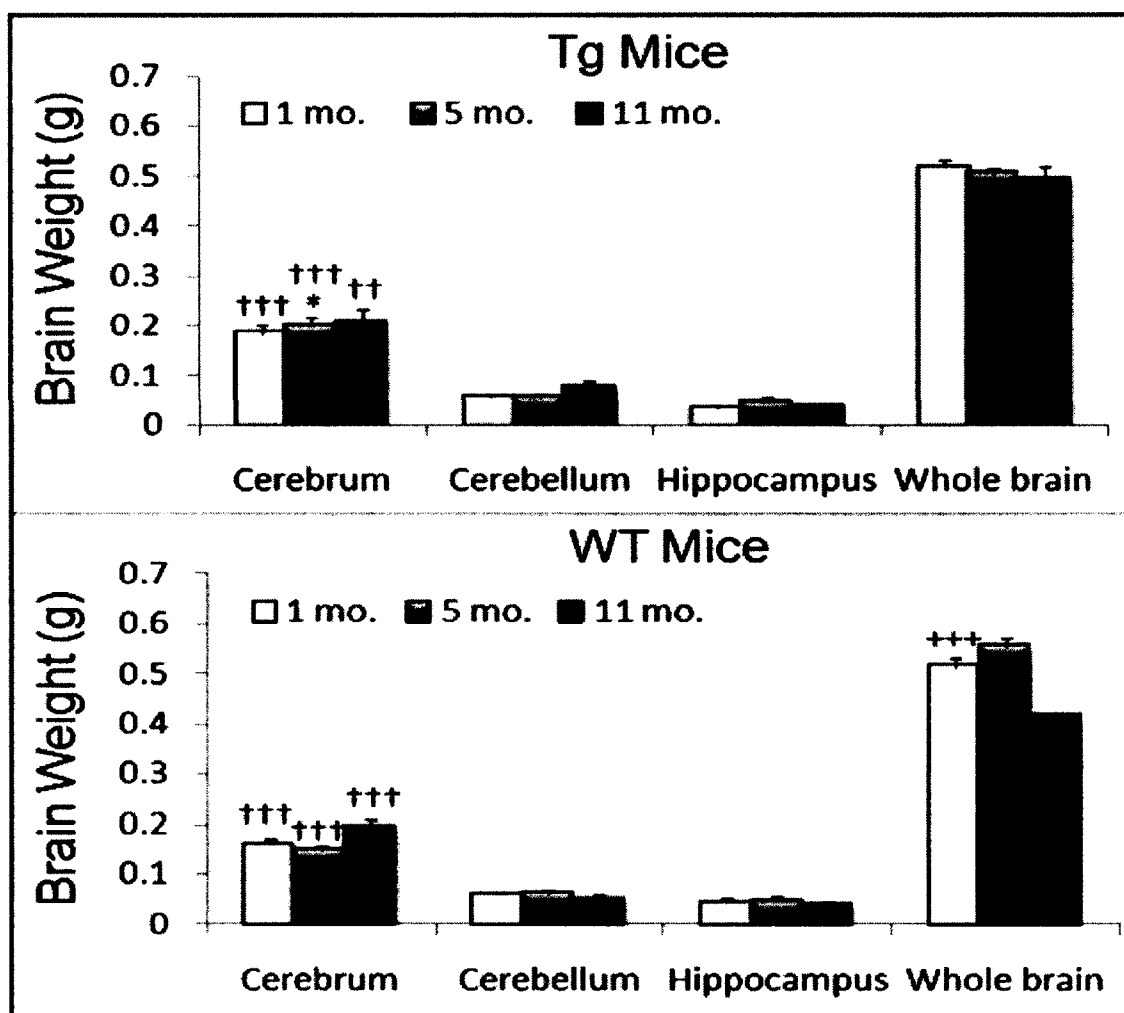


Figure 6: Comparison of wet brain weight in cerebrum, cerebellum, hippocampus, and total weight of AD-Tg/WT mice at 3 age stages. Data are presented as means  $\pm$  SEM for 30 animals. Age effect: 1-month vs. 5-month vs. 11-month. †††  $P < 0.001$ . Genotype effect: Tg vs. WT. \*  $P < 0.05$ . Tissue effect: hippocampus vs. cerebrum vs. cerebellum. ††  $P < 0.01$ , †††  $P < 0.001$ .



### 3.1.3 Tissue Glutathione Status

HPLC was used to measure the level of GSH and GSSG in three anatomic positions of brain tissue of AD-Tg/WT mice at 1-, 5- 11-month. The GSH/GSSG ratio was calculated from these quantitative measurements. The results are shown in Figure 7. The GSH content of AD-Tg mice in the cerebrum at 1-month was the highest, and the levels decreased 17% and 40% at 5-, and 11-month, respectively ( $P = 0.03$ ). On the contrary, age-matched wild type mice had significant increases in the GSH amount in cerebellum with age; 42% and 78% increases at 5-month and 11-month, respectively, with respect to 1-month-old mice ( $P = 0.03$ ).

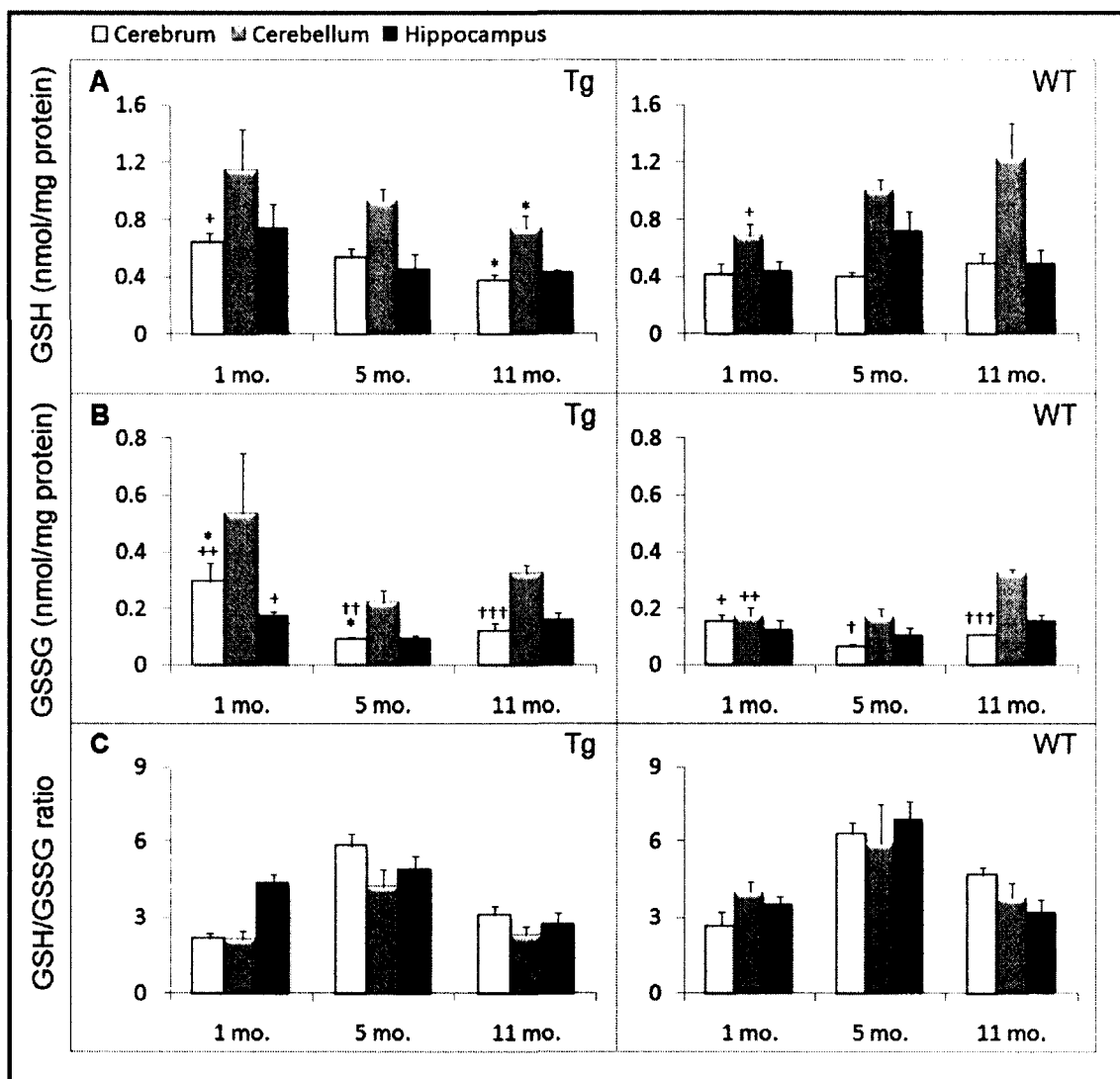


Figure 7: Glutathione (GSH) and oxidized glutathione (GSSG) levels and GSH/GSSG ratio in 1-, 5- and 11-month-old Tg and WT specific brain regions. Both (A) GSH and (B) GSSG levels were determined by reverse-phase high performance liquid chromatography (HPLC) following derivatization of samples with 1-fluoro-2, 4-dinitrobenzene (FDNB) as described in Methods; and (C) calculated GSH/GSSG ratio. GSH and GSSG are expressed as nmol/mg proteins and presented as means  $\pm$  SEM ( $n=5$ /group). Age effect: 1-month vs. 5-month vs. 11-month. +  $P < 0.05$ , ++  $P < 0.01$ . Genotype effect: Tg vs. WT. \*  $P < 0.05$ . Tissue effect: hippocampus vs. cerebrum vs. cerebellum. †  $P < 0.05$ , ††  $P < 0.01$ , †††  $P < 0.001$ .

As shown in Figure 7B, there was a significant decrease of 45% in GSSG production in hippocampus at 5-month-old Tg compared with 1-month-old young mice ( $P = 0.01$ ). However, a 69% increase in GSSG level from 5-month-old to 11-month-old

( $P = 0.01$ ) was observed. Similarly, in Tg cerebrum, a significant decrease of GSSG from 0.29 to 0.09 nmol/mg protein was observed from 1-month to 5-month-old, followed by a rise to 0.12 nmol/mg protein at 11-month-old ( $P = 0.009$ ). In particular, there was a decline of 46%, 45% and 39% of the GSH/GSSG ratio in the cerebrum, the cerebellum and the hippocampus, respectively, in aged transgenic animals at 11-month-old compared with the 5-month-old mice. Additionally, the aging effect on GSSG was observed in WT mice. Specifically, one-way ANOVA for GSSG level of WT type showed a 63% and 56% significant increase from 5-month-old to 11-month-old in the cerebrum ( $P = 0.02$ ) and in the cerebellum ( $P < 0.01$ ), respectively.

The results in Figure 7 further revealed significant genotype differences in the GSH redox status between Tg and WT mice. The Tg cerebrum exhibited a GSH value of 0.38 nmol/mg of protein, which is 20% less than its WT counterpart ( $P=0.03$ ). Also, GSH content was increased by 64% in 11-month-old WT mouse cerebellum than the Tg counterpart ( $P=0.04$ ). Genotypic differences in GSSG levels were evident in 1-month-old ( $P = 0.02$ ) and 5-month-old ( $P = 0.03$ ) cerebrum. Specifically, significant GSSG increases of 90% and 44% in Tg and WT were observed at these two stages.

In terms of brain regions, a significant difference in GSH content was observed for AD-Tg mice at 1-month-old. In young mice, the highest baseline level of GSH was seen in the cerebellum and the lower values in the hippocampus and cerebrum. This trend generally continued in aged mice. Regarding GSSG variation in different brain regions, the cerebrum exhibited decreases of 59% and 62% than cerebellum for 5-month Tg ( $P = 0.004$ ) and at 11-month Tg ( $P < 0.001$ ), respectively. For WT, significant decreases of

62% and 61% in GSSG in the cerebrum than in the cerebellum were observed for 5-month-old ( $P = 0.01$ ) and at 11-month-old ( $P < 0.001$ ), respectively.

One-way ANOVA for blood GSH level in Tg mice (Table 2) showed a significant increase of 1.6 fold in 11-month-old compared with 1-month-old ( $P < 0.005$ ). Moreover, significant age effect was observed in GSSG levels between 1-month and 11-month, with an increase of 37% with aging ( $P < 0.005$ ). Blood GSH level in Tg mice at 1-month is 50% less than its WT counterpart ( $P = 0.05$ ). It is notable that both GSH and GSSG levels in the blood were significantly higher than in brain tissues regardless of genotype. For example, basal GSH level in the blood of 11-month-old Tg, 8.39 nmol/mg protein (Table 2) was 20-fold higher than that in the hippocampus (0.47 nmol/mg protein) at the same age group (Figure 7A).

#### 3.1.4 Blood Glutathione Status

One-way ANOVA for blood GSH level in Tg mice (Table 2) showed a significant increase of 1.6 fold in 11-month-old compared with 1-month-old ( $P < 0.005$ ). Moreover, significant age effect was observed in GSSG levels between 1-month and 11-month, with an increase of 37% with aging ( $P < 0.005$ ). Blood GSH level in Tg mice at 1-month is 50% less than its WT counterpart ( $P = 0.05$ ). It is notable that both GSH and GSSG levels in the blood were significantly higher than in brain tissues regardless of genotype. For example, basal GSH level in the blood of 11-month-old Tg, 8.39 nmol/mg protein (Table 2) was 20-fold higher than that in the hippocampus (0.47 nmol/mg protein) at the same age group (Figure 7A).

Table 2: Blood glutathione status.

Blood	Tg			WT		
	1-mo. (n=5)	5-mo. (n=5)	11-mo. (n=5)	1-mo. (n=5)	5-mo. (n=5)	11-mo. (n=5)
GSH	3.19 ± 1.17 <sup>++*</sup>	8.27 ± 0.65	8.39 ± 1.07	6.24 ± 0.75	8.61 ± 0.85	9.08 ± 1.71
GSSG	7.01 ± 1.90 <sup>++*</sup>	15.99 ± 1.36	18.25 ± 2.35	12.40 ± 0.49	16.21 ± 2.55	18.75 ± 7.95
GSH/GSSG	0.45 ± 0.14	0.52 ± 0.03	0.46 ± 0.03	0.50 ± 0.04	0.53 ± 0.07	0.48 ± 0.04

GSH and GSSG levels are expressed in  $\mu\text{mol/ml}$  and presented as means  $\pm$  SEM with the number of mice per group indicated in parenthesis. Age effect: 1-month vs. 5-month vs. 11-month. ++  $P < 0.01$ . Genotype effect: Tg vs. WT. \*  $P < 0.05$ .

### 3.1.5 Mixed-disulfide Status

Next, we examined protein glutathione levels. Significant age differences were found in Pr-SSG contents at all 3 age stages in Tg-cerebrum ( $P = 0.03$ ), Tg-cerebellum ( $P = 0.04$ ), and Tg-blood ( $P = 0.04$ ) with increases of Pr-SSG levels from 1-month to 11-month-old (Figure 8). Also, 5-month-old animals exhibited significant decreases of 1.5- and 5.4- and 4.8-fold in Pr-SSG levels in these brain regions and blood, respectively, when compared with 1-month-old. Similar to what was observed in GSSG fluctuations with aging in Tg mice (see Figure 7B), we observed a dip in GSSG levels at 5-month-old rather than a steady increase in Pr-SSG with aging.

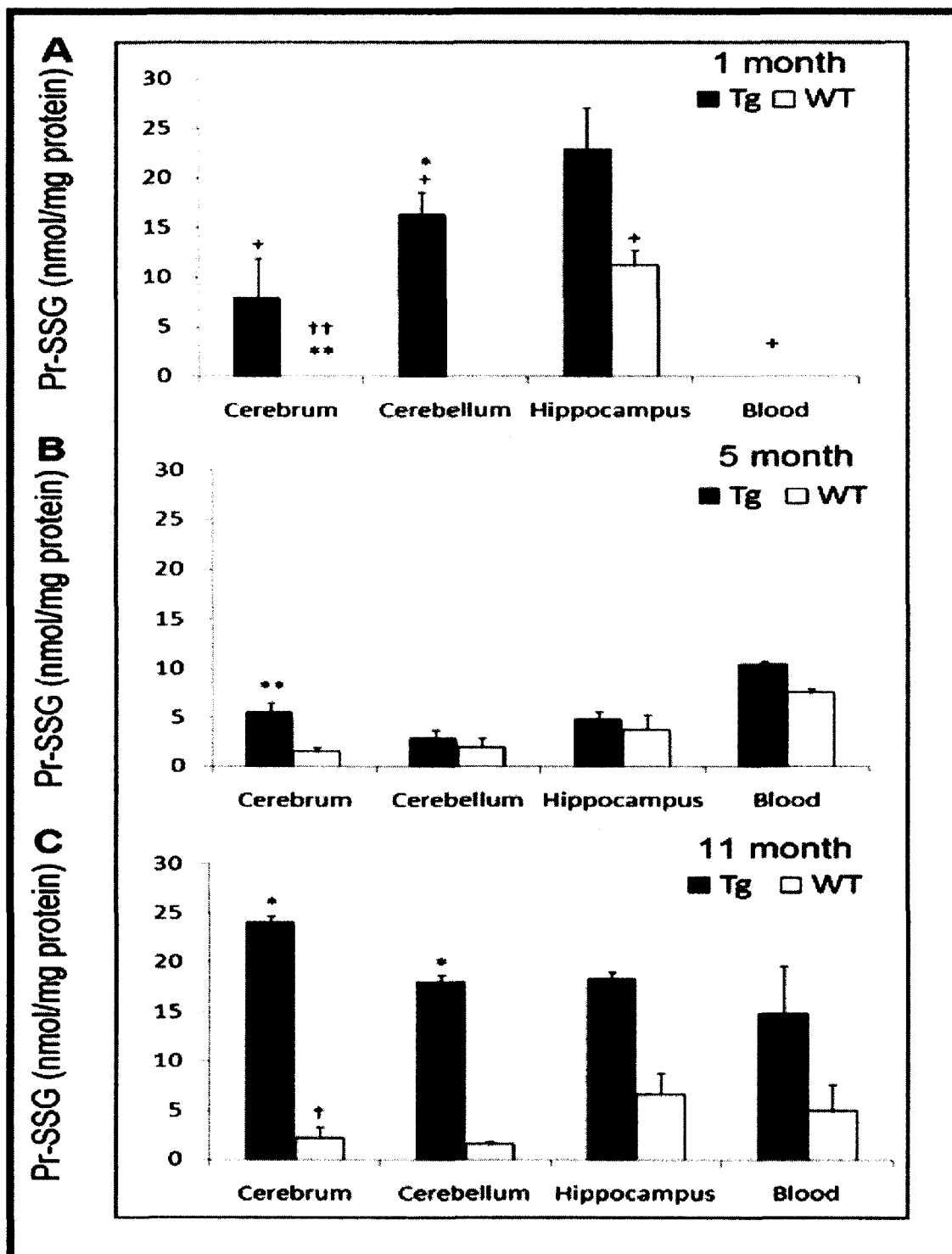


Figure 8: Levels of S-glutathionylated proteins (Pr-SGG) in specific brain regions in 1-, 5- and 11-month-old Tg and WT mice. Data are expressed as nmol/mg proteins and presented as means  $\pm$  SEM. Error bars do not appear in panel A, because samples cannot be detectable in cerebrum, cerebellum and blood of WT mice. Age effect: 1-month vs. 5-month vs. 11-month. +  $P < 0.05$ . Genotype effect: Tg vs. WT. \*  $P < 0.05$ , \*\*  $P < 0.01$ . Tissue effect: hippocampus vs. cerebrum vs. cerebellum. †  $P < 0.05$ , ††  $P < 0.01$ .

No Pr-SSG was detected at 1-month-old mice in WT brain tissues except in the hippocampus, whereas high Pr-SSG levels were found in Tg brain tissues at this early stage. As shown in Figure 8, the levels of Pr-SSG in Tg-cerebrum were 1.6- and 8-fold higher than its WT counterparts at 5-month ( $P=0.006$ ) and 11-month ( $P=0.01$ ), respectively. Additionally, the cerebellum showed a significant genotype effect at 1-month ( $P=0.03$ ) and 11-month ( $P=0.04$ ).

No significant tissue effect was seen in the different Tg brain regions, but differences between the hippocampus and other brain regions were observed in WT mice at 1-month ( $P=0.005$ ) and at 11-month ( $P=0.04$ ). As compared to WT-cerebrum and cerebellum, the hippocampus was the only region that started to show the detectable levels of Pr-SSG at 1-month-old. At 11-month-old, hippocampal Pr-SSG in WT was 27% higher than cerebellum. These findings support the notion that increased formation of Pr-SSG contributes to the specific vulnerability of the hippocampal zone of the AD brain.

### 3.1.6 Enzymatic Activity

Because of the observed changes in glutathione redox (Figures 7 and 8), we also examined the two key enzymes of the glutathione redox cycle: GPx converts GSH to GSSG in the presence of hydroperoxides, GR catalyzes the conversion of GSSG to GSH with a cofactor, NADPH. Statistical analysis of GR and GPx activities was done by one-way ANOVA shown in Figure 9. The results indicate no age or genotyping difference in GR activity. Also, no genotyping effect was observed in GPx. However, GPx activity shows significant increase in aging for both AD-Tg ( $P<0.001$ ) and WT mice ( $P=0.01$ ). In specific, comparing the two age stages (1-mo. v.s. 24-mo.), GPx activity increased from 24.7 to 43.5 nmol/min/ml in AD-Tg and from 26.1 to 43.5 nmol/min/ml in WT brain. The

relative higher increase in GPx activity compared to GR activity suggests that glutathione redox cycling might be compromised in the brain of older mice.

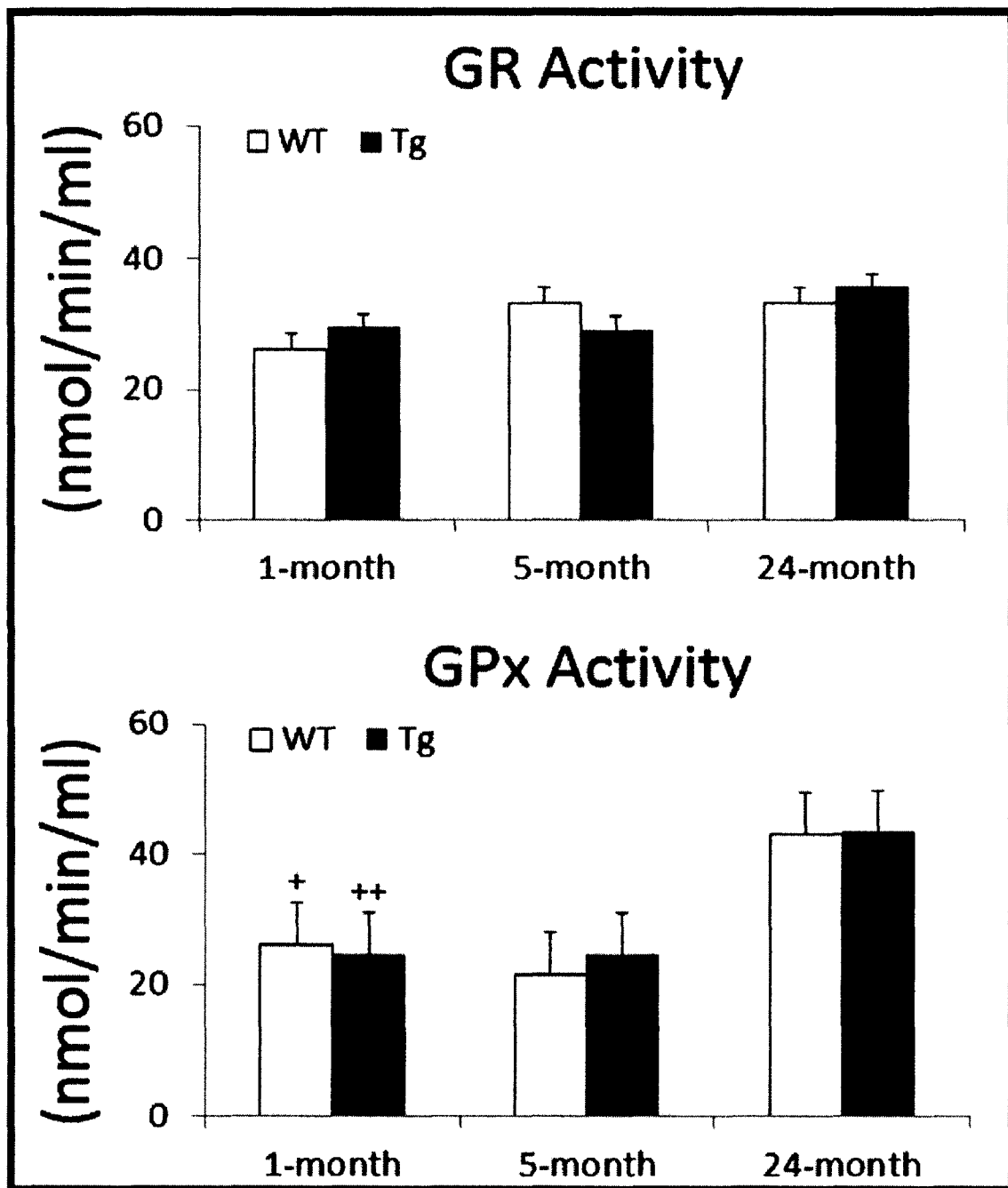


Figure 9: Activities of glutathione reductase (GR) and glutathione peroxidase (GPx) in AD-Tg/WT mouse brain at 1-, 5- and 24-month. Data are expressed as nmol/min/ml and presented as means  $\pm$  SEM. Age effect: 1-month vs. 5-month vs. 11-month. +  $P < 0.05$ , ++  $P < 0.01$ .



## 3.2 Oxidized Protein

### 3.2.1 Grx-catalyzed Deglutathionylation

Proteins were first heavily alkylated with NEM to block residual protein thiols and then subjected to deglutathionylation to generate newly formed free thiols. The ability to specifically identify and further reduce Pr-SSG is crucial for the selectivity of this derivatization method. Grx belongs to the thiol-disulfide oxidoreductase family [66]. Grx catalyze the reversible reduction of the Pr-SSG to free SH group through a monothiol mechanism by relying solely on the N-terminal Cys22 [57, 67, 68]. Cys 22 residue of Grx will become *S*-glutathionylated itself. The reduced form of Grx can then be regenerated using GSH coupled to GSSG reductase [68]. Since native Grx can recognize protein disulfides and reduce them also, it potentially produces false positive artifacts [69]. So we elected to utilize the mutant enzyme C14S, C65Y of glutaredoxin-3 (Grx-3) mainly due to its preference for the reduction of protein bound *S*-glutathiols [70]. The selectivity of this reductive treatment was also demonstrated in a Pr-SSG proteomic study [44]. It was noted by Mannervik that at least 0.5 mM GSH is required to ensure optimal activity of Grx [71]. We followed the optimal concentrations of all enzymes involved in deglutathionylation cycling [58].

### 3.2.2 Detection and Validation

In the present work we provide a novel approach for monitoring *S*-glutathionylated proteins based on the selective enzymatic recognition of Pr-SSG, fluorescent labeling and quantification by CGE-LIF analysis. To validate the analytical system, we chose to analyze *in vitro* oxidized BSA. As stated in the method section, various controls including (a) Dylight 488 maleimide dye alone; (b) BSA-SSG without

Grx-3 catalyzed deglutathionylation step; (c) BSA-SSG pretreated with DTT to reduce the protein bound disulfides; (d) native BSA without *S*-glutathionylation were performed to validate the detection of *S*-glutathionylation using this method.

Firstly, we studied the CGE-LIF analysis of the fluorescent dye, Dylight 488 maleimide. This analysis is to differentiate the peaks of dye itself from those of *S*-glutathionylated proteins and further identify how differently they distribute in terms of migration time. Trace 1 in Figure 10 demonstrated that the Dylight 488 maleimide alone shows multiple peaks occurring between 347 and 573 s, whereas *in vitro* *S*-glutathionylated BSA (trace 2 in Figure 10) exhibits a new additional peak appearing at 796 s, indicating the detection of *S*-glutathionols. Altogether, it validated the reactivity of Dylight 488 maleimide toward the disulfide group in the treated BSA.

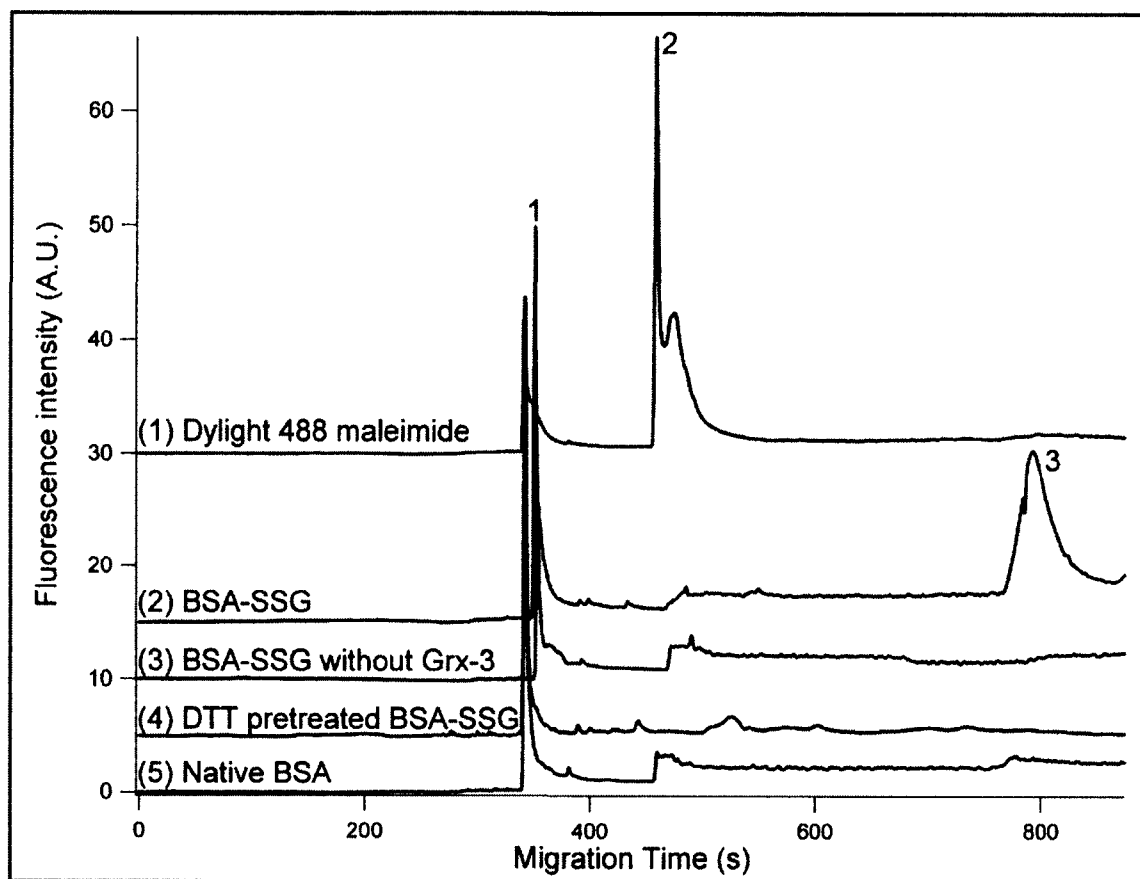


Figure 10: *In vitro* S-glutathionylated bovine serum albumin (BSA-SSG) and validation of the method using controls. (1) Electropherograms of Dylight 488 maleimide; (2) BSA-SSG; (3) BSA-SSG without glutaredoxin (Grx) reduction; (4) BSA-SSG pretreated with dithiothreitol (DTT); (5) native BSA. Hydrodynamic injection at pH 8 and 11 kpa for 4 s; separation in gel containing 15% dextran (64-76 kDa), 0.5% SDS, 20 mM Tris and 20 mM Tricine at -570 V/cm. 1 & 2 indicate Dylight 488 maleimide. Top trace is offset in the y-axis for the clarity.

Secondly, a control experiment was performed in the presence of all the derivatization steps except Grx deglutathionylation, and no peak at 796 sec for the BSA-SSG was observed (Trace 3 in Figure 10). Grx mediated deglutathionylation is essential to enzymatically reduce S-glutathionyls and further generate newly generated free thiols for consecutive labeling. Thus, the omission of the deglutathionylation step and no S-glutathionyl detection in this negative control further validates the requirement of the enzymatic cycling for the labeling reaction.

Furthermore, the selectivity of *S*-glutathionyls labeling was also exploited in native BSA and BSA-SSG pretreated with reducing agent, DTT. After the DTT treatment, the protein-bound *S*-glutathionyls was reduced and hence the consecutive labeling of *S*-glutathionyls was abolished. In native BSA, no *S*-glutathionyls are available for labeling. As we expected, in both controls, no peak around 796 s was observed in both traces 4 and 5 of Figure 10. All these observations further indicate the selectivity of this method.

Dylight 488 fluorophore tagged Pr-SSG will lead to an increase in molecular weight (Mw). The addition of NEM (124 Da), reduction of *S*-glutathionyls (-307 Da) and maleimide labeling (800 Da) will result in an increase of Mw of 617 Da. Proteomic study disclosed that the majority of identified *S*-glutathionylated proteins have Mw ranging from 25 to 70 kDa [44]. Therefore, the Mw shift of 617 Da is insignificant compared with the *S*-glutathionylated protein size itself, and this derivatization procedure will have little effect on the protein mobility in the CGE separation.

### 3.2.3 Evaluation of NEM Removal

After alkylating the free thiols, the NEM was removed using Amicon Amicon ultra-4 (Mw cutoff of 3000 Da) spin columns. If the removal were not complete, the remaining NEM will compete with Dylight 488 maleimide by reacting with freshly reduced thiols from *S*-glutathionyls. This would cause a decrease or no signals for the detection of *S*-glutathionylated proteins. Therefore, we investigated whether the levels of NEM removal were associated with the numbers of ultracentrifugation washes. Figure 11 displays a peak at approximately 796 s representing BSA-SSG after six washes with desalting column, whereas no peak detected for *S*-glutathionyl after only three washes.

This observation indicated that by doubling the desalting wash times, the excess NEM was completely removed, which eliminated its interference of binding reduced *S*-glutathionyls.

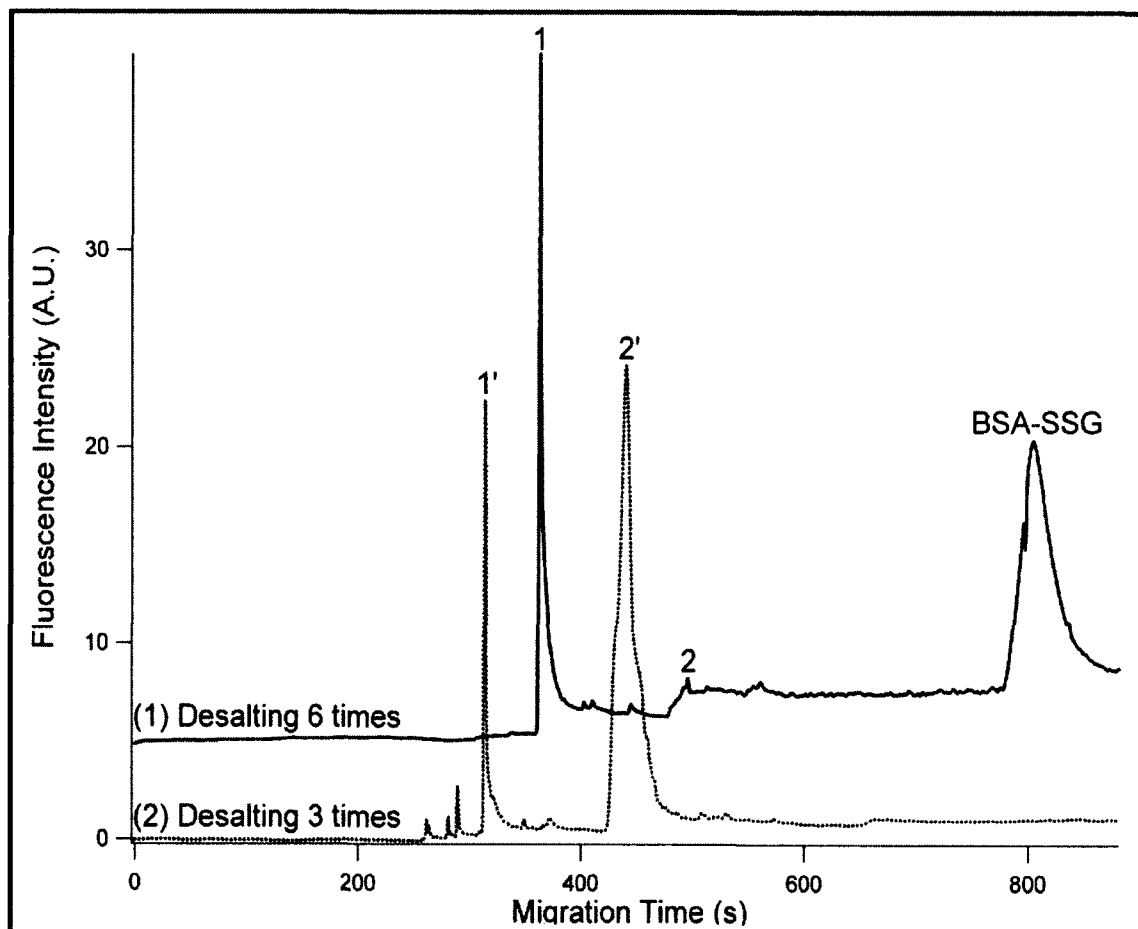


Figure 11: Comparison of desalting efficiency using spin columns at different times. Completely removing blocking reagents is crucial in this experiment. Remaining N-ethylmaleimide (NEM) can cause unnecessary blocking to freshly formed thiol groups. Double the desalting times will solve this problem. Top trace shows clear peaks for maleimide and *S*-glutathionylated bovine serum albumin (BSA-SSG) (1 and 2 indicate Dylight 488 maleimide using spin columns for 6 times). Bottom trace shows no peak for BSA-SSG (1' and 2' indicate Dylight 488 maleimide using spin columns for 3 times). All the experimental conditions are the same as in Figure 10. Top trace is offset in the y-axis for the clarity.

### 3.2.4 Assessment of Blocking Efficiency

The derivatization procedure only works when only *S*-glutathionylated cysteine residue will be derivatized and fluorescently labeled. If the free thiols were not completely blocked with NEM, then the remaining nonblocked cysteines would be labeled with Dylight 488 maleimide and produce a false artifact in the electropherogram. Hence, we studied the blocking efficiency using various concentrations (10, 30 and 40 mM) of two blocking reagents, NEM and IAA without deglutathionylation step. As seen in Figure 12, 40 mM of NEM was considered as the optimal concentration to completely block all the free thiols in BSA-SSG.

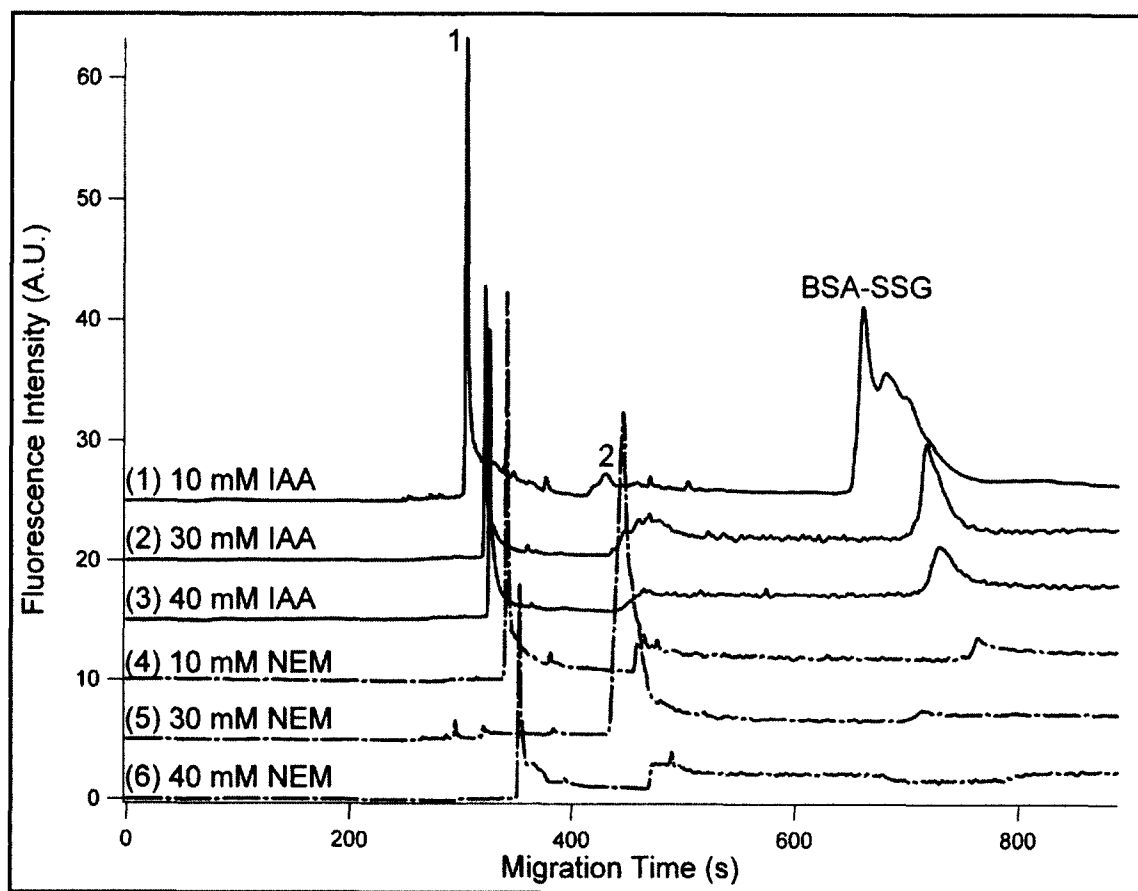


Figure 12: Comparison of blocking efficiency between Iodoacetic acid (IAA) and N-ethylmaleimide (NEM) at three concentration conditions. *S*-glutathionylated bovine serum albumin (BSA-SSG) samples were reacted with IAA and NEM, respectively. Top 3 traces indicate 10, 30 and 40 mM IAA with solid lines. Bottom 3 traces indicate 10, 30 and 40 mM NEM. 1 & 2 indicate Dylight 488 maleimide. All the experimental conditions are the same as in Figure 10. Top trace is offset in the y-axis for the clarity.

### 3.2.5 Assay Reproducibility and Accuracy

The concentration of *S*-glutathionyl groups in *S*-glutathionylated BSA was determined by Ellman's colorimetric assay, which was expressed as 92.41 nmol *S*-glutathionyl per 1 mg BSA protein. Therefore, the concentrations of a serial dilution (1-, 1.3-, 2-, 4-fold and 10-fold dilution) of BSA-SSG were calculated ranging from 92.41 to 9.24 nmol/mg protein. In Ellman's assay, immobilized TCEP was used because: (1) It allows recovering reduced BSA in high yield without dialyzing or desalting steps; (2) It

eliminates the possibility of the remaining TCEP reacting with Ellman's reagent, DTNB; (3) it does not interfere with consecutive thiols-reactive reagent, i.e. maleimide crosslinkers. The calibration curve was generated by separately injecting a serial dilution of *S*-glutathionylated BSA in triplicate onto CE (Figure 13). The integrated fluorescence peak area and corresponding *S*-glutathiol (in moles) are indicated as *y* and *x* in the calibration curve, respectively [72].

$$y = (5 \pm 0.12) \times 10^{15} x - (2.28 \pm 3); \quad R^2 = 0.996 \quad \text{Eq. 2}$$

LOD and LOQ are defined as the amount for which the S/N is 3 and 10, respectively. In this CGE-LIF study, the LOD and LOQ of *S*-glutathionyl groups assessed by Equation 2 were 1.8 and 6 attomole, respectively, which are the lowest LOD and LOQ reported to date.



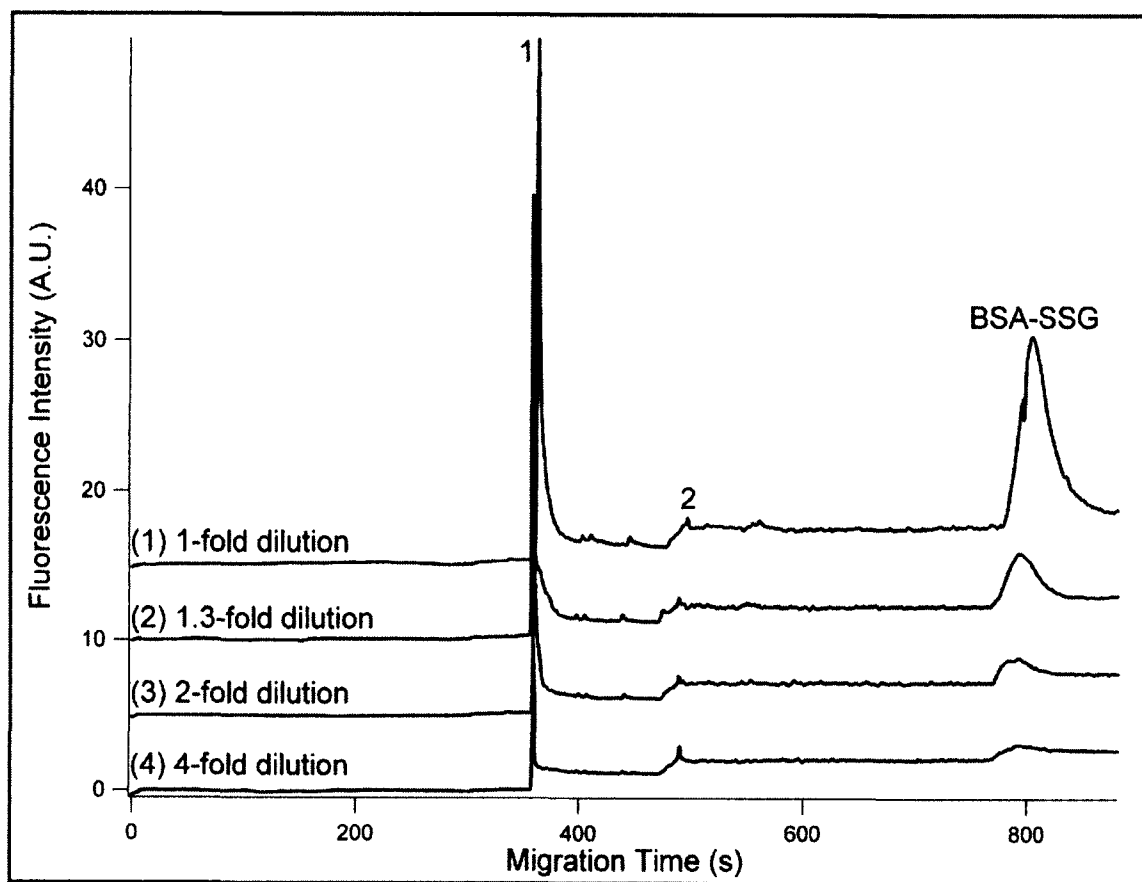


Figure 13: Electropherograms of a series of dilution (1-, 1.3-, 2-, 4-fold) of *S*-glutathionylated bovine serum albumin (BSA-SSG) labeled with Dylight 488 maleimide. 1 & 2: Dylight 488 maleimide. All the experimental conditions are the same as in Figure 10. Top trace is offset in the y-axis for the clarity.

The reproducibility of the method was determined by performing three replicate injections of the *in vitro* *S*-glutathionylated BSA solution. The RSD values for migration time and peak area were 2.0% and 0.5%, respectively, suggesting good reproducibility in the measurement of *S*-glutathionylation abundance in one sample. The precision of the method was determined by replicate injection of the test model, *in vitro* *S*-glutathionylated BSA on three consecutive days. The RSD values of migration time and peak area were 5.5% and 0.7%, respectively, for the day-to-day precision assay. The accuracy was determined by performing a standard spiking method, where known

amounts of *S*-glutathionylated BSA (BSA-SSG) standard was mixed with previously analyzed BSA-SSG and further detected by CGE-LIF method in triplicates. The concentration of BSA-SSG was subsequently quantified by the calibration curve. The percentage of the spiked BSA-SSG analyte recovered by the assay indicates that the accuracy of the method was 93.5%.

### 3.2.6 *S*-glutathionylation Determination

To illustrate the potential of this novel analytical method, we directly applied it to the analysis of MQ-induced *S*-glutathionylation. Figure 14a (traces 1 and 2) demonstrates wide peaks (738s - 1103s), indicating a broad range of proteins susceptible to *S*-glutathionylation in this oxidative stress cell model. A negative control carried by eliminating the Grx-catalyzed deglutathionylation (shown in trace 3 of Figure 14a) also highlighted the specificity of this derivatization method and the necessity of this reduction step.

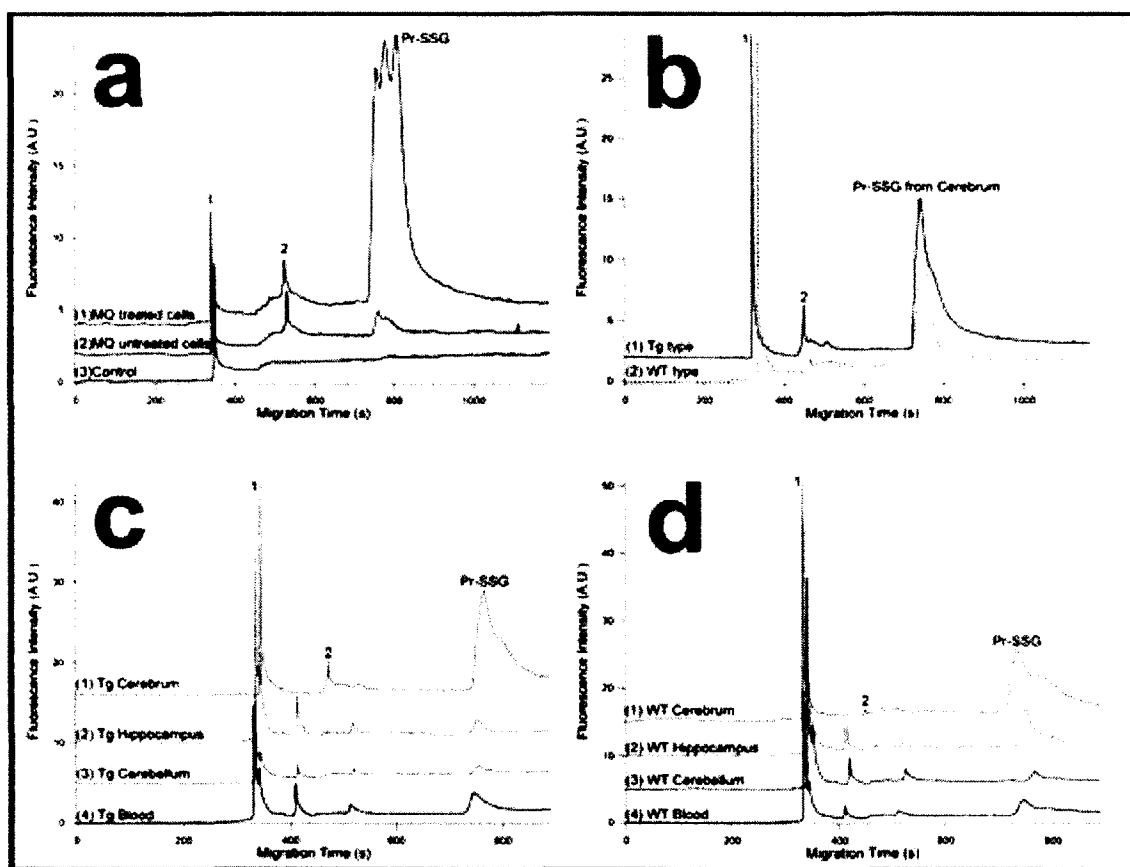


Figure 14: Quantitative electrophoretic profiling of menadione (MQ) mediated *S*-glutathionylation (Pr-SSG) in human colon adenocarcinoma (HT-29) cells and Pr-SSG of brain tissues and blood in AD-Tg/WT mice. (a) Electropherograms of Pr-SSG from HT-29 cells labeled with Dylight 488 maleimide. Trace 1 demonstrates Pr-SSG from MQ treated HT-29 cells. Traces 2 and 3 indicate MQ untreated HT-29 cells and MQ treated HT-29 cells without deglutathionylation, respectively. (b) Electropherograms of Pr-SSG in cerebrum of AD-Tg/WT mice at 5-month. (c) Electropherograms of Pr-SSG from 3 anatomical positions (cerebrum, cerebellum and hippocampus) in brain tissue and blood sample of AD-Tg mouse. (d) Electropherograms of Pr-SSG from 3 anatomic brain regions and blood of AD-WT mouse. 1 & 2: Dylight 488 maleimide. All the experimental conditions are the same as in Figure 10. Top trace is offset in the y-axis for the clarity.

Based on the Equation 2, and the measured peak area for the *S*-glutathionylated peaks, the total *S*-glutathionyls content in the injected volume for MQ-treated and untreated HT-29 cells were calculated as  $(326 \pm 15)$  fmol (average  $\pm$  SD;  $n=3$ ) and  $(41 \pm 3.4)$  fmol, (average  $\pm$  SD;  $n=3$ ), respectively. For the CE analysis, only 1.1 nL volumes of samples were hydrodynamically injected, which leads to 1.41 ng and 1.40 ng of total

proteins for the MQ treated and untreated cells, respectively. Therefore, the treatment with MQ resulted in 8-fold increase in protein-bound *S*-glutathionyls contents ( $232 \pm 10.6$  nmol/mg protein) compared with untreated cells ( $29.3 \pm 2.5$  nmol/mg protein). MQ, a redox cycling quinone can form the toxic species, the semiquinone (SQ $\cdot$ ) radical through the one-electron metabolism catalyzed by NADPH-ubiquinone oxidoreductase (ubQO). Also, MQ can be replenished by reaction between SQ $\cdot$  and O $_2$  with concomitant free radical generation of superoxide anion (O $_2^{\cdot-}$ ) [45]. Our results are in close agreement with other reported values for Pr-SSG in this MQ mediated oxidative stress model [45]. In addition, the relative standard deviation (RSD) was 4-7% indicative of reproducibility of LIF detection of Dylight 488 labeled *S*-glutathionyls in multiple CE injections.

### 3.2.7 Monitoring Pr-SSG in Mice Brain

Another direct biological application of this CGE-LIF method was demonstrated in characterizing the electrophoretic profiles in nanogram (ng) amounts of whole blood and brain tissues including the hippocampus, the cerebrum and the cerebellum from 5-month-old AD-Tg mice. The fluorescence of Dylight 488 maleimide-labeled *S*-glutathionyls was detected in a migration window between 725 and 927 s in both Tg and WT mice (Figure 14c and 14d). The quantitative amounts of Pr-SSG in different biological samples were calculated and listed in Table 3. To further improve separation of protein mixture based on size, an additional experiment for gel condition test was performed by detection of Pr-SSG in the cerebrum of AD-Tg/WT mice at 5-month old using gel matrix containing 10% dextran (Mw: 64-76 KDa), 0.5% SDS, 20 mM Tris, and 20 mM Tricine. The only difference between original (15% dextran) and this new experiment (10% dextran) is gel percentage, where the same Mw dextran was used. The

result is shown in Figure 15, which indicates gel percentages affect the Pr-SSG separation efficiency. To obtain further optimum resolution, gel concentration and 2D-CE will be investigated in a future study.

Table 3: *S*-glutathionyl contents.

Sample Sources	AD-Tg Mice	WT mice
Cerebrum	10.38 ± 4.51 (nmol/mg)	11.99 ± 4.29 (nmol/mg)
Cerebellum	3.31 ± 0.96 (nmol/mg)	1.06 ± 0.13 (nmol/mg)
Hippocampus	1.36 ± 0.11 (nmol/mg)	3.37 ± 0.58 (nmol/mg)
Whole blood	16.3 ± 2.25 (μM)	27.4 ± 2.96 (μM)

The B6.Cg mice model is associated with early onset of AD so that it was selected for the study of neurodegenerative alternation, *S*-glutathionylation, with the AD progression. Mice genotyping was accomplished with melting curve analysis and the results are shown in Figure 16. Since the appearance of amyloid pathology and cognitive impairment are generated in transgenic mice at 6, 7-month of age, it is intriguing for us to study 5-month-old mice pair and explore whether *S*-glutathionylation formation precedes the appearance of amyloid plaque. We demonstrated the feasibility of applying this newly developed CE-LIF method to detect and quantify *S*-glutathionylated proteins in whole blood and specific brain regions including the hippocampus, the cerebrum and the cerebellum from a 5-month-old AD mice pair (data shown in Table 3). Although no statistical evaluation regarding genotyping can be undertaken in this initial animal study, this method proves to be a valuable tool for future investigation into characterizing *S*-glutathionylation abundance and electrophoretic profile with AD progression. To further understand the cause of early onset AD, a large scale animal study including AD-Tg/WT mice pair at different age stages such as 1-, 5-, and 11-month-old, indicative of long

before, immediately before and long after amyloid plaque accumulation, is necessary for examining whether *S*-glutathionylation formation is an early event in the AD progression. Additionally, we envision that this method can serve as a platform for study disease etiology and serve as prescreening of AD if different *S*-glutathionylation patterns indeed occur with progression.

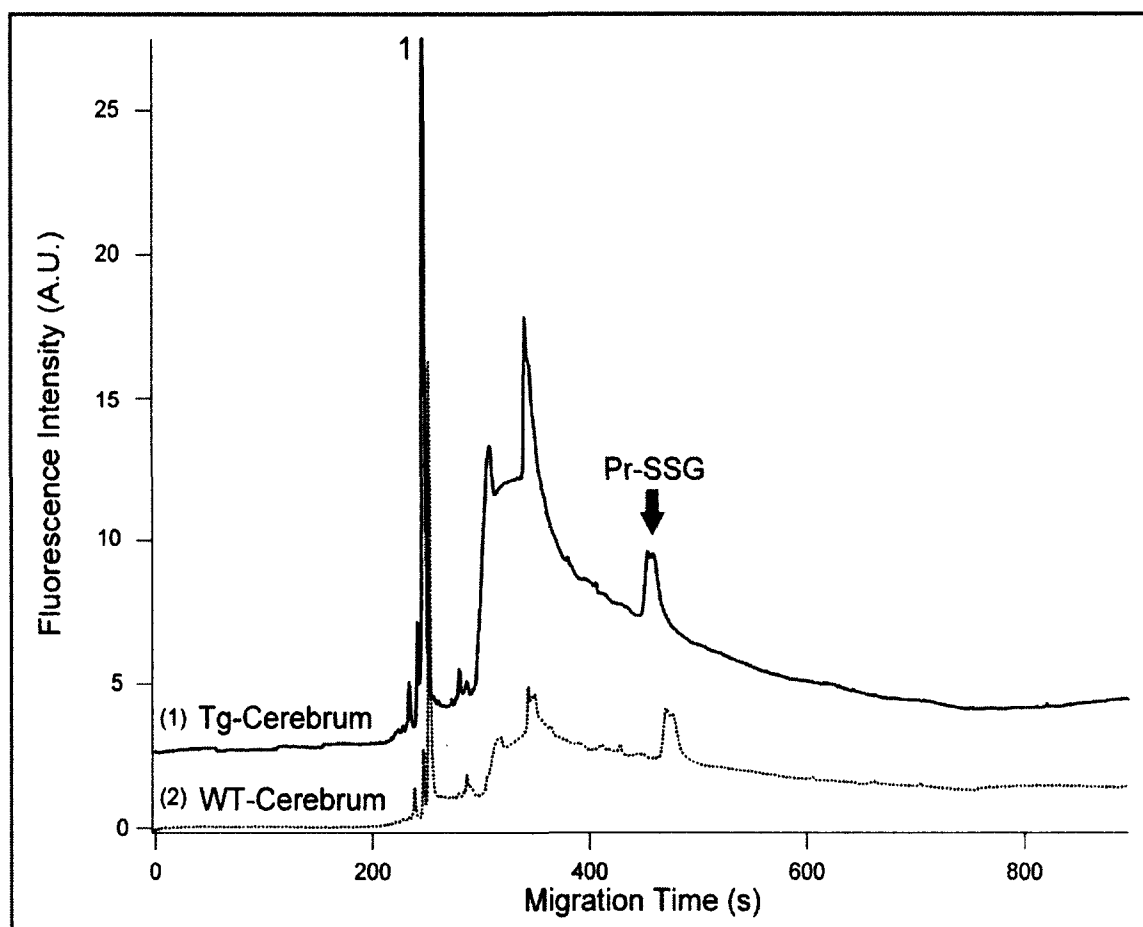


Figure 15: Gel condition test for *S*-glutathionylated protein (Pr-SSG) in cerebrum of AD-Tg/WT mice at 5-month old using gel matrix containing 10% dextran (Mw: 64-76KDa), 0.5% SDS, 20 mM Tris and 20 mM Tricine. 1: Dylight 488 maleimide. All the experimental conditions are the same as in Figure 10. Top trace is offset in the y-axis for the clarity.

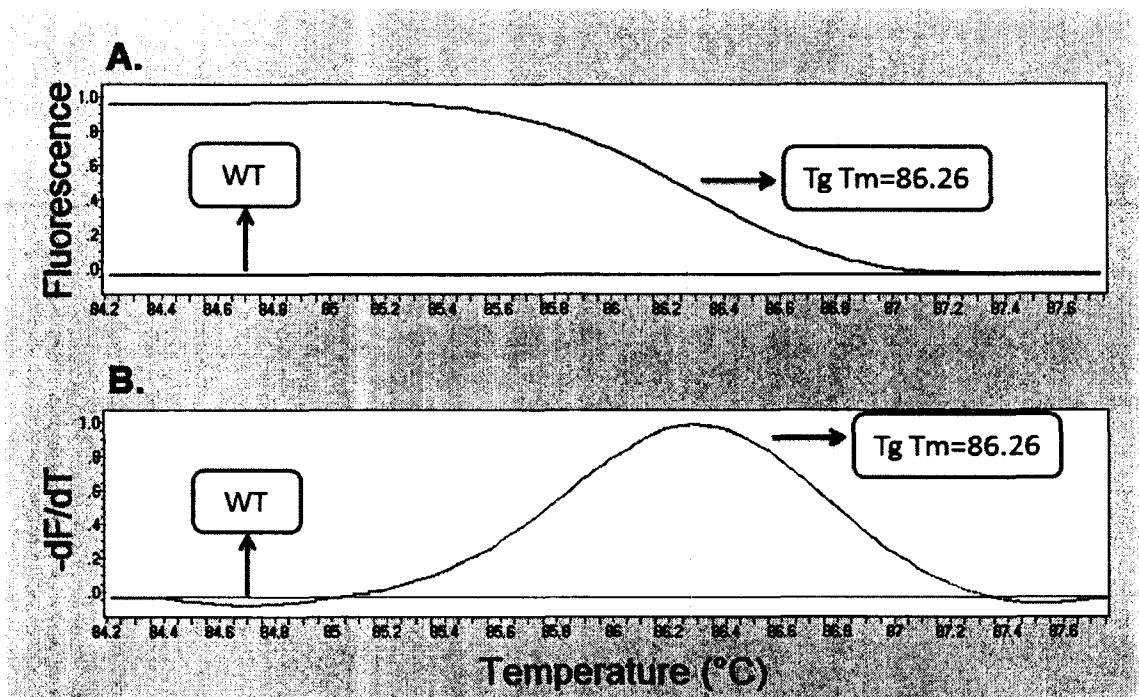


Figure 16: Melting curves (A) and melting peaks (B) of App gene. Melting temperature ( $T_m$ ) of App gene is  $86.0 \pm 0.6$  °C (peak area=18).

The quantitative data listed *S*-glutathionylated protein levels in specific brain regions. Previous studies reported that the levels of reduced GSH in 4-month-old mouse brain varied in different anatomical positions, with cortex > cerebellum > hippocampus [73, 74]. However, in another rat study, no brain region associated the difference in *S*-glutathionyl expression was observed [75]. The discrepancy might be due to the use of different species. Currently, our data is not conclusive to discuss whether *S*-glutathionylation level varies with brain regions with AD progression. However, this new method has explicitly displayed the potential to lead a complete study to answer the biological question, such as whether regional vulnerability of the AD brain tissue is reflected in differences in *S*-glutathionylated protein pattern.

The results demonstrated the extent of protein *S*-glutathionylation in whole blood, averaging  $16.3 \mu\text{M}$ , which is equal to  $7.15 \text{ nmol/mg}$  protein. The level of Pr-SSG in

human blood was reported as 138  $\mu\text{M}$  [14]. The discrepancy between the two values might be due to the differences of species [14]. Blood protein-bound glutathione concentration may reflect glutathione status in other less readily accessible tissues, such as brain biopsy, thus of blood measurement has been considered as an index for of whole body oxidative stress status, and serves as an important biomarkers diagnostically [76]. Altogether, with Mw pattern distribution characterized from the CGE separation, we envision that the method can be further extended to investigate the *S*-glutathionyls patterns classification in blood samples from the involvement of AD disease progression using chemometric tools such as principal component analysis. If difference in electrophoretic profiles exists, this method could potentially become a pre-screening tool for early detection of AD.

Our method of coupling Grx-catalyzed derivatization and labeling of protein bound *S*-glutathionyls to CGE-LIF detection has exhibited several great merits, including low LOD, fast analysis time (within 15 min) and potential for Mw pattern classification. It reached the limit of *S*-glutathionyls detection of 1.8 attomole, which is  $10^9$  fold less than the conventional Ellman's assay [77] and significantly faster than traditional SDS-PAGE analysis which might take up to 2 days. It may facilitate the glutathione homeostasis study in minuscule biological samples, such as single cells or biopsy tissues.

### 3.2.8 Pr-SSG in Protein Profiles

We previously developed an ultrasensitive CGE-LIF method for the detection and quantification of *S*-glutathionyl, reaching the lowest limit of Pr-SSG detection at 1.8 attomole level, reported to date [78]. Here, we used this analytical method to quantify *S*-



glutathionyl abundance in brain and blood preparations obtained from 5 pairs of AD-Tg/WT mice at the three age stages (10 animals/age group, total of 30 animals).

After calibration, each biological sample was analyzed in triplicate. Based on Equation 2 and the measured peak area for *S*-glutathionylated peaks, the total *S*-glutathionyl content (in fmol) for each injected protein sample preparation (in ng) was calculated. The results in Figure 17e and 17f suggest that *S*-glutathionyl levels of Tg mice brains increased with aging ( $P < 0.001$ ) except at the 5-month-old, and Pr-SSG levels at 1-, 5- and 11-month-olds were  $43.0 \pm 7.2$ ,  $36.6 \pm 7.0$  and  $129.8 \pm 14.2$  nmol/mg protein, respectively. No significant change with aging was observed in the WT mouse brain. For the genotype effect, there is a significant increase in *S*-glutathionylation abundance in Tg brain tissues compared with controls' at the 1-month ( $P < 0.05$ ) and 11-month-olds ( $P < 0.001$ ). For blood samples, Pr-SSG contents increased with aging for both control and Tg mice ( $P < 0.001$ ). Specifically at the three AD staging, Pr-SSG levels were measured as  $10.6 \pm 1.0$ ,  $18.0 \pm 1.3$  and  $32.1 \pm 4.1$  nmol/mg protein, respectively, whereas Tg counterparts had Pr-SSG levels of  $10.7 \pm 2.5$ ,  $33.3 \pm 7.1$  and  $46.9 \pm 11.4$  nmol/mg protein, respectively. In terms of the genotype effect, blood Pr-SSG abundance in Tg mice at 5-month ( $P < 0.01$ ) and 11-month-olds ( $P < 0.5$ ) was significantly higher than their age-matched control mice. These results are in agreement with the results of previous studied [78]. All Pr-SSG values are expressed as mean  $\pm$  standard deviation (S.D.).

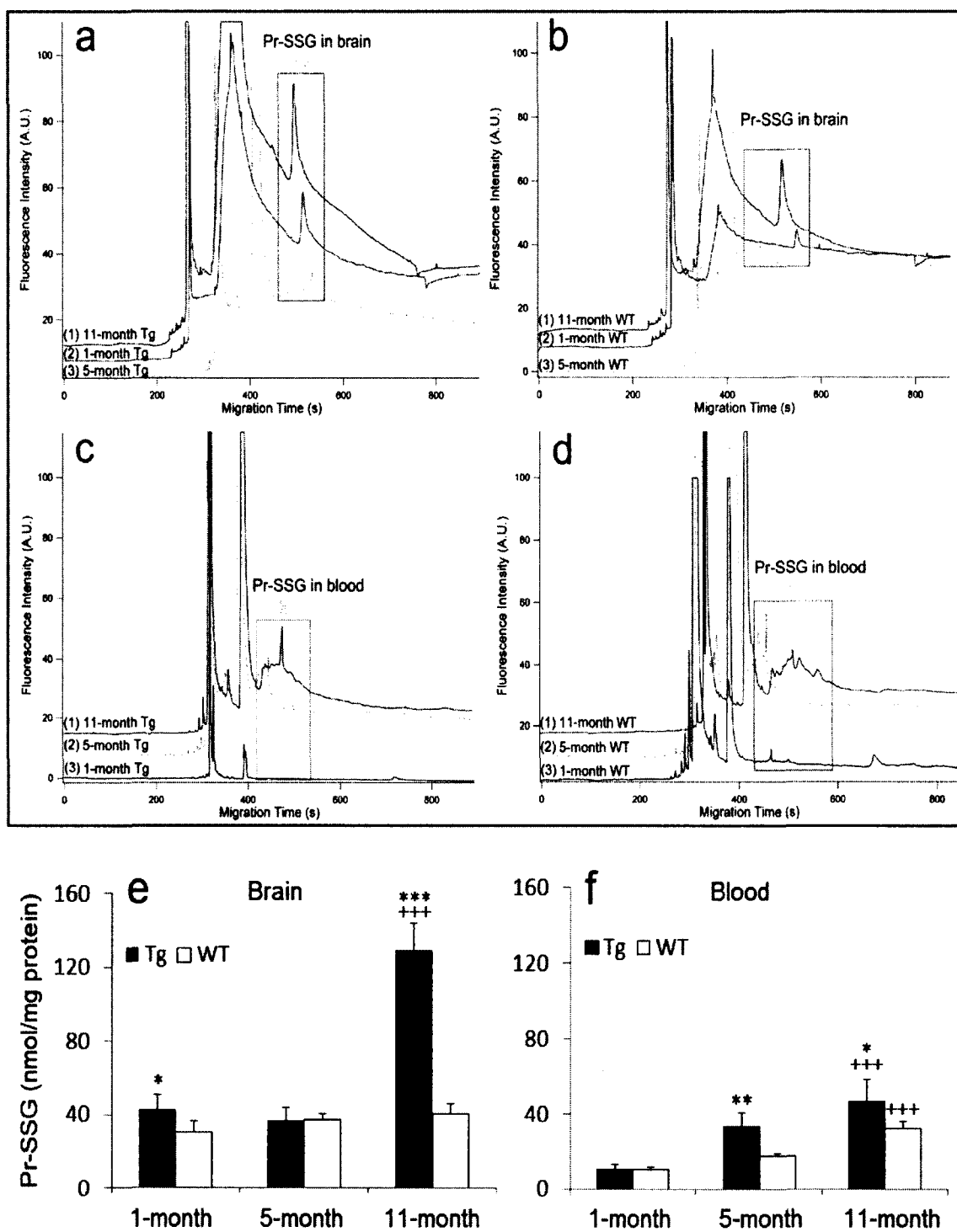


Figure 17: Electropherograms of *S*-glutathionylated protein (Pr-SSG) of Tg (a)/WT (b) mouse brain and Tg (c)/WT (d) blood at 1-, 5- and 11-month-old. Yellow arrows point out Pr-SSG peaks at the 3 age stages. The unlabeled peaks belong to Dylight 488 maleimide. Pr-SSG levels in AD-Tg/WT brain (e) and blood (f) samples at the 3 age groups. Age effect: 1-month vs. 5-month vs. 11-month. +++P < 0.001. Genotype effect: Tg vs. WT. \* P < 0.05, \*\* P < 0.01, \*\*\*P < 0.001.

### 3.2.9 Principal Component Analysis

Due to the nature of CE separation, this electrophoretic method also produces a protein molecular weight (Mw) based profile of *S*-glutathionylated proteins. These complex data matrices are desirable for powerful multivariate analysis. The primary research objectives are used to assess whether reactive oxygen species (ROS) induced protein oxidative stress such as *S*-glutathionylated proteins distribution as a function of Mw (1) differs between AD and control subjects; and (2) exhibits different features at different stages of AD progression. We evaluated the utility of the combination of *S*-glutathionyls profiling and PCA analysis for AD diagnosis. Particular attention was paid to the number of PCs, as they are viewed as a critical factor to determine the outcome of the PCA model. As seen in Table 4, the first three PCs from brain tissues and blood samples, account for up to 80.10% and 82.37% of the total variance in six age/genotype groups, respectively. Figure 18 shows that the brain and blood in the six age/genotype groups were distinguished by principal component scores. Since it can sometimes be difficult to appreciate the degree to which these individual groups are separated in a three-dimensional plot, we have also prepared a two-dimensional score plot for each genotype-WT and Tg shown in Figure 19.

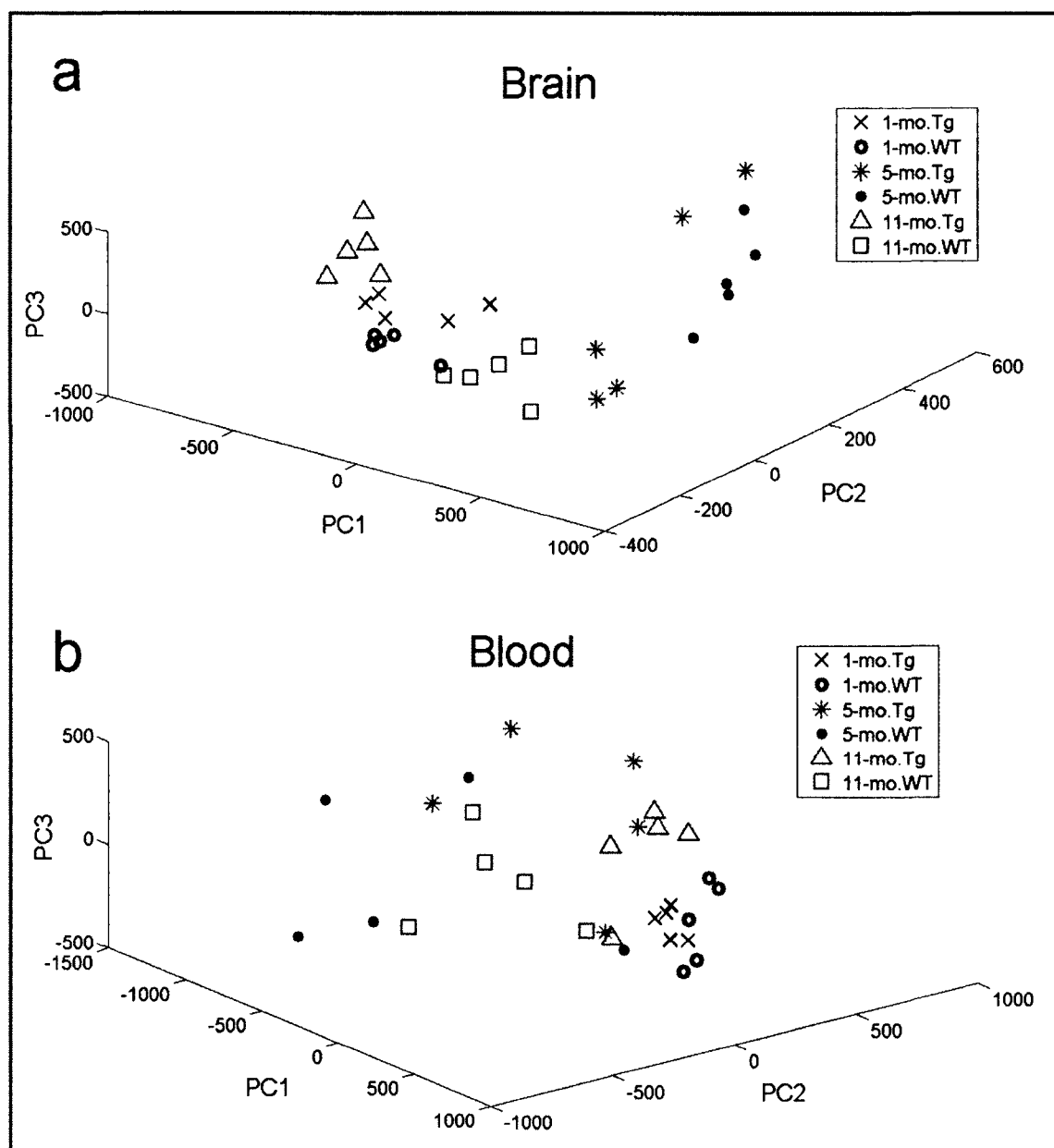


Figure 18: The score plots of PCA analysis for the brain (a) and blood (b) S-glutathionylated protein electropherograms.

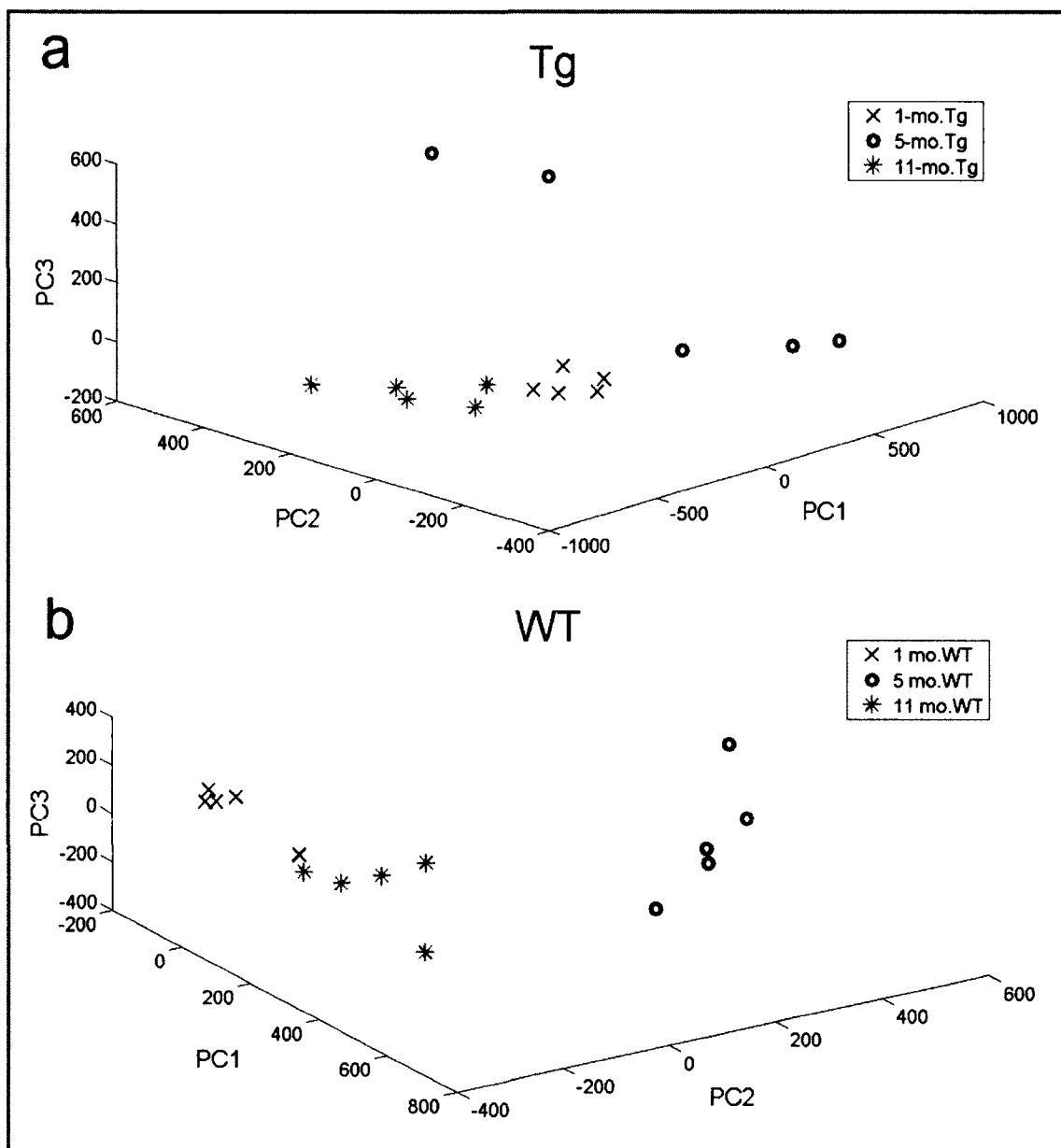


Figure 19: Principle component analysis (PCA) of brain Pr-SSG electropherograms. Score plot of PCA-analyzed samples using the first three PCs for the three Tg (a) and WT (b) groups.

Table 4: PCA variance in brain tissues and blood samples.

Brain	Variance	Cumulative variance	Blood	Variance	Cumulative variance
PC1	53.22%	53.20%	PC1	56.84%	56.84%
PC2	20.71%	73.90%	PC2	16.53%	73.37%
PC3	6.56%	80.10%	PC3	9.00%	82.37%
PC4	5.17%	85.20%	PC4	6.06%	88.43%
PC5	4.59%	89.80%	PC5	3.07%	91.51%
PC6	2.15%	92.40%	PC6	1.80%	93.31%

### 3.2.10 Prediction of Molecular Weight

PCA can be utilized to evaluate the “importance” of variables, such as protein Mw values converted from the migration time (see Figure 4 for details) by examining loading vectors of PCs. The contribution of protein Mw to this PCA model was evaluated by inspecting the loading vector of the first PC shown in Figure 20. The first PC accounts for 53.22% of the total variance in Table 4. The contribution of any given Mw value to the total variance was determined by the loading vector value: the higher loading vector value indicates the bigger contribution of the corresponding Mw. Arbitrarily, 50% of the loading vector maximum (0.03/dashed line) was set as the threshold to inspect which regions were considered as the most contributors to this model variance. The main Mw regions in mice brains are found at 1.4 kDa and 8.4~20.3 kDa. For blood samples, the Mw ranges are located at 8.3 kDa and 13.2~37.2 kDa. The first region is associated with small, non-protein fluorescent species present in the sample. The second region predicts the Mw range where the most age-related and genotype-related *S*-glutathionylations occur.

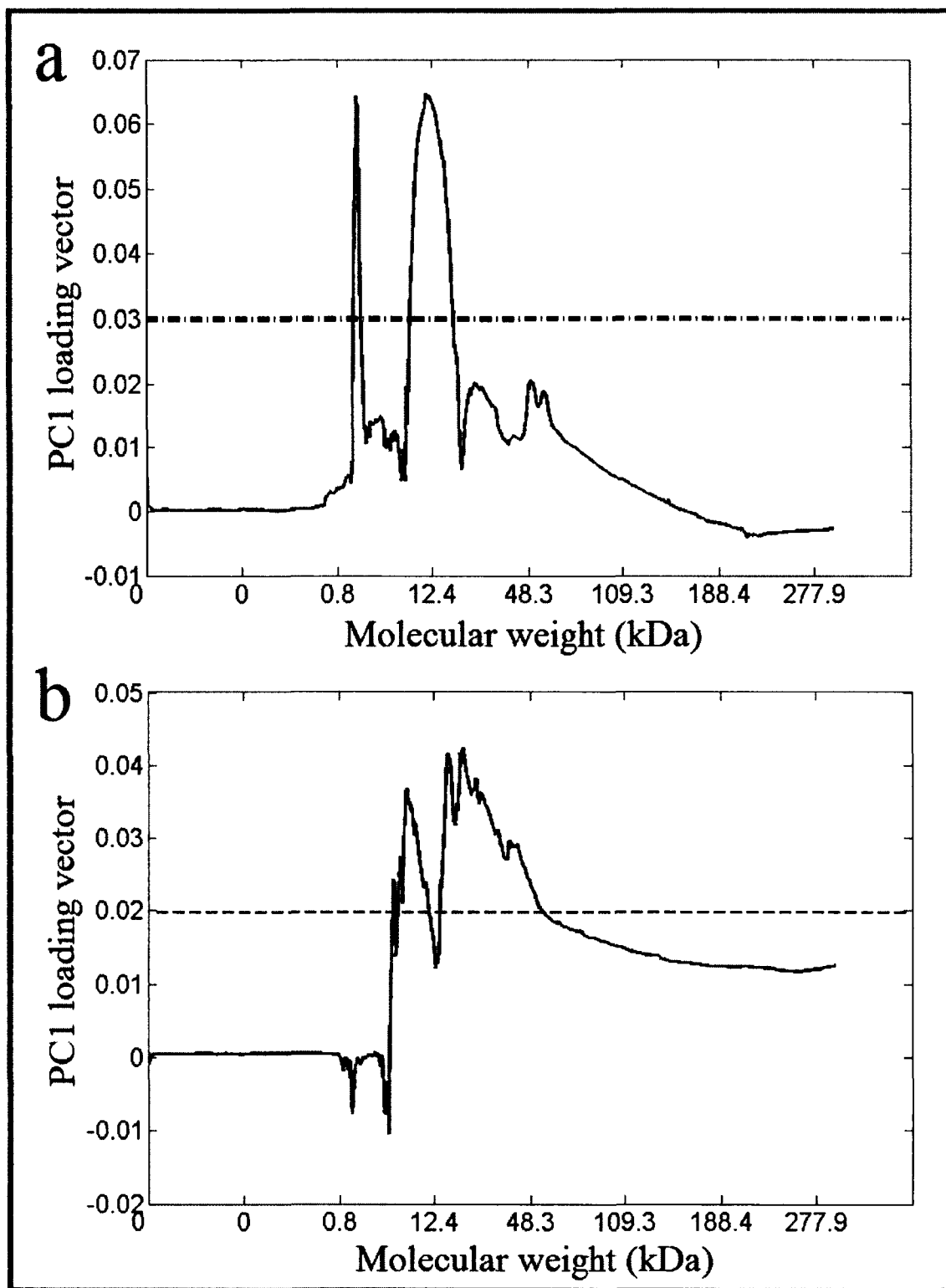


Figure 20: Loading vector of the first principle component (PC) of mice PCA in brain (a) and blood (b). The loading vector represents how variables contribute to the variance explained by the first PC. The variables with the most contribution found above the threshold (dashed line).

### 3.2.11 Sample Categorization

Classification of the each sample data into one of six groups based on its electropherogram profile feature was achieved using a K-means clustering method. The boxplots of classification accuracy based on a 5-fold cross-validation method are shown in Figure 21. The binary classifiers for the discrimination of genotype at the three age groups are shown in Figure 21a and 21b. The accuracies of distinguishing the WT versus Tg genotype at the three age stages of brain/blood samples were found to range from 70.00% to 100.00%, with sufficient discrimination power. Regardless of the data sample type, at 5-month, the classification accuracy was always the lowest with half the data samples testing no better than chance classification. At 1-month and 11-month-olds, most data can be correctly classified to be either WT or Tg genotype. Next, the age of the Tg and WT mice can be distinguished better than chance as seen in Figure 21c, with accuracies ranging from 93%-100% and 66.67%-73.34% for brain tissues and blood samples, respectively. Figure 21d shows the combined age/genotype classification results. An overall classification accuracy of 70.02% can be achieved using brains and 60.00% using blood samples. So, the disease progression stage contributed significantly to group separation for both AD and controls, while genotyping contributed very largely to group separation at 1- and 11-month-olds, except at 5-month old, right before the amyloid deposition.



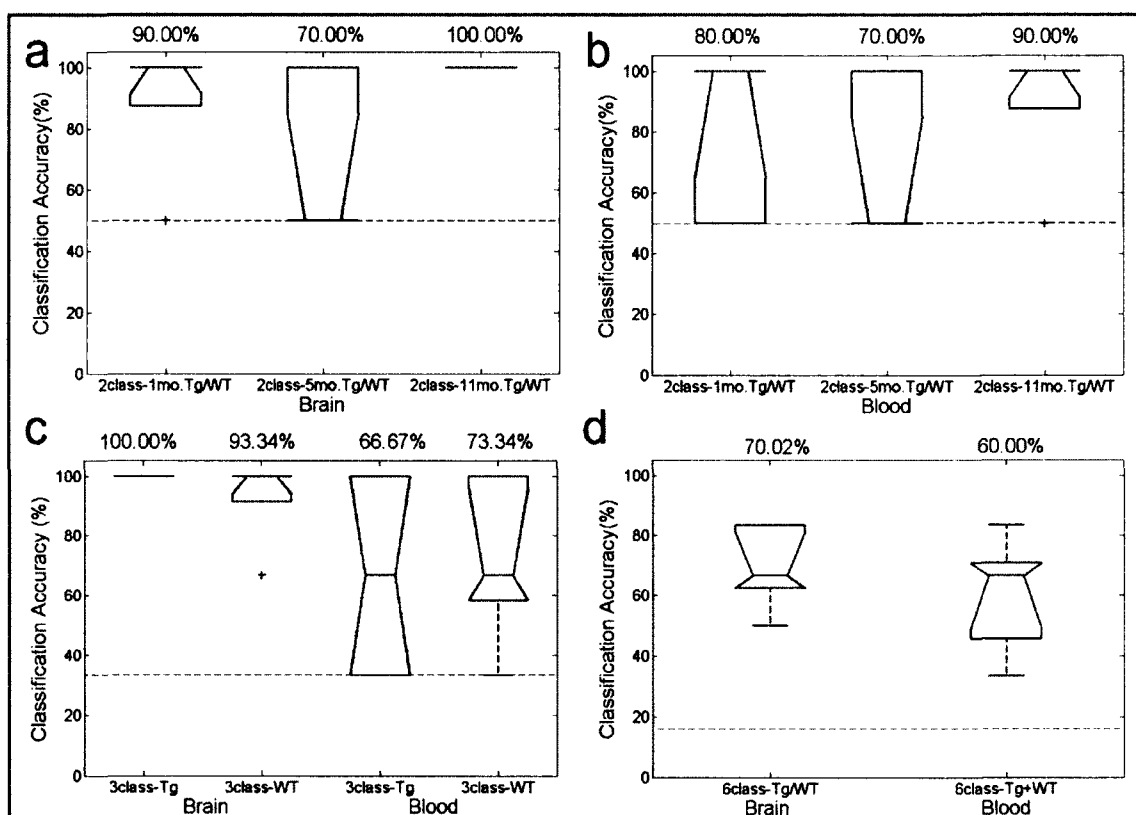


Figure 21: Boxplots for 5-fold cross-validation classification accuracy data for age/genotype groups of brain and blood *S*-glutathionylated protein. (a) and (b) show the binary classification accuracies for the discrimination of genotype in the three age groups. (c) shows the three-class age discrimination in Tg and WT mice using blood and brain samples. (d) shows the overall six-group classification of both age & genotype. In each of these subplots, the horizontal dotted line represents the accuracy of a chance (random) classifier. The mean classification accuracy for each group is also shown on the top of the each bar chart.

A leave-one-out validation method was also applied to test the classification accuracy for the age and genotype. To classify samples into one of six groups based on their *S*-glutathonylation profiles, six disjoint PCA models were used for pattern recognition and sample classification. The normalized Gaussian distribution probabilities of membership using *S*-glutathionylated protein electrophoretic profiling data of both brain tissues and blood samples were computed. Table 5 showed the final results using brain data, with 28 correct assignments out of 30 samples (>95% confidence). The

difference between AD and control at the three disease progression stages in the brain can be separated out even further, thus obtaining the correct classification. Using the blood data from Table 6, however, only 13 out of 30 samples were assigned correctly with >95% confidence. Despite the seemingly low accuracy level using blood samples, this result is still more than twice as high as the random classifier. It is probably more appropriate in single-trial classification applications where a new brain or blood sample is compared with Gaussian clusters obtained from an existing data base of existing AD v.s. non-AD samples.

Table 5: Probability of membership in the six age/genotype group—brain.

Sample	1-mo. Tg	1-mo. WT	5-mo. Tg	5-mo. WT	11-mo. Tg	11-mo. WT
1-mo. Tg1	<b>1.00</b>	3.15E-13	1.56E-21	0	0	2.34E-28
1-mo. Tg2	<b>0.93</b>	4.74E-08	0	0	0.07	0
1-mo. Tg3	<b>1.00</b>	6.69E-04	0	0	9.61E-05	0
1-mo. Tg4	<b>0.95</b>	6.26E-16	0	0	0.05	0
1-mo. Tg5	<b>1.00</b>	0	9.57E-16	0	0	0
1-mo. WT1	4.21E-14	<b>1.00</b>	0	0	1.87E-03	0
1-mo. WT2	0	<b>1.00</b>	0	0	1.52E-23	0
1-mo. WT3	1.03E-16	<b>1.00</b>	0	0	1.85E-04	0
1-mo. WT4	0	<b>1.00</b>	3.50E-18	0	2.92E-12	2.36E-15
1-mo. WT5	7.49E-07	<b>1.00</b>	0	0	4.58E-04	1.07E-20
5-mo. Tg1	3.96E-03	0	0.37	0	0	<b>0.63</b>
5-mo. Tg2	0	1.36E-13	<b>0.96</b>	8.54E-14	0	0.04
5-mo. Tg3	0	0	<b>1.00</b>	2.55E-12	0	0
5-mo. Tg4	0	2.66E-21	<b>1.00</b>	4.72E-09	0	2.86E-12
5-mo. Tg5	0	0	<b>0.95</b>	0.05	0	0
5-mo. WT1	0	0	0.02	<b>0.98</b>	0	0
5-mo. WT2	0	0	3.95E-15	<b>1.00</b>	0	3.93E-16
5-mo. WT3	0	0	3.51E-06	<b>1.00</b>	0	0
5-mo. WT4	0	0	9.18E-15	<b>1.00</b>	0	0
5-mo. WT5	0	0	4.78E-12	<b>1.00</b>	0	0
11-mo. Tg1	0	1.05E-12	0	0	<b>1.00</b>	0
11-mo. Tg2	6.67E-20	0	0	0	<b>1.00</b>	0
11-mo. Tg3	0	0	0	0	<b>1.00</b>	0
11-mo. Tg4	0.04	0	0	0	<b>0.96</b>	0
11-mo. Tg5	0	0	0	0	<b>1.00</b>	0
11-mo. WT1	0	1.47E-03	5.07E-12	0	0	<b>1.00</b>
11-mo. WT2	7.17E-25	6.08E-05	1.83E-08	0	0	<b>1.00</b>
11-mo. WT3	9.69E-28	1.57E-04	3.01E-16	0	0	<b>1.00</b>
11-mo. WT4	2.59E-18	2.02E-17	2.67E-06	0	0	<b>1.00</b>
11-mo. WT5	0	1.77E-06	2.28E-04	0	0	<b>1.00</b>

Notes: Mo = Month; Tg = Transgenic; WT = Wild-type; The highest probability value in the each row indicates that a sample belong to a particular class (boldface). The italic numbers indicate the correct classification with confidence level above 95%.

Table 6: Probability of membership in the six age/genotype group—blood.

Sample	1-mo. Tg	1-mo. WT	5-mo. Tg	5-mo. WT	11-mo. Tg	11-mo. WT
1-mo. Tg1	<b>0.97</b>	0.03	2.42E-08	1.07E-03	4.09E-06	7.72E-04
1-mo. Tg2	<b>0.99</b>	3.17E-11	5.73E-11	7.24E-04	3.76E-03	9.06E-04
1-mo. Tg3	<b>1.00</b>	1.48E-05	2.85E-08	7.59E-04	1.40E-04	6.53E-04
1-mo. Tg4	<b>0.99</b>	3.50E-10	2.07E-10	9.22E-04	3.82E-03	1.35E-03
1-mo. Tg5	<b>0.98</b>	8.69E-12	9.84E-07	2.06E-03	9.24E-03	4.06E-03
1-mo. WT1	0	<b>1.00</b>	8.02E-05	2.68E-03	3.22E-04	4.34E-07
1-mo. WT2	0.05	<b>0.94</b>	8.78E-06	3.58E-03	1.18E-08	1.53E-03
1-mo. WT3	0.02	<b>0.98</b>	1.90E-04	3.65E-03	3.76E-08	1.85E-03
1-mo. WT4	0	<b>0.94</b>	0.06	1.49E-03	8.21E-06	2.00E-07
1-mo. WT5	0	<b>0.99</b>	9.52E-03	3.93E-04	8.49E-07	1.26E-10
5-mo. Tg1	1.46E-11	1.03E-28	0.23	0.09	0.32	<b>0.35</b>
5-mo. Tg2	0	0	<b>1.00</b>	2.14E-04	3.66E-04	5.43E-18
5-mo. Tg3	0	0	<b>0.53</b>	0.14	0	0.33
5-mo. Tg4	0	3.77E-25	0.24	2.24E-04	<b>0.76</b>	2.88E-15
5-mo. Tg5	0	0	<b>0.98</b>	0.02	0	3.12E-08
5-mo. WT1	2.10E-07	2.04E-15	0.22	0.14	<b>0.32</b>	<b>0.32</b>
5-mo. WT2	0	0	<b>0.60</b>	0.38	0	0.02
5-mo. WT3	0	0	1.41E-09	<b>0.81</b>	0	0.19
5-mo. WT4	0	0	0	<b>0.98</b>	0	0.02
5-mo. WT5	0	0	0	<b>0.96</b>	0	0.04
11-mo. Tg1	5.95E-08	1.48E-24	0.09	0.11	<b>0.53</b>	0.28
11-mo. Tg2	0	0	0	6.01E-12	<b>1.00</b>	0
11-mo. Tg3	0	3.94E-05	0.13	1.63E-03	<b>0.87</b>	3.54E-12
11-mo. Tg4	0	3.56E-15	0.24	6.28E-05	<b>0.76</b>	1.11E-16
11-mo. Tg5	0	3.87E-23	0.24	3.20E-03	<b>0.76</b>	6.12E-11
11-mo. WT1	1.19E-15	0	0.30	0.11	0.09	<b>0.49</b>
11-mo. WT2	0	0	0.03	0.11	3.20E-22	<b>0.86</b>
11-mo. WT3	0	0	0.01	0.31	1.12E-09	<b>0.67</b>
11-mo. WT4	0	0	0.41	0.10	0	<b>0.49</b>
11-mo. WT5	0	0	6.84E-20	0.38	5.56E-29	<b>0.62</b>

Notes: Mo = Month; Tg = Transgenic; WT = Wild-type; The highest probability value in the each row indicates that a sample belong to a particular class (boldface). The italic numbers indicate the correct classification with confidence level above 95%.

Finally, we performed a receiver operating characteristics (ROC) analysis for both brain tissues and blood samples with only classifying AD and non-AD phenotypes, without taking disease progression staging into consideration. The 30 brain electropherograms (5 pairs of AD and WT at each of three age stages) that were used to differentiate AD and non-AD phenotypes reached 100.00% in both sensitivity and specificity (as shown in Figure 22a). Also, Figure 22b suggests that the validation cohort of the 30 blood electrophoretic profiles achieved high discrimination power, with sensitivity of 93.33% and specificity of 90.00%. These preliminary results suggest that PCA is a powerful method for multivariate analysis of complex data, such as electropherograms describing *S*-glutathionyl profiles for the diagnosis of AD.

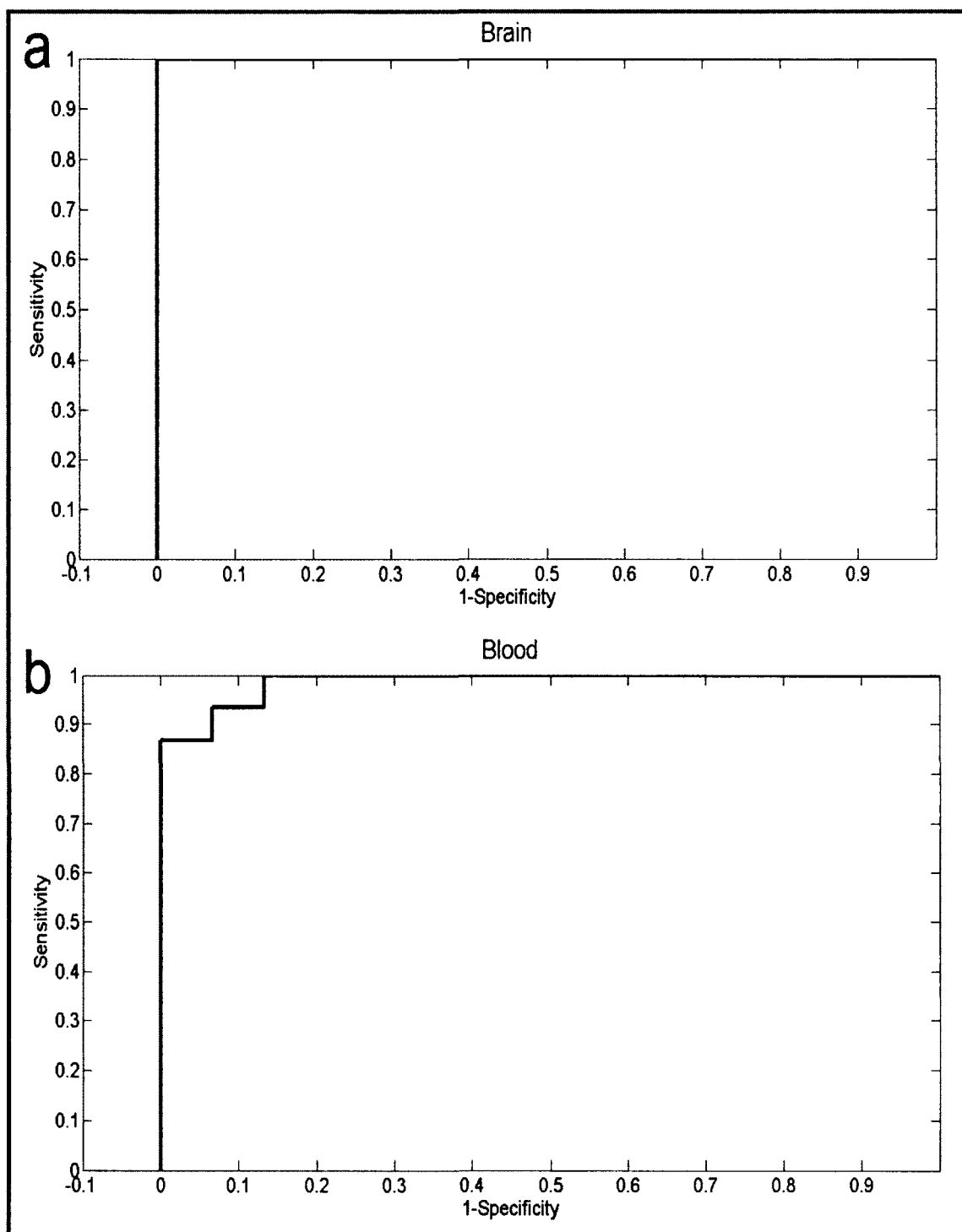


Figure 22: Results of the receiver operating characteristic (ROC) analyses generated by the threshold percentage votes needed to classify a *S*-glutathionylation electropherogram. The area under the curve was calculated as 1 and 0.9867 for brain (a) and blood (b), respectively.

### 3.3 Damaged DNA

We developed a procedure for the analysis of 8-OHdG comprising immunoaffinity and indirect fluorescence labeling of 8-OHdG, their separation by CE, and on-line detection by LIF. To monitor the damage to the DNA base guanine in transgenic AD mice, we developed an assay that utilizes the very low sensitivity of the capillary electrophoresis coupled with laser induced fluorescence detection. In addition, this assay takes advantage of the specificity provided by the monoclonal antibody N45.1 to 8-OHdG. Simple manipulation comprises of urine centrifugation, incubation with the antibody, and capillary electrophoresis separation.

#### 3.3.1 Calibration Curve

To test the feasibility of the assay, we used N45.1 mouse monoclonal antibody that is specific to 8-OHdG. First of all, capillary electrophoresis validated no presence of impurities in primary antibody (Figure 23 trace 5). Next, it separated the unbound secondary antibody at 135 s and 278 s (Figure 23 trace 4), and a complex of the secondary antibody along with primary antibody (Figure 23 trace 3). In addition, a complex of 8-OHdG ( $10 \text{ ng}\cdot\mu\text{L}^{-1}$ ) with primary and the secondary antibodies was analyzed for generating a calibration curve (Figure 23 trace 2). Furthermore, the 8-OHdG complex ( $1000 \text{ ng}\cdot\mu\text{L}^{-1}$ ) peak was determined in this study by comparison of the migration time and spiking at 162 s. (Figure 23 trace 1).

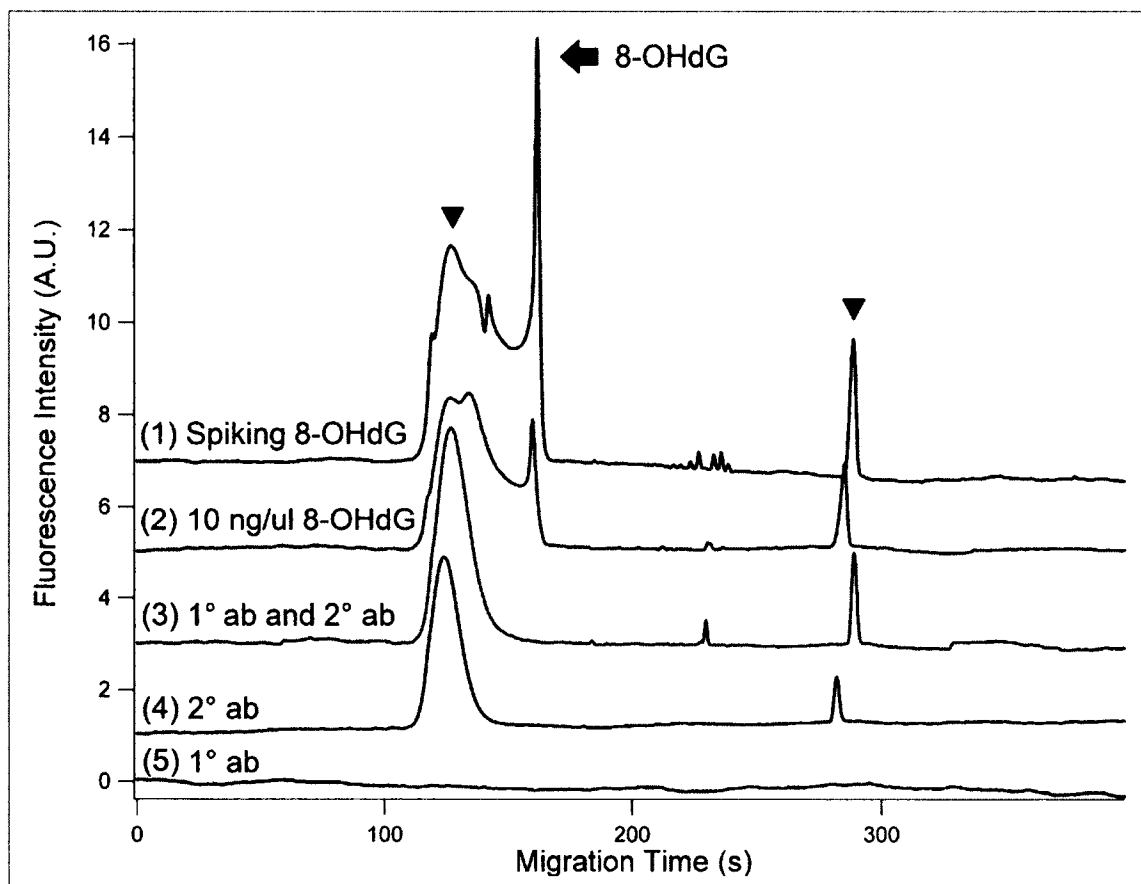


Figure 23: Electropherograms of validation tests in positive and negative controls. (1) a complex with  $1000 \text{ ng}\cdot\mu\text{L}^{-1}$  8-hydroxy-2'-deoxyguanosine (8-OHdG) standard; (2) a complex with  $10 \text{ ng}\cdot\mu\text{L}^{-1}$  8-OHdG standard; (3) a complex with primary and secondary antibody; (4) secondary antibody alone; (5) primary antibody alone. Hydrodynamic injection at pH 9.5 and 0.5 psi for 5 s; separation in 20mM sodium tetraborate buffer at 400 V/cm. Arrowhead: secondary antibody; Arrow: 8-OHdG complex. Top trace is offset in the y-axis for the clarity.

To estimate the limits of detection, a calibration curve was constructed by plotting the measurement of the average peak area ( $y$ ) versus the amount of 8-OHdG ( $x$ ) in Figure 24. The five-point calibration from 2.2 to 11 fmol showed the linear detection of 8-OHdG with correlation coefficient of 0.96. The Equation 3 for the regression line is:

$$y = (1.23 \pm 0.31) \times 10^{15} x + (3.00 \pm 2.52); \quad R^2 = 0.96. \quad \text{Eq. 3}$$



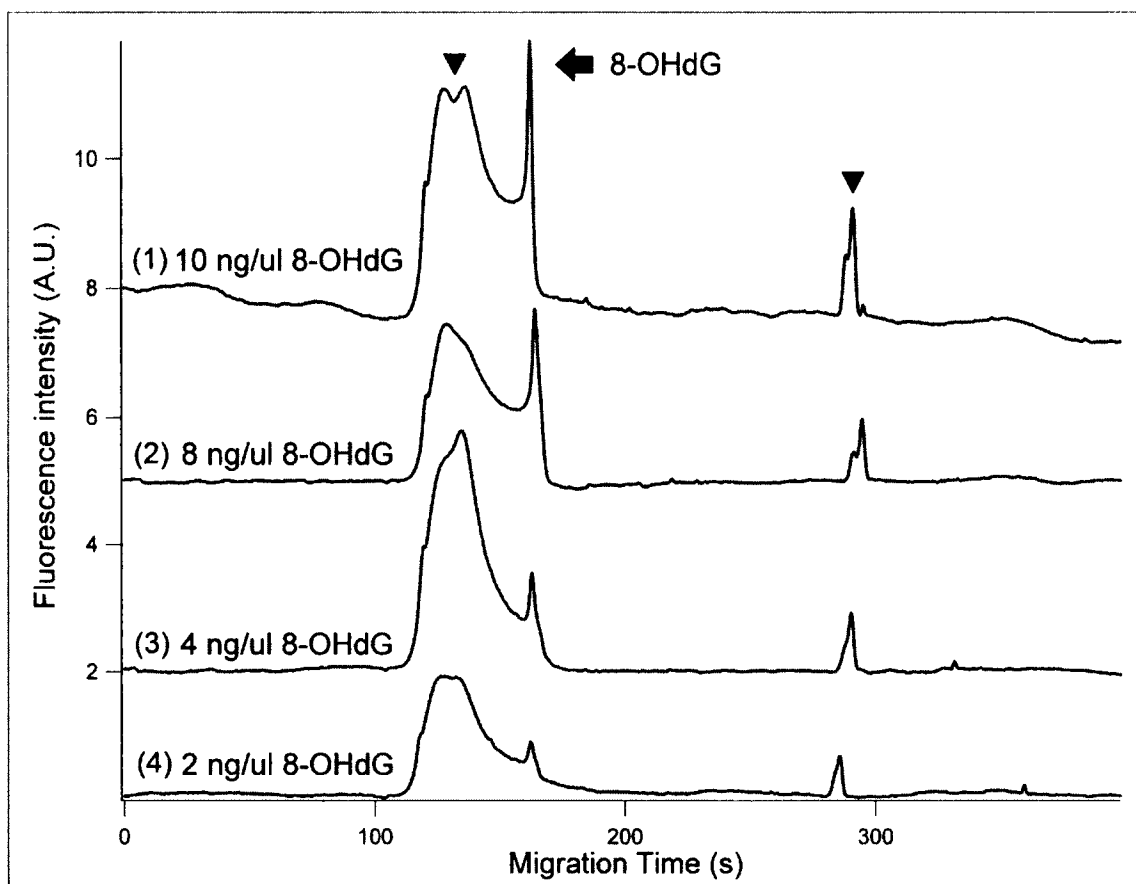


Figure 24: Electropherograms of calibration curve of 8-hydroxy-2'-deoxyguanosine (8-OHdG) standard with different concentrations. Arrowhead: secondary antibody; Arrow: 8-OHdG complex. All the experimental conditions are the same as in Figure 23. Top trace is offset in the y-axis for the clarity.

### 3.3.2 Analysis of 8-OHdG in Mice Urine

To illustrate the potential of this analytical method, we directly applied it to the analysis of 8-OHdG in AD-Tg mice urine. We performed experiments using urine samples from 11-month-old, male, transgenic mice. The electropherograms of the 8-OHdG in urine and the standard is shown in Figure 25. This is a very fast and sensitive method with an overall analytical run time of 10 min. The peaks at 164 s indicated the identification of 8-OHdG in the urine sample. A good separation was obtained for 8-OHdG complex from secondary antibody and complex of primary and secondary

antibody. Based on Equation 3, and the measured peak area for the 8-OHdG peak, the total 8-OHdG content in the injected volume for AD transgenic mice urine was calculated as 0.51 fmole. For the CE analysis, only 0.31 nL volumes of samples were hydrodynamically injected, which leads to urinary concentration of 8-OHdG of 1.64  $\mu\text{M}$ .

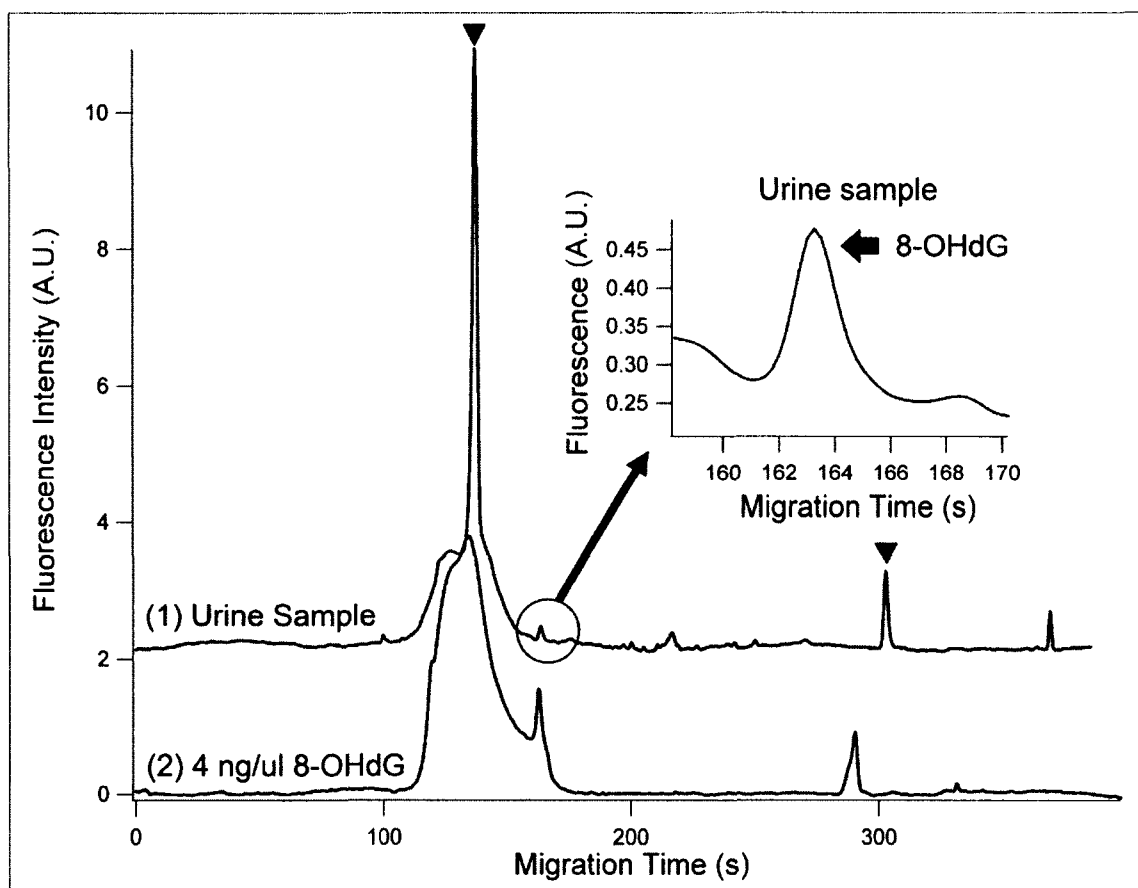


Figure 25: Electropherograms of urine sample and 8-hydroxy-2'-deoxyguanosine (8-OHdG) standard. Arrowhead: secondary antibody; Arrow: 8-OHdG complex. All the experimental conditions are the same as in Figure 23.

The critical issue in detecting 8-OHdG in the urine sample is to avoid interference from other compounds. This is achieved by using antibody that has high selectivity for 8-OHdG compound. Among 500 papers published on urinary 8-OHdG detection, ELISA method has been used primarily. There is ongoing debate whether the kit is specific to

recognize other urine components than 8-OHdG. Toyokuni's group stated that the antibody N45.1 is highly specific to 8-OHdG, showing weak or no cross reactivity with the urine component such as uric acid, urea, creatine and creatinine [79]. Although it can recognize both the modified base (8-oxoguanine) as well as the deoxyribose structure, the modified base has to be at least two orders of magnitude higher in concentration to be a competitor for the monoclonal antibody [79].

On the other hand, Song's group suggested that although ELISA is a very popular technology for detection of 8-OHdG, it overestimated the amount of the antigen in the samples, after examining 8-OHdG using both HPLC with ELISA [80]. They conclude that one of the major reasons for the overestimation of urinary 8-OHdG detection in the urine is caused by the cross reactivity of N45.1 with urea in the urine sample. Urea is weakly recognized by the anti-8-OHdG antibody since both of them share a common -NH-CO-N structure [80].

For our developed method, even if there were similar compounds in the urine and cross reacted with the antibody, CE with high resolution and high sensitivity will offer great promise to separate these interferences. For the capillary zone electrophoresis, the borate buffer (a mixture of sodium tetraborate and boric acid) at pH 9.5 was employed. Because at this pH level, the boric acid proton dissociation occurs, which further leads to an increase in coupling sugar moiety of 8-OHdG with boric acid [81]. However, both urea and creatinine are uncharged species, the transport of which is controlled by the electroosmotic flow [81]. Therefore, the 8-OHdG and other possible interference can be separated by charge to size ratio.

The urinary excretion of damaged nucleotides, 8-OHdG from both mtDNA and nDNA serves as an essential biomarker of oxidative stress reflecting the rate of damage in steady state. We have demonstrated this sensitive method combining both CE-LIF separation and immuno-affinity characteristics capable of studying low abundant 8-OHdG in small amount of urine sample. Because 8-OHdG is considered as a biomarker of oxidative DNA damage, we cannot exclusively conclude that the results are only related to AD. However, it allows us to determine oxidative status. Moreover, our results clearly show the screening capability of 8-OHdG using this new developed method from extracellular matrix (urine). The potential of using this method as a diagnostic biomarker in AD progression in a larger set of subjects deserves further study. Additionally, this method can serve as a tool to monitor the oxidative stress response of AD subjects with therapeutic antioxidant treatment.

### 3.3.3 Assay Repeatability and Accuracy

The reproducibility of this method was evaluated with both injection and analytical repeatabilities. To assess injection repeatability, five replicate injections of labeled 8-OHdG were examined, while five different labeled 8-OHdG samples prepared by the same procedure were studied for analytical repeatability. In the measurement of analysis repeatability, the relative standard deviation (RSD) values for migration time and peak area were 11.32% and 5.52%, respectively. In addition, day-to-day assays by replicate injection of the 8-OHdG solution during five consecutive days were examined to study the precision of the method. The RSD values of migration time and peak area were 19.3% and 24.3%, respectively.

The accuracy was determined by performing a standard spiking method, where known amounts of labeled 8-OHdG standard was mixed with analyzed 8-OHdG and further detected by CE-LIF method in triplicate. The 8-OHdG LOD concentration of 28.61 nM was subsequently determined by the calibration curve. The percentage of the spiked 8-OHdG recovered by the assay indicates the accuracy of the method was 93.14%.

## CHAPTER 4

### DISCUSSION

#### 4.1 Glutathione Homeostasis

The aims of the present study were to quantify tissue glutathione (GSH and GSSG) and *S*-glutathionylated protein (mixed-disulfides, Pr-SGG) levels in the brain and blood at three ages (1-, 5- and 11-month-old) in a transgenic mice model of AD and compared these levels to those found in wild type (WT) litter mates. In addition, tissue differences in glutathione levels were investigated in the hippocampus, the cerebrum and the cerebellum regions of Tg and WT brains.

As indicated in Figure 6, the absolute brain weight in 5-month WT mice was 12% higher than their AD counterparts. Interestingly, the 11-month Tg mice demonstrated a significant (20%) increase in brain weight as compared to WT animals at the same age. Moreover, one-way ANOVA analysis showed that the total protein of AD-Tg brains significantly increases from 2.5 (at 5-month-old) to 3.4 mg/ml (11-month-old) with aging. The blood brain barrier (BBB) might be compromised in aged Tg mice, which would contribute to increased fluid filtration, perhaps even serum protein from vessel lumen to the brain. This suggestion is supported by previous autopsy finding that an enhanced expression of aquaporin 4, the protein channels involved in water transport, leads to edema formation in AD [82]. This interesting observation suggests an association

of AD with brain inflammation, a subject of future investigation in our laboratory using this AD mouse model.

#### 4.1.1 Age Effect

In this work, we tried to address the hypothesis that oxidative stress, specifically, the formation of GSSG and *S*-glutathionylated proteins is an early event prior to amyloid plaque manifestation in AD progression. Our current use of 1-month-old mice that have not developed amyloid pathologies revealed that substantial increase in protein-thiol oxidation (Pr-SSG formation) occurred in the absence of neuropathological markers, thus supporting the view that an early loss of cerebral glutathione redox balance preceded disease manifestation. Additional support comes from previous studies demonstrating that the aging process is associated with the generation of reactive oxygen species and disturbance of glutathione homeostasis in the brain [49, 83]. The 11-month-old aged mice long after A $\beta$  generation represented a suitable model for AD progression. Our results demonstrated significant age-related reduction of tissue GSH levels in the cerebrum and associated decreases in the GSH/GSSG ratio in all brain regions from 5-month (right before A $\beta$  deposit) to 11-month, a stage when A $\beta$  deposits are abundant. This age-related decline in brain GSH level and the GSH/GSSG ratio is consistent with reduced GSH synthesis, as evidenced by a decrease in  $\gamma$ -glutamylcysteine ligase, the rate-limiting enzyme in GSH synthesis during aging [84]. Surprisingly, the brain GSSG levels in 5-month-old mice were lower than 1-month-old, suggesting that the 5-month-old brain may be more resistant to oxidative stress. The “dip-down” at 5-month was observed for both GSSG and Pr-SSG levels with a corresponding increase in the GSH/GSSG ratio in all brain regions. Thus, it appears that the transgenes induce a stress response to compensate

for its expression and this leads to an early increase in *S*-glutathionylation but the animals reach an equilibrium, probably due to the large excess capacity at the middle age. Then the response repeats during plaque deposition at a later stage.

The study of GSH redox state in blood not only serves as an index of oxidative stress status, but also offers a comparison between age-related differences in GSH redox status between the brain and blood. Interestingly, Pr-SSG was not detectable in the blood of 1-month-old mice, regardless of genotype; however, Pr-SSG levels were significantly elevated in 5- and 11-month-olds, respectively. The summation of the total thiol pool revealed that approximately 80~90% of blood thiols are in the form of oxidized disulfides of which 40-50% are protein bound. Furthermore, the concentrations of GSH plus GSSG in blood were 2-to-3 fold higher than those in brain tissues. It is notable that the level of GSH was increased 1.6 fold in blood from 1- to 5-month-old in Tg mice. While the significance of this increase is unresolved, typically higher blood GSH could act to scavenge superoxide and hydroxyl radical.

The dramatic increase in Pr-SSG in blood at 5-month coupled to the dip in GSSG and Pr-SSG in the brain (Figure 8) suggests an interesting scenario, namely, that an increase in brain-to-blood export of GSSG at an age right before A $\beta$  manifestation. The consequent increase in systemic oxidative stress would be consistent with increased formation of *S*-glutathionylated proteins (Pr-SSG) in the blood. It is not clear whether this mixed-disulfide increase is primarily due to GSSG export from brain or perhaps collectively from some other tissues such as the liver. Although these hypothetical scenarios require further investigation and validation, it is confirmed by previous findings that aging enhanced a cell's ability to export GSSG as a mechanism to maintain cellular



redox homeostasis [85, 86]. Some of the proteins responsible for GSSG export have been identified; reportedly, the multidrug resistant protein 1 (Mrp1) mediates GSSG efflux and maintains GSH homeostasis. Mrp1 is expressed in brain tissues, and has been implicated in GSSG export in primary cultures of rat astrocytes [87] and mouse astrocytes [88]. Mrps function as organic anion export pumps, and accept glutathione *S*-conjugates as substrates [89-91]. Altogether, these results support the contention that oxidative stress occurs before amyloid plaque deposition in AD brain, an early event in AD progression [92-94]. Our current study suggests that intracellular brain GSH/GSSG status is differentially regulated during AD progression, and that the rate of GSH synthesis and/or GSSG export are likely to play important roles in cellular GSH redox homeostasis. Our main goal of this study is to characterize glutathione redox status in details; and these observations will further facilitate future studies into why these changes occur. Particularly, we will investigate whether these changes in glutathione redox status are closely related to the change in gamma-glutamylcysteine (for GSH synthesis) or MRP-1 (for GSH and GSSG export). Additionally, we will examine whether the change in GSH/GSSG is attributed from apoptosis induced by amyloid aggregation.

#### 4.1.2 Genotype Effect

The level of GSH in the cerebrum and the cerebellum of 11-month Tg mice were decreased as compared to WT litter mates, while GSSG was elevated in 1- and 5-month Tg animals. Moreover, the data in Figure 8 demonstrated the existence of significant mixed-disulfides, suggesting that oxidative modification of protein thiols was evident in various brain regions, most dramatically in Tg mice. For example, at 11-month, *S*-glutathionylated proteins (Pr-SSG) were substantially elevated in the three regions of the

brain and blood in Tg animals as compared to the WT counterpart. Even at 1-month old, baseline Pr-SSG in Tg animals was higher than the WT counterpart, which might be due to the fact of growth stress in Tg mice at an early stage before evidence of A $\beta$  generation. Plus, it is noteworthy that the content of protein-bound glutathione was variable, from 15 to 24 nmol/mg in the different brain regions of 11-month-old Tg animals and represented a major percentage of total glutathione (range of free GSH was between 0.1 and 0.8 nmol/mg). Previous studies demonstrated a wide range in the GSH/GSSG ratio in the brain, from 2 to 200, under conditions of oxidative stress, disease or aging [75, 95, 96]. In our study, the GSH/GSSG ratio ranged from 2 to 7; the ratio in all brain regions in aged Tg mice (11-month olds) were significantly lower than their WT counterpart. This is consistent with a relatively more oxidized basal intracellular environment and suggests that the Tg brain would be selectively vulnerable to ROS damage.

#### 4.1.3 Specific Brain Region Effect

The three brain tissues of the hippocampus, the cerebrum and the cerebellum were examined to evaluate whether regional differences exist in cellular GSH redox status and whether elevation in GSSG and Pr-SSG formation was associated with regional vulnerability during AD progression. Notably, the basal level of Pr-SSG was high in the hippocampus, even in the age-matched WT mice, suggesting that, regardless of genotype, the hippocampus is likely to be a vulnerable region of the brain to oxidative stress. Significantly, AD is associated with hippocampal damage and loss of cognitive functions of the brain. Thus, the finding of altered tissue redox status before the onset of amyloid plaque formation underscores the importance of evaluating redox changes at early stage AD progression for early detection.

GSH is present in millimolar (mM) concentrations in the brain [9]. However, previous reports of GSH abundance among various brain regions were inconsistent [74, 75, 97]. Studies by Zhu [75] and Liu [97] showed that GSH levels were similar in all brain regions, including the cortex, the cerebellum and the hippocampus in Sprague-Dawley and Fisher 344 rats, respectively. In other studies, Abbott et al., reported that in 4-month-old mice, the levels of GSH varied in different anatomic regions of the brain with the cortex exhibiting the highest value followed by the cerebellum and the hippocampus [73, 74]. However, our results indicate the cerebellum in both AD-Tg and wild type mice have the highest GSH level among all the brain regions examined, regardless of age difference (Figure 7). Interestingly, the cerebellum is the region of the brain that is most resistant to age-associated AD pathology. The discrepancy between the studies of Zhu and Liu [74, 75, 97] and those of Abbott et al. [73, 74] and our current work could be due to species differences (rat vs. mice) as well as differences in animal strains, housing, environmental and dietary factors. Although there were many GSH/GSSG studies using AD mouse model [98-100], we have performed the systematical measurements in differentiating the ROS induced GSH/GSSG and Pr-SSG alternations using three aspects -- age, genotypes and brain regions.

In summary, the present study has characterized the age-dependent status of glutathione and mixed-disulfide in specific regions of the brain and blood of a transgenic mouse model of AD, which provided the ground work for future investigation into the relationship between GSH and A $\beta$  regulation, as well as into the mechanism of GSH redox control in AD brain. The results will have important implication for age-dependent and regional selective pathobiology of AD progression.

To our knowledge, this is the first time such a study was undertaken and these observations can serve as a supporting platform for future investigation. For example, two opposite regimes, glutathione stimulator- N-acetyl-L-cysteine (NAC) and inhibitor- diamine can be employed to further pinpoint whether alteration of GSH/GSSG ratio can accelerate or decelerate amyloid plaque onset. Another interesting example will involve studying how the fluctuation in GSH correlate with the change in NOX (NADPH oxidase 1/2), NOS (nitric oxide synthesis), and mitochondrial function. Altogether, an understanding of regional and age differences in GSH and mixed-disulfide redox status will provide important insights into differential antioxidant capacity and oxidative susceptibility in the specific regions of AD brain.

The data from this study demonstrated that altered GSH redox balance in specific brain regions is age- and genotype-linked in the transgenic model of AD (B6.Cg). Collectively, the data shows that GSH redox imbalance and subsequent S-glutathionylation of proteins are early events, and provides a time line for when these redox changes occur during AD progression. These results will underpin investigations into the mechanism of AD-associated oxidative disruption of brain GSH homeostasis; this information will be useful in future study of longitudinal changes in oxidative stress and cognitive behavior in AD in this Tg mouse model.

## 4.2 Pr-SSG Profiles

The issue for the early screening of individuals who will progress to AD is a very critical one. Although various imaging tools that facilitate the identification are present, using capillary electrophoresis combined with PCA analysis to characterize oxidized protein biomarkers would be a powerful tool. In our approach, we used principal

component scores as quantitative markers for the each mouse *S*-glutathionylation electrophoretic profile. The spatially distributed six groups in three dimensional PCA plots were observed. Additionally, we used a cross validation method to determine the use of principal component scores, and to predict the classification. This analysis provides a great estimate at the early stage of AD progression.

#### 4.2.1 Pr-SSG Electrophoretic Profiles

*S*-glutathionyl levels in brain tissues and blood samples of AD-Tg/WT mice at different age stages were quantitatively determined using CGE-LIF. Overall, our study demonstrated that Pr-SSG in AD-Tg mouse brain significantly increased with aging except at 5-month-old. The difference of *S*-glutathionylation between Tg and WT indicated that *S*-glutathionylation might be an early event prior to the AD progression. The principal component scores, served as quantitative markers, were able to discriminate AD from WT types, and even differentiate various AD staging groups.

We assessed the performance of *S*-glutathionylation profiles in the classification of unknown samples. Specifically, we carried out a “leave-one-out” prediction for a “six-class” prediction for “Alzheimer’s” or “control” phenotype at the three disease progression [101]. It was shown in Tables 5 and 6 that the sensitivity and accuracy of using blood *S*-glutathionylation profiles appears suboptimal compared with brain oxidative stress. Also, from PCA plot (Figure 18B), it was observed that the difference in these six group classification was more pronounced in brain tissues than blood samples. This observation may suggest that peripheral blood-based markers reflect mechanism of the central nervous system (CNS) in AD, to some extent, but not completely. Peripheral blood is a highly convenient source of biomarkers, which has been studied in research

settings. However, it is unclear how and what proteins that originate as a result of brain pathology, would be transited from the brain to the blood, since blood brain barrier may limit the potential diagnostic blood-based markers to small or lipophilic molecules, or ones with specific transporters [102].

However, it is notable that these observations of subpar prediction using blood *S*-glutathionylation profiles are only correct when including a consideration of AD progression stages. Not considering AD staging but only predicting AD and non-AD phenotypes, the most critical issue, the predicting specificity and sensitivity using blood *S*-glutathionylation profiles reached 93.33% and 90.00%, respectively. Other reports have also pointed to that the APP metabolism alteration and oxidative imbalance does not only exist in neuronal plaque, but also in peripheral blood [103]. Hence, the oxidative imbalance in the blood of AD subjects could mirror physiological events in CNS, to some extent [104]. In our case, the change of blood *S*-glutathionylation profile is sufficient enough to be detected and used for prediction. Even though brain proteins that pass into the blood stream become diluted into a complex medium, it displays that our CGE-LIF analytical method is sensitive to detect these low abundant oxidative stress related biomarkers. These *S*-glutathionylated proteins can provide insight into processes such as inflammation and oxidative damage. This study remains fully validated by future studies such as determining key biomarkers to predict pathological diagnosis and further narrow treatment options. Despite the absence of precise knowledge about the identity of these biomarkers, we can still distinguish AD from non-AD, which is a very attractive feature of this method. Our results show clinical usefulness of a panel of unknown biomarkers associated with *S*-glutathionylation from the blood.

#### 4.2.2 Diagnostic Use

Surprisingly, the classification accuracy assessed for 5-month *S*-glutathionylation spectral PCA analysis has great variance, while 1-month and 11-month mice have significantly higher classification accuracy than random chance. This interesting finding suggests that targeted oxidized proteins long before and long after amyloid plaque deposition are indicative predictors of AD screening. However, immediately before amyloid plaque formation, the oxidative stress induced *S*-glutathionylation becomes ambiguous in terms of classification. This could be attributed by various factors, such as antioxidant capacity surge to overcome the protein modification at 5-month right before plaque deposition. What is more interesting is that our previous study of characterizing *S*-glutathionylation redox status showed that brain GSSG and Pr-SSG levels in 5-month-old mice were lower than 1-month-olds, suggesting that the 5-month-old brain may be more resistant to oxidative stress [105]. Our electrophoretic spectra of targeted *S*-glutathionylation at 5-month-old seems to be agreeable to the previous observation on the “dip-down” for Pr-SSG levels at 5 months, which suggests an abrupt change in the redox status from its normal trend of increasing oxidative stress with aging. Thus, it appears that the transgenes initially induce a stress response to compensate for its expression and this leads to the early increase in *S*-glutathionylation, but the oxidative stress balance reaches equilibrium, probably due to the large excess of antioxidant capacity at the middle age. Then the response repeats during plaque deposition at the later stage. At this end, our data suggests that 5-month (right before plaque manifestation) brain and blood oxidative stress profile seems not completely reliable for AD and non-AD phenotype

classification. Currently, it is unknown what precise mechanisms are involved in oxidative stress at this stage.

On the other hand, we demonstrated the high accuracy of genotyping classification at 1- and 11-month mice, based on PCA analysis of *S*-glutathionylated proteins electrophoretic profiles. Our finding indicates that the measurement of molecular weight based electrophoretic profiling of blood and brain *S*-glutathionylated proteins are sensitive to change, even at the early stage of the disease long before the plaque deposition. Also, our results highlight a unique method to use the electrophoretic technique for separation of oxidized protein biomarkers and further analyze them with PCA for monitoring the AD progression. We find that the electrophoretic characteristics of oxidized proteins can serve as a predictor of AD progression and the early stage screening.

#### 4.2.3 Protein Biomarkers

To predict what Mw range indicates the most *S*-glutathionylated proteins associated with aging and genotyping effects, the electropherograms were analyzed by combining the loading vector of the first PC. The useful range extends up to 875 seconds that corresponds to 277.9 kDa. The migration time of Pr-SSG in the brain and blood is between 350 and 470 seconds which correspond to the Mw region at 8.4~20.3 kDa and 13.2~37.2 kDa, respectively. A previous proteome-based study showed that several key proteins within these molecular weight ranges: Deoxyhemoglobin (15.8 kDa),  $\alpha$ -crystalline B (20.1kDa) and GAPDH (36.1 kDa) were identified as *S*-glutathionylated proteins with the loss of functions [16]. *S*-glutathionylation proteomics study in AD brain shows the number of oxidized proteins increased and these identified proteins are



involved in various cellular processes such as the glucose or energy metabolism, and synaptic plasticity with loss of their functions [16]. These results indicate the *S*-glutathionylation involvement in AD brain and that it plays a key role in AD pathogenesis.

Therefore, the particular Mw ranges of *S*-glutathionylated proteins predicted by fast profiling from CGE-LIF and PCA could serve as a powerful tool to locate the specific and precise Mw regions of interest. This prescreening would be instrumental for complex global proteomic study because it helps tease out the most crucial biomarkers within specific Mw range.

#### 4.2.4 Spectral Separation

By focusing on proteins that are susceptible to oxidative stress, we were able to identify AD phenotype. The simplicity and novelty of the method is that it allows the simultaneous monitoring of all proteins with various expression levels of oxidative damage, instead of investigating the abundance of each protein biomarker using various biochemical assays such as ELISA, western blot or microarray. These biomarkers, although unknown, are preferentially prone to *S*-glutathionylation in brain tissues and blood samples. This method naturally investigates a panel of protein biomarkers that are sensitive to *S*-glutathionylation. Besides, our omnibus measures of *S*-glutathionylated proteome profiles with known abundance distribution as a function of Mw are promising approaches for the development of blood-based diagnostic tests for AD. These proteins are expected to have various functions such as  $\beta$ -amyloid generation, the inflammatory response and proteolytic inhibition. Compared with function imaging based AD

diagnosis, our method is less costly, so it is a great alternative addition to the AD diagnosis.

Given the complexity implicated in AD pathogenesis, including amyloid plaque formation, inflammation, oxidative stress disturbance [106, 107], and lipid metabolism [108], the diagnostic accuracy of biomarkers may be improved by combining several blood-based biomarkers related to different mechanisms [109]. Ray et al. found that a panel of 18 signaling proteins in blood plasma together may indicate the early molecular change in AD progression and are further used to identify MCI patients who progressed to AD years later [110]. Hence, a confirmation in larger populations and an incorporation of additional oxidative stress mechanisms such as carbonylation, nitrosylation and nitration profiles may further improve the sensitivity and specificity of this approach.

#### 4.2.5 Transgenic Mouse Model

Our chosen transgenic mouse model mostly mimics the early-onset Familial AD (FAD) rather than the late-onset FAD because of APP and presenilin-1 (PS-1) genes mutations [111] and the lack of ApoE-4 gene inheritance.

Since AD is a very complicated disease, it is a major obstacle to find an ideal animal model that recapitulates the full spectrum of AD neuropathology, such as amyloid plaques, tangles, cell dysfunction/loss and aging. Some aged primates and dogs exhibit AD-like neuropathology; however, it is not practical to use them as models due to the high cost and extensive time involved. Rodents, along with several other animal species such as guinea pigs, *Drosophila*, *Caenorhabditis elegans*, and yeast have been considered for AD research because they are relatively cheap to maintain and can be genetically engineered. But none of these species develop AD pathology on aging [112]. Among

them, transgenic mice models are considered preferable because they have a similar central nervous system (CNS) and the general neurobiology to humans. However, the relative short time window (10 months) of AD-Tg mouse model could make some challenges to studying the effect of aging. In addition, humans are less resistant to neurotoxins and more easily develop AD with mutant APP compared to rodent models. We know that the rodent models have not been able to effectively demonstrate all AD aspects in a single animal [113].

In the end, it has been a significant limitation for the entire AD research field to create an animal model that replicates the multiple AD characteristics [114]. Because of this, currently we cannot simply relate the pathology resulted from the double mutation expression in this artificial mouse model to an aged human brain.

Even though transgenic mice cannot represent all aspects of AD, our current model helped us developed an invaluable tool for characterizing and detecting the molecular changes in the ROS induced oxidative stress damage, particularly, *S*-glutathionylation in the early-onset FAD. This PCA analysis of *S*-glutathionylation spectral profiles can be readily extrapolated to study the age effect on AD development using a different animal model such as ApoE4 mice crossed with PD-APP mice [115, 116]. Most importantly, our method has great potential to analyze *S*-glutathionylation profiles of human blood samples.

### 4.3 8-OHdG Detection

We developed a CE-LIF system to analyze urinary 8-OHdG. This method demonstrates the detection and screening of 8-OHdG in urine using immuno-affinity labeling coupled with CE-LIF. Our method is unique in that, (1) it reaches high

specificity with using CE separation method; plus, (2) it keeps the ease of use provided by the immunoaffinity concept. The sample preparation can be completely excluded, because it requires no solid phase extraction for urine. The ultrasensitive assay described here is not limited to detection of 8-OHdG but can be expanded to other oxidative lesion when appropriate affinity probes are available. Likewise, it has an enormous potential for high throughput clinical applications as well as direct monitoring for the early diagnosis and monitoring DNA oxidative stress progression.

## **APPENDIX A**

### **CHEMICALS AND REAGENTS**

### A.1 GSH and GSSG Determination

Mice identification tags were purchased from Hasco Tag in Dayton, KY. *APP* and *PSENI* primers were from IDT, Coralville, Iowa. Master mix for PCR was from Idaho Technology Inc., Salt Lake City, Utah. Grx was from IMCO in Stamford, CT. GSH and GSSG were from Calbiochem. Diamide was from Research Organics Inc., Cleveland, OH. Five 5'-Dithiobis (2-nitrobenzoic acid) (DTNB) was bought from Biosynth in Itasca, IL. Iodoacetic acid (IAA), 1-fluoro-2, 4-dinitrobenzen (FDNB) and triton X-100 were obtained from Alfa Aesar in Ward Hill, MA. N-Ethylmaleimide (NEM), immobilized TCEP disulfide reducing gel, bicinchoninic acid (BCA) protein assay kit was from Thermo Scientific, Rockford, IL. Sodium dodecyl sulfate (SDS), sodium phosphate dibasic, potassium phosphate monobasic, tris (hydroxymethyl)-aminomethane, tricine, ethylenediaminetetraacetic acid (EDTA), sodium hydroxide, hydrochloric acid and trichloroacetic acid (TCA) were all from Sigma, St. Louis, MO. Glutathione reductase assay kit and glutathione peroxidase assay kit were both purchased from Cayman Chemical Company in Ann Arbor, MI.

### A.2 Pr-SSG Detection

Sodium dodecyl sulfate (SDS), 2-[4-(2-hydroxyethyl)piperazin-1-yl] ethanesulfonic acid (HEPES), ethylenediaminetetraacetic acid (EDTA), methanol, sodium hydroxide, hydrochloric acid, neocuproine, dextran from *Leuconostoc mesenteroides* (average Mw 64-76 kDa), trypsin inhibitor (20 kDa), glyceraldehyde-3-phosphate dehydrogenase (GAPDH, 36 kDa), albumin from chicken egg white (44 kDa), bovine serum albumin (BSA, 66 kDa), bovine gamma globulin (BGG, 140 kDa), trichloroacetic acid (TCA) were all from Sigma. Amicon ultra-4 (Mw cutoff of 3 kDa)

spin columns were purchased from Millipore. Recombinant Grx-3 (C14S, C65Y) from *Escherichia coli* was obtained from IMCO. Glutathione reductase (GR) was from Roche. Nicotinamide adenine dinucleotide phosphate (NADPH), reduced glutathione (GSH), and glutathione disulfide (GSSG) were all from Calbiochem. Diamide was from Research Organics Inc. Five 5'-Dithiobis (2-nitrobenzoic acid) (DTNB) was from Biodynth. DL-dithiothreitol (DTT) was from Fluka. Iodoacetic acid (IAA) and Triton X-100 were obtained from Alfa Aesar. Ultra Trol dynamic pre-coat LN was from Target Discovery. N-Ethylmaleimide (NEM), Dylight 488 maleimide, dimethyl sulfoxide (DMSO), immobilized tris-2-carboxyethyl phosphate disulfide (TCEP) reducing gel, bicinchonic acid (BCA) protein assay kit were all purchased from Thermo Scientific.

### A.3 8-OHdG Detection

Aqueous solution of the reagents was prepared using 18 ohm water from Milli-Q water purification system (Millipore, Bedford, MA). All chemicals were analytical grade quality. 8-hydroxy-2-deoxyguanosine was purchased from Sigma-Aldrich (St. Louis, MO). N45.1 anti 8-OHdG monoclonal antibody was obtained from Genox Corporation (Baltimore, MD). IgG Alexa fluor 488 goat secondary antibody was obtained from Invitrogen (Ontario, Canada). Sodium tetraborate, DMSO, methanol, sodium hydroxide, and hydrochloric acid were obtained from VWR International (Suwanee, GA). Commercially flexible fused silica capillary was obtained from Polymicro Technologies (Phoenix, AZ). The separation buffer consisted of 20 mM sodium tetraborate, pH 9.5.

**APPENDIX B**

**ANIMAL USE APPROVAL**



INSTITUTIONAL ANIMAL CARE AND USE COMMITTEE  
OFFICE OF BIOLOGICAL SERVICES  
Louisiana Tech University

OLAW Assurance #: A3300-01  
USDA Registration #: 72-R-0010

3 February 2011

Dr. June Feng  
Biomedical Engineering  
Louisiana Tech University  
Campus P.O. Box # 58

cc: Dr. Les Guice, Vice President, Research  
and Development

Dear Dr. Feng:

The Louisiana Tech University's Institutional Animal Care and Use Committee (IACUC) has been carried out a review of your amended experimental protocol entitled:

***Understanding the Molecular Mechanism of Alzheimer's Disease: Quantitative Proteomics of Oxidatively Modified Proteins using iTRAQ Analysis and a Novel Proteomic Reactor.***

The proposed procedures have scientific merit and were found to provide reasonable and adequate safeguards for the comfort of the animals, the safety of the researchers and the participating students.

When you are prepared to order additional animals please contact me by e-mail to me at [jgspauld@latech.edu](mailto:jgspauld@latech.edu).

Please remember that you are required to keep adequate and accurate records of all procedures, results, and the number of animals used in this protocol for three years after termination of the project. These records must be available for review by the IACUC or state and federal animal use agencies. Each year in October you will be required to complete a summary of animals used for the United States Agricultural Agency (USDA). Note that failure to follow this protocol as approved may result in the termination of research. If you have any questions please send e-mail to me at [jgspauld@latech.edu](mailto:jgspauld@latech.edu). This protocol must be submitted for renewal review in April 2012.

Sincerely,

  
James G. Spaulding, Chair  
Louisiana Tech University IACUC

## REFERENCES

- [1] Association as “2011 Alzheimer’s Disease Facts and Figure,” *Alzheimer's Dementia*, vol. 7, (no. 2), 2011.
- [2] C.E. Jackson and P.J. Snyder, “Electroencephalography and event-related potentials as biomarkers of mild cognitive impairment and mild Alzheimer's disease,” *Alzheimer's and Dementia*, vol. 4, pp. 137-143, 2008.
- [3] J.A. Ricardo, M.C. Franca, Jr., F.O. Lima, C.L. Yassuda, and F. Cendes, “The impact of EEG in the diagnosis and management of patients with acute impairment of consciousness,” *Arq Neuropsiquiatr*, vol. 70, (no. 1), pp. 34-9, Jan 2012.
- [4] M.S. Chong, W.S. Lim, and S. Sahadevan, “Biomarkers in preclinical Alzheimer's disease,” *Curr Opin Investig Drugs*, vol. 7, (no. 7), pp. 600-7, Jul 2006.
- [5] M.J. de Leon, S. DeSanti, R. Zinkowski, P.D. Mehta, D. Pratico, S. Segal, C. Clark, D. Kerkman, J. DeBernardis, J. Li, L. Lair, B. Reisberg, W. Tsui, and H. Rusinek, “MRI and CSF studies in the early diagnosis of Alzheimer's disease,” *J Intern Med*, vol. 256, (no. 3), pp. 205-23, Sep 2004.
- [6] V. Chauhan and A. Chauhan, “Oxidative stress in Alzheimer's disease,” *Pathophysiology*, vol. 13, (no. 3), pp. 195-208, Aug 2006.
- [7] J.T. Coyle and P. Puttfarcken, “Oxidative stress, glutamate, and neurodegenerative disorders,” *Science*, vol. 262, (no. 5134), pp. 689-95, Oct 29 1993.
- [8] K. Aoyama, M. Watabe, and T. Nakaki, “Regulation of neuronal glutathione synthesis,” *J Pharmacol Sci*, vol. 108, (no. 3), pp. 227-38, Nov 2008.
- [9] R. Dringen, “Glutathione metabolism and oxidative stress in neurodegeneration,” *Eur J Biochem*, vol. 267, (no. 16), pp. 4903, Aug 2000.
- [10] I. Martin and M.S. Grotewiel, “Oxidative damage and age-related functional declines,” *Mech Ageing Dev*, vol. 127, (no. 5), pp. 411-23, May 2006.

- [11] K.M. Gate, I. Lartaud, P. Giummelly, R. Legrand, A. Pompella, and P. Leroy, "Accurate measurement of reduced glutathione in gamma-glutamyltransferase-rich brain microvessel fractions," *Brain Res*, vol. 1369, pp. 95-102, Jan 19.
- [12] F. Tchanchou, M. Graves, E. Rogers, D. Ortiz, and T.B. Shea, "N-acetyl cysteine alleviates oxidative damage to central nervous system of ApoE-deficient mice following folate and vitamin E-deficiency," *J Alzheimers Dis*, vol. 7, (no. 2), pp. 135-8; discussion 173-80, Apr 2005.
- [13] A. Meister and M.E. Anderson, "Glutathione," *Annu Rev Biochem*, vol. 52, pp. 711-60, 1983.
- [14] W.A. Kleinman, D. Komninou, Y. Leutzinger, S. Colosimo, J. Cox, C.A. Lang, and J.P. Richie, Jr., "Protein glutathiolation in human blood," *Biochem Pharmacol*, vol. 65, (no. 5), pp. 741-6, Mar 1 2003.
- [15] I.A. Cotgreave and R.G. Gerdes, "Recent trends in glutathione biochemistry--glutathione-protein interactions: a molecular link between oxidative stress and cell proliferation?," *Biochem Biophys Res Commun*, vol. 242, (no. 1), pp. 1-9, Jan 6 1998.
- [16] S.F. Newman, R. Sultana, M. Perluigi, R. Coccia, J. Cai, W.M. Pierce, J.B. Klein, D.M. Turner, and D.A. Butterfield, "An increase in S-glutathionylated proteins in the Alzheimer's disease inferior parietal lobule, a proteomics approach," *J Neurosci Res*, vol. 85, (no. 7), pp. 1506-14, May 15 2007.
- [17] R.C. Cumming and D. Schubert, "Amyloid-beta induces disulfide bonding and aggregation of GAPDH in Alzheimer's disease," *FASEB J*, vol. 19, (no. 14), pp. 2060-2, Dec 2005.
- [18] I. Dalle-Donne, R. Rossi, D. Giustarini, R. Colombo, and A. Milzani, "Actin S-glutathionylation: evidence against a thiol-disulphide exchange mechanism," *Free Radic Biol Med*, vol. 35, (no. 10), pp. 1185-93, Nov 15 2003.
- [19] C. Muscari, M. Pappagallo, D. Ferrari, E. Giordano, C. Capanni, C.M. Caldarera, and C. Guarnieri, "Simultaneous detection of reduced and oxidized glutathione in tissues and mitochondria by capillary electrophoresis," *J Chromatogr B Biomed Sci Appl*, vol. 707, (no. 1-2), pp. 301-7, Apr 10 1998.
- [20] P. Monostori, G. Wittmann, E. Karg, and S. Turi, "Determination of glutathione and glutathione disulfide in biological samples: an in-depth review," *J Chromatogr B Analyt Technol Biomed Life Sci*, vol. 877, (no. 28), pp. 3331-46, Oct 15 2009.
- [21] N. Ercal, P. Yang, and N. Aykin, "Determination of biological thiols by high-performance liquid chromatography following derivatization by ThioGlo maleimide reagents," *J Chromatogr B Biomed Sci Appl*, vol. 753, (no. 2), pp. 287-92, Apr 5 2001.

- [22] E. Camera and M. Picardo, "Analytical methods to investigate glutathione and related compounds in biological and pathological processes," *J Chromatogr B Analyt Technol Biomed Life Sci*, vol. 781, (no. 1-2), pp. 181-206, Dec 5 2002.
- [23] C.S. Yang, S.T. Chou, L. Liu, P.J. Tsai, and J.S. Kuo, "Effect of ageing on human plasma glutathione concentrations as determined by high-performance liquid chromatography with fluorimetric detection," *J Chromatogr B Biomed Appl*, vol. 674, (no. 1), pp. 23-30, Dec 1 1995.
- [24] Y.K. Mohammad Arif, Faizule Hassan, T.M. Zaved Waise, Md. Ehsanul Hoque Mazumder and Shafiqur Rahman, "Increased DNA damage in blood cells of rat treated with lead as assessed by comet assay," *Bangladesh J Pharmacological* vol. 3, pp. 97-101, 2008.
- [25] K.C. Cheng, D.S. Cahill, H. Kasai, S. Nishimura, and L.A. Loeb, "8-Hydroxyguanine, an abundant form of oxidative DNA damage, causes G---T and A---C substitutions," *J Biol Chem*, vol. 267, (no. 1), pp. 166-72, Jan 5 1992.
- [26] J. Cadet, M. Berger, T. Douki, and J.L. Ravanat, "Oxidative damage to DNA: formation, measurement, and biological significance," *Rev Physiol Biochem Pharmacol*, vol. 131, pp. 1-87, 1997.
- [27] T. Kondo, T. Ohshima, and Y. Ishida, "Age-dependent expression of 8-hydroxy-2'-deoxyguanosine in human pituitary gland," *Histochem J*, vol. 33, (no. 11-12), pp. 647-51, Nov-Dec 2001.
- [28] C.G. Fraga, M.K. Shigenaga, J.W. Park, P. Degan, and B.N. Ames, "Oxidative damage to DNA during aging: 8-hydroxy-2'-deoxyguanosine in rat organ DNA and urine," *Proc Natl Acad Sci U S A*, vol. 87, (no. 12), pp. 4533-7, Jun 1990.
- [29] C. Richter, J.W. Park, and B.N. Ames, "Normal oxidative damage to mitochondrial and nuclear DNA is extensive," *Proc Natl Acad Sci U S A*, vol. 85, (no. 17), pp. 6465-7, Sep 1988.
- [30] P. Mecocci, U. MacGarvey, A.E. Kaufman, D. Koontz, J.M. Shoffner, D.C. Wallace, and M.F. Beal, "Oxidative damage to mitochondrial DNA shows marked age-dependent increases in human brain," *Ann Neurol*, vol. 34, (no. 4), pp. 609-16, Oct 1993.
- [31] M.A. Lovell, S.P. Gabbita, and W.R. Markesbery, "Increased DNA oxidation and decreased levels of repair products in Alzheimer's disease ventricular CSF," *J Neurochem*, vol. 72, (no. 2), pp. 771-6, Feb 1999.
- [32] J. Wang, W.R. Markesbery, and M.A. Lovell, "Increased oxidative damage in nuclear and mitochondrial DNA in mild cognitive impairment," *J Neurochem*, vol. 96, (no. 3), pp. 825-32, Feb 2006.

- [33] W.R. Markesbery and M.A. Lovell, "DNA oxidation in Alzheimer's disease," *Antioxid Redox Signal*, vol. 8, (no. 11-12), pp. 2039-45, Nov-Dec 2006.
- [34] L. Lyras, N.J. Cairns, A. Jenner, P. Jenner, and B. Halliwell, "An assessment of oxidative damage to proteins, lipids, and DNA in brain from patients with Alzheimer's disease," *J Neurochem*, vol. 68, (no. 5), pp. 2061-9, May 1997.
- [35] P. Mecocci, U. MacGarvey, and M.F. Beal, "Oxidative damage to mitochondrial DNA is increased in Alzheimer's disease," *Ann Neurol*, vol. 36, (no. 5), pp. 747-51, Nov 1994.
- [36] P. Mecocci, M.C. Polidori, A. Cherubini, T. Ingegneri, P. Mattioli, M. Catani, P. Rinaldi, R. Cecchetti, W. Stahl, U. Senin, and M.F. Beal, "Lymphocyte oxidative DNA damage and plasma antioxidants in Alzheimer disease," *Arch Neurol*, vol. 59, (no. 5), pp. 794-8, May 2002.
- [37] K. Sakumi, M. Furuichi, T. Tsuzuki, T. Kakuma, S. Kawabata, H. Maki, and M. Sekiguchi, "Cloning and expression of cDNA for a human enzyme that hydrolyzes 8-oxo-dGTP, a mutagenic substrate for DNA synthesis," *J Biol Chem*, vol. 268, (no. 31), pp. 23524-30, Nov 5 1993.
- [38] H. Wiseman and B. Halliwell, "Damage to DNA by reactive oxygen and nitrogen species: role in inflammatory disease and progression to cancer," *Biochem J*, vol. 313 ( Pt 1), pp. 17-29, Jan 1 1996.
- [39] H. Kasai and S. Nishimura, "Hydroxylation of deoxyguanosine at the C-8 position by ascorbic acid and other reducing agents," *Nucleic Acids Res*, vol. 12, (no. 4), pp. 2137-45, Feb 24 1984.
- [40] H.T.K. Michael C. Peoples, "Recent developments in analytical methodology for 8-hydroxy-2-deoxyguanosine and related compounds," *Journal of Chromatography B*, vol. 827, pp. 5-15, 2005.
- [41] Q. Zhang, X. Zhang, J. Chen, Y. Miao, and A. Sun, "Role of caspase-3 in tau truncation at D421 is restricted in transgenic mouse models for tauopathies," *Journal of Neurochemistry*, vol. 109, pp. 476-484, 2009.
- [42] M.L. Circu, S. Stringer, C.A. Rhoads, M.P. Moyer, and T.Y. Aw, "The role of GSH efflux in staurosporine-induced apoptosis in colonic epithelial cells," *Biochem Pharmacol*, vol. 77, (no. 1), pp. 76-85, Jan 1 2009.
- [43] M.L. Circu, M.P. Moyer, L. Harrison, and T.Y. Aw, "Contribution of glutathione status to oxidant-induced mitochondrial DNA damage in colonic epithelial cells," *Free Radic Biol Med*, vol. 47, (no. 8), pp. 1190-8, Oct 15 2009.

- [44] C. Lind, R. Gerdes, Y. Hamnell, I. Schuppe-Koistinen, H.B. von Lowenhielm, A. Holmgren, and I.A. Cotgreave, "Identification of S-glutathionylated cellular proteins during oxidative stress and constitutive metabolism by affinity purification and proteomic analysis," *Arch Biochem Biophys*, vol. 406, (no. 2), pp. 229-40, Oct 15 2002.
- [45] M.L. Circu, C. Rodriguez, R. Maloney, M.P. Moyer, and T.Y. Aw, "Contribution of mitochondrial GSH transport to matrix GSH status and colonic epithelial cell apoptosis," *Free Radic Biol Med*, vol. 44, (no. 5), pp. 768-78, Mar 1 2008.
- [46] N. Patsoukis and C.D. Georgiou, "Determination of the thiol redox state of organisms: new oxidative stress indicators," *Anal Bioanal Chem*, vol. 378, (no. 7), pp. 1783-92, Apr 2004.
- [47] R.E. Hansen and J.R. Winther, "An introduction to methods for analyzing thiols and disulfides: Reactions, reagents, and practical considerations," *Anal Biochem*, vol. 394, (no. 2), pp. 147-58, Nov 15 2009.
- [48] M. Okouchi, N. Okayama, and T.Y. Aw, "Hyperglycemia potentiates carbonyl stress-induced apoptosis in naive PC-12 cells: relationship to cellular redox and activator protease factor-1 expression," *Curr Neurovasc Res*, vol. 2, (no. 5), pp. 375-86, Dec 2005.
- [49] P. Klatt and S. Lamas, "Regulation of protein function by S-glutathiolation in response to oxidative and nitrosative stress," *Eur J Biochem*, vol. 267, (no. 16), pp. 4928-44, Aug 2000.
- [50] R.E. Hansen, H. Qstergaard, P. Norgaard, and J.R. Winther, "Quantification of protein thiols and dithiols in the picomolar range using sodium borohydride and 4,4'-dithiodipyridine," *Analytical Biochemistry*, vol. 363, pp. 77-82, 2007.
- [51] A.J. Gow, Q. Chen, D.T. Hess, B.J. Day, H. Ischiropoulos, and J.S. Stamler, "Basal and stimulated protein S-nitrosylation in multiple cell types and tissues," *J Biol Chem*, vol. 277, (no. 12), pp. 9637-40, Mar 22 2002.
- [52] Y. Zhang and N. Hogg, "Formation and stability of S-nitrosothiols in RAW 264.7 cells," *Am J Physiol Lung Cell Mol Physiol*, vol. 287, (no. 3), pp. L467-74, Sep 2004.
- [53] A. Martinez-Ruiz and S. Lamas, "Detection and identification of S-nitrosylated proteins in endothelial cells," *Methods Enzymol*, vol. 396, pp. 131-9, 2005.
- [54] N.L. Reynaert, K. Ckless, A.S. Guala, E.F.M. Wouters, A.v.d. Vliet, and Y.M.W. Janssen-Heininger, "In site detection of S-glutathionylated proteins following glutaredoxin-1 catalyzed cysteine derivatization," *Biochimica et Biophysica Acta*, vol. 1760, pp. 380-387, 2006.

- [55] G. Cheng, Y. Ikeda, Y. Iuchi, and J. Fujii, "Detection of S-glutathionylated proteins by glutathione S-transferase overlay," *Arch Biochem Biophys*, vol. 435, (no. 1), pp. 42-9, Mar 1 2005.
- [56] G.L. Ellman, "Tissue sulfhydryl groups," *Arch Biochem Biophys*, vol. 82, (no. 1), pp. 70-7, May 1959.
- [57] N.L. Reynaert, K. Ckless, A.S. Guala, E.F. Wouters, A. van der Vliet, and Y.M. Janssen-Heininger, "In situ detection of S-glutathionylated proteins following glutaredoxin-1 catalyzed cysteine derivatization," *Biochim Biophys Acta*, vol. 1760, (no. 3), pp. 380-7, Mar 2006.
- [58] Y. Hamnell-Pamment, C. Lind, C. Palmberg, T. Bergman, and I.A. Cotgreave, "Determination of site-specificity of S-glutathionylated cellular proteins," *Biochem Biophys Res Commun*, vol. 332, (no. 2), pp. 362-9, Jul 1 2005.
- [59] J. Feng and E.A. Arriaga, "Quantification of carbonylated proteins in rat skeletal muscle mitochondria using capillary sieving electrophoresis with laser-induced fluorescence detection," *Electrophoresis* vol. 29, (no. 2), pp. 475-482, 2008.
- [60] J. Feng, M. Navratil, L.V. Thompson, and E.A. Arriaga, "Principal component analysis reveals age-related and muscle-type-related differences in protein carbonyl profiles of muscle mitochondria," *J Gerontol A Biol Sci Med Sci*, vol. 63, (no. 12), pp. 1277-88, Dec 2008.
- [61] J. MacQueen, "Some methods for classification and analysis of multivariate observations," in Book Some methods for classification and analysis of multivariate observations, *Series Some methods for classification and analysis of multivariate observations*, Editor ed.^eds., City: *University of California Press* 1, 1967, pp. 281-297.
- [62] V. Franc and V. Hlavác, "Statistical Pattern Recognition Toolbox for Matlab," Czech Technical University Prague 2004.
- [63] B.S. Everitt, *The Cambridge Dictionary of Statistics*, Cambridge Cambridge University Press, 2006.
- [64] R. Kohavi, "A Study of Cross-Validation and Bootstrap for Accuracy Estimation and Model Selection," *Proceedings of the Fourteenth International Joint Conference on Artificial Intelligence*, vol. 2, (no. 12), pp. 1137-1143, 1995.
- [65] J. Shao, "Linear Model Selection by Cross-Validation," *Journal of the American Statistical Association*, vol. 88, (no. 422), pp. 486-495, 1993.
- [66] M.D. Shelton, P.B. Chock, and J.J. Mieryl, "Glutaredoxin: role in reversible protein s-glutathionylation and regulation of redox signal transduction and protein translocation," *Antioxid Redox Signal*, vol. 7, (no. 3-4), pp. 348-66, Mar-Apr 2005.

- [67] S.A. Gravina and J.J. Mieyal, "Thioltransferase is a specific glutathionyl mixed disulfide oxidoreductase," *Biochemistry*, vol. 32, (no. 13), pp. 3368-76, Apr 6 1993.
- [68] Y. Yang, S. Jao, S. Nanduri, D.W. Starke, J.J. Mieyal, and J. Qin, "Reactivity of the human thioltransferase (glutaredoxin) C7S, C25S, C78S, C82S mutant and NMR solution structure of its glutathionyl mixed disulfide intermediate reflect catalytic specificity," *Biochemistry*, vol. 37, (no. 49), pp. 17145-56, Dec 8 1998.
- [69] A. Holmgren and F. Aslund, "Glutaredoxin," *Methods Enzymol*, vol. 252, pp. 283-92, 1995.
- [70] K. Nordstrand, F. Aslund, A. Holmgren, G. Otting, and K.D. Berndt, "NMR structure of Escherichia coli glutaredoxin 3-glutathione mixed disulfide complex: implications for the enzymatic mechanism," *J Mol Biol*, vol. 286, (no. 2), pp. 541-52, Feb 19 1999.
- [71] B. Mannervik and K. Axelsson, "Role of cytoplasmic thioltransferase in cellular regulation by thiol-disulphide interchange," *Biochem J*, vol. 190, (no. 1), pp. 125-30, Jul 15 1980.
- [72] C. Chassaing, J. Gonin, C.S. Wilcox, and I.W. Wainer, "Determination of reduced and oxidized homocysteine and related thiols in plasma by thiol-specific pre-column derivatization and capillary electrophoresis with laser-induced fluorescence detection," *J Chromatogr B Biomed Sci Appl*, vol. 735, (no. 2), pp. 219-27, Dec 10 1999.
- [73] Y. Kang, V. Viswanath, N. Jha, X. Qiao, J.Q. Mo, and J.K. Andersen, "Brain gamma-glutamyl cysteine synthetase (GCS) mRNA expression patterns correlate with regional-specific enzyme activities and glutathione levels," *J Neurosci Res*, vol. 58, (no. 3), pp. 436-41, Nov 1 1999.
- [74] L.C. Abbott, H.H. Nejad, W.G. Bottje, and A.S. Hassan, "Glutathione levels in specific brain regions of genetically epileptic (tg/tg) mice," *Brain Res Bull*, vol. 25, (no. 4), pp. 629-31, Oct 1990.
- [75] Y. Zhu, P.M. Carvey, and Z. Ling, "Age-related changes in glutathione and glutathione-related enzymes in rat brain," *Brain Res*, vol. 1090, (no. 1), pp. 35-44, May 23 2006.
- [76] A. Pastore, G. Federici, E. Bertini, and F. Piemonte, "Analysis of glutathione: implication in redox and detoxification," *Clin Chim Acta*, vol. 333, (no. 1), pp. 19-39, Jul 1 2003.
- [77] T.S. LeGrand and T.Y. Aw, "Chronic hypoxia alters glucose utilization during GSH-dependent detoxication in rat small intestine," *Am J Physiol*, vol. 274, (no. 2 Pt 1), pp. G376-84, Feb 1998.



- [78] C. Zhang, C. Rodriguez, M.L. Circu, T.Y. Aw, and J. Feng, "S-Glutathionyl quantification in the attomole range using glutaredoxin-3-catalyzed cysteine derivatization and capillary gel electrophoresis with laser-induced fluorescence detection," *Anal Bioanal Chem*, vol. 401, (no. 7), pp. 2165-75, Oct 2011.
- [79] S. Toyokuni, T. Tanaka, Y. Hattori, Y. Nishiyama, A. Yoshida, K. Uchida, H. Hiai, H. Ochi, and T. Osawa, "Quantitative immunohistochemical determination of 8-hydroxy-2'-deoxyguanosine by a monoclonal antibody N45.1: its application to ferric nitrilotriacetate-induced renal carcinogenesis model," *Lab Invest*, vol. 76, (no. 3), pp. 365-74, Mar 1997.
- [80] M.F. Song, Y.S. Li, Y. Ootsuyama, H. Kasai, K. Kawai, M. Ohta, Y. Eguchi, H. Yamato, Y. Matsumoto, R. Yoshida, and Y. Ogawa, "Urea, the most abundant component in urine, cross-reacts with a commercial 8-OH-dG ELISA kit and contributes to overestimation of urinary 8-OH-dG," *Free Radic Biol Med*, vol. 47, (no. 1), pp. 41-6, Jul 1 2009.
- [81] V. Kvasnicova, E. Samcova, A. Jursova, and I. Jelinek, "Determination of 8-hydroxy-2'-deoxyguanosine in untreated urine by capillary electrophoresis with UV detection," *J Chromatogr A*, vol. 985, (no. 1-2), pp. 513-7, Jan 24 2003.
- [82] P. Moftakhar, M.D. Lynch, J.L. Pomakian, and H.V. Vinters, "Aquaporin expression in the brains of patients with or without cerebral amyloid angiopathy," *J Neuropathol Exp Neurol*, vol. 69, (no. 12), pp. 1201-9, Dec.
- [83] I. Rebrin, S. Kamzalov, and R.S. Sohal, "Effects of age and caloric restriction on glutathione redox state in mice," *Free Radic Biol Med*, vol. 35, (no. 6), pp. 626-35, Sep 15 2003.
- [84] R. Liu and J. Choi, "Age-associated decline in gamma-glutamylcysteine synthetase gene expression in rats," *Free Radic Biol Med*, vol. 28, (no. 4), pp. 566-74, Feb 15 2000.
- [85] S. Leichtweis, C. Leeuwenburgh, J. Bejma, and L.L. Ji, "Aged rat hearts are not more susceptible to ischemia-reperfusion injury *in vivo*: role of glutathione," *Mech Ageing Dev*, vol. 122, (no. 6), pp. 503-18, May 15 2001.
- [86] H. Sies and P. Graf, "Hepatic thiol and glutathione efflux under the influence of vasopressin, phenylephrine and adrenaline," *Biochem J*, vol. 226, (no. 2), pp. 545-9, Mar 1 1985.
- [87] T. Minich, J. Riemer, J.B. Schulz, P. Wielinga, J. Wijnholds, and R. Dringen, "The multidrug resistance protein 1 (Mrp1), but not Mrp5, mediates export of glutathione and glutathione disulfide from brain astrocytes," *J Neurochem*, vol. 97, (no. 2), pp. 373-84, Apr 2006.

- [88] P.T. Ronaldson and R. Bendayan, "HIV-1 viral envelope glycoprotein gp120 produces oxidative stress and regulates the functional expression of multidrug resistance protein-1 (Mrp1) in glial cells," *J Neurochem*, vol. 106, (no. 3), pp. 1298-313, Aug 2008.
- [89] P. Borst, R. Evers, M. Kool, and J. Wijnholds, "A family of drug transporters: the multidrug resistance-associated proteins," *J Natl Cancer Inst*, vol. 92, (no. 16), pp. 1295-302, Aug 16 2000.
- [90] R.G. Deeley, C. Westlake, and S.P. Cole, "Transmembrane transport of endo- and xenobiotics by mammalian ATP-binding cassette multidrug resistance proteins," *Physiol Rev*, vol. 86, (no. 3), pp. 849-99, Jul 2006.
- [91] A. Ilias, Z. Urban, T.L. Seidl, O. Le Saux, E. Sinko, C.D. Boyd, B. Sarkadi, and A. Varadi, "Loss of ATP-dependent transport activity in pseudoxanthoma elasticum-associated mutants of human ABCC6 (MRP6)," *J Biol Chem*, vol. 277, (no. 19), pp. 16860-7, May 10 2002.
- [92] G. Aliev, M.A. Smith, D. Seyidov, M.L. Neal, B.T. Lamb, A. Nunomura, E.K. Gasimov, H.V. Vinters, G. Perry, J.C. LaManna, and R.P. Friedland, "The role of oxidative stress in the pathophysiology of cerebrovascular lesions in Alzheimer's disease," *Brain Pathol*, vol. 12, (no. 1), pp. 21-35, Jan 2002.
- [93] G. Perry, A. Nunomura, K. Hirai, A. Takeda, G. Aliev, and M.A. Smith, "Oxidative damage in Alzheimer's disease: the metabolic dimension," *Int J Dev Neurosci*, vol. 18, (no. 4-5), pp. 417-21, Jul-Aug 2000.
- [94] M.A. Smith, G. Perry, and W.A. Pryor, "Causes and consequences of oxidative stress in Alzheimer's disease," *Free Radic Biol Med*, vol. 32, (no. 11), pp. 1049, Jun 1 2002.
- [95] A. Samuele, A. Mangiagalli, M.T. Armentero, R. Fancellu, E. Bazzini, M. Vairetti, A. Ferrigno, P. Richelmi, G. Nappi, and F. Blandini, "Oxidative stress and pro-apoptotic conditions in a rodent model of Wilson's disease," *Biochim Biophys Acta*, vol. 1741, (no. 3), pp. 325-30, Sep 25 2005.
- [96] J.W. Lipton, S. Gyawali, E.D. Borys, J.B. Koprach, M. Ptaszny, and S.O. McGuire, "Prenatal cocaine administration increases glutathione and alpha-tocopherol oxidation in fetal rat brain," *Brain Res Dev Brain Res*, vol. 147, (no. 1-2), pp. 77-84, Dec 30 2003.
- [97] R.M. Liu, "Down-regulation of gamma-glutamylcysteine synthetase regulatory subunit gene expression in rat brain tissue during aging," *J Neurosci Res*, vol. 68, (no. 3), pp. 344-51, May 1 2002.

- [98] T. Garcia, J.L. Esparza, M.R. Nogues, M. Romeu, J.L. Domingo, and M. Gomez, "Oxidative stress status and RNA expression in hippocampus of an animal model of Alzheimer's disease after chronic exposure to aluminum," *Hippocampus*, vol. 20, (no. 1), pp. 218-25, Jan.
- [99] R.R. Resende, A.S. Alves, L.R. Britto, and H. Ulrich, "Role of acetylcholine receptors in proliferation and differentiation of P19 embryonal carcinoma cells," *Exp Cell Res*, vol. 314, (no. 7), pp. 1429-43, Apr 15 2008.
- [100] B.N. Ames and J. Liu, "Delaying the mitochondrial decay of aging with acetylcarnitine," *Ann N Y Acad Sci*, vol. 1033, pp. 108-16, Nov 2004.
- [101] C. Zhang, C.C. Kuo, A.W. Chiu, and J. Feng, "Prediction of S-glutathionylated Proteins Progression in Alzheimer's Transgenic Mouse Model Using Principle Component Analysis," *J Alzheimers Dis*, vol. 30, (no. 4), pp. 919-34, Jan 1 2012.
- [102] M.C. Irizarry, "Biomarkers of Alzheimer disease in plasma," *NeuroRx*, vol. 1, (no. 2), pp. 226-34, Apr 2004.
- [103] J. Choi, C.A. Malakowsky, J.M. Talent, C.C. Conrad, and R.W. Gracy, "Identification of oxidized plasma proteins in Alzheimer's disease," *Biochem Biophys Res Commun*, vol. 293, (no. 5), pp. 1566-70, May 24 2002.
- [104] E. Straface, P. Matarrese, L. Gambardella, R. Vona, A. Sgadari, M.C. Silveri, and W. Malorni, "Oxidative imbalance and cathepsin D changes as peripheral blood biomarkers of Alzheimer disease: a pilot study," *FEBS Lett*, vol. 579, (no. 13), pp. 2759-66, May 23 2005.
- [105] C. Zhang, C. Rodriguez, J. Spaulding, T.Y. Aw, and J. Feng, "Age-dependent and tissue-related glutathione redox status in a mouse model of Alzheimer's disease," *J Alzheimers Dis*, vol. 28, (no. 3), pp. 655-66, 2012.
- [106] A. Castegna, M. Aksenov, V. Thongboonkerd, J.B. Klein, W.M. Pierce, R. Booze, W.R. Markesbery, and D.A. Butterfield, "Proteomic identification of oxidatively modified proteins in Alzheimer's disease brain. Part II: dihydropyrimidinase-related protein 2, alpha-enolase and heat shock cognate 71," *J Neurochem*, vol. 82, (no. 6), pp. 1524-32, Sep 2002.
- [107] A. Castegna, M. Aksenov, M. Aksenova, V. Thongboonkerd, J.B. Klein, W.M. Pierce, R. Booze, W.R. Markesbery, and D.A. Butterfield, "Proteomic identification of oxidatively modified proteins in Alzheimer's disease brain. Part I: creatine kinase BB, glutamine synthase, and ubiquitin carboxy-terminal hydrolase L-1," *Free Radic Biol Med*, vol. 33, (no. 4), pp. 562-71, Aug 15 2002.
- [108] D.A. Butterfield, A. Castegna, C.M. Lauderback, and J. Drake, "Evidence that amyloid beta-peptide-induced lipid peroxidation and its sequelae in Alzheimer's disease brain contribute to neuronal death," *Neurobiol Aging*, vol. 23, (no. 5), pp. 655-64, Sep-Oct 2002.

- [109] C.E. Teunissen, D. Lütjohann, K. von Bergmann, F. Verhey, F. Vreeling, A. Wauters, E. Bosmans, H. Bosma, M.P. van Boxtel, M. Maes, J. Delanghe, H.J. Blom, M.M. Verbeek, P. Rieckmann, C. De Bruijn, H.W. Steinbusch, and J. de Vente, "Combination of serum markers related to several mechanisms in Alzheimer's disease," *Neurobiol Aging*, vol. 24, (no. 7), pp. 893-902, Nov 2003.
- [110] S. Ray, M. Britschgi, C. Herbert, Y. Takeda-Uchimura, A. Boxer, K. Blennow, L.F. Friedman, D.R. Galasko, M. Jutel, A. Karydas, J.A. Kaye, J. Leszek, B.L. Miller, L. Minthon, J.F. Quinn, G.D. Rabinovici, W.H. Robinson, M.N. Sabbagh, Y.T. So, D.L. Sparks, M. Tabaton, J. Tinklenberg, J.A. Yesavage, R. Tibshirani, and T. Wyss-Coray, "Classification and prediction of clinical Alzheimer's diagnosis based on plasma signaling proteins," *Nat Med*, vol. 13, (no. 11), pp. 1359-62, Nov 2007.
- [111] D.J. Selkoe, "The genetics and molecular pathology of Alzheimer's disease: roles of amyloid and the presenilins," *Neurol Clin*, vol. 18, (no. 4), pp. 903-22, Nov 2000.
- [112] C.D. Link, "Transgenic invertebrate models of age-associated neurodegenerative diseases," *Mech Ageing Dev*, vol. 122, (no. 14), pp. 1639-49, Sep 30 2001.
- [113] K. Duff and F. Suleman, "Transgenic mouse models of Alzheimer's disease: how useful have they been for therapeutic development?," *Brief Funct Genomic Proteomic*, vol. 3, (no. 1), pp. 47-59, 2004.
- [114] L. Li, T. Cheung, J. Chen, and K. Herrup, "A comparative study of five mouse models of Alzheimer's disease: cell cycle events reveal new insights into neurons at risk for death. ," *International Journal of Alzheimer's Disease*, vol. 2011, pp. 10, 2011.
- [115] D.M. Holtzman, K.R. Bales, T. Tenkova, A.M. Fagan, M. Parsadanian, L.J. Sartorius, B. Mackey, J. Olney, D. McKeel, D. Wozniak, and S.M. Paul, "Apolipoprotein E isoform-dependent amyloid deposition and neuritic degeneration in a mouse model of Alzheimer's disease," *Proc Natl Acad Sci U S A*, vol. 97, (no. 6), pp. 2892-7, Mar 14 2000.
- [116] D.M. Holtzman, A.M. Fagan, B. Mackey, T. Tenkova, L. Sartorius, S.M. Paul, K. Bales, K.H. Ashe, M.C. Irizarry, and B.T. Hyman, "Apolipoprotein E facilitates neuritic and cerebrovascular plaque formation in an Alzheimer's disease model," *Ann Neurol*, vol. 47, (no. 6), pp. 739-47, Jun 2000.